

**STUDY ON CHANNEL ESTIMATION AND
EQUALIZATION METHODS FOR OFDM BASED
NEXT GENERATION WIRELESS
COMMUNICATION SYSTEMS UNDER HIGHER
MOBILE ENVIRONMENTS**

MARCH 2017

PONGSATHORN REANGSUNTEA

**STUDY ON CHANNEL ESTIMATION AND
EQUALIZATION METHODS FOR OFDM BASED
NEXT GENERATION WIRELESS
COMMUNICATION SYSTEMS UNDER HIGHER
MOBILE ENVIRONMENTS**

by

Pongsathorn Reangsuntea, B.Eng., M.Eng.

Submitted in fulfillment of the requirements
for the Degree of Doctor of Engineering

Supervisor: Professor Hideo Kobayashi

Division of Systems Engineering
Graduate School of Engineering

Mie University

March 2017



I declare that this chapter contains no material which has been accepted for a degree or diploma by the University or any other institution, except by way of background information and duly acknowledged in the thesis, and, that, to the best of my knowledge and belief, this thesis contains no material previously published or written by another person, except where due acknowledgement is made in the text of the thesis.

Signed:_____

Pongsathorn Reangsuntea

Date:_____

This thesis may be made available for loan and limited copying in accordance with the
Mie University Copyright Act 2017

Signed:_____

Pongsathorn Reangsuntea

Date:_____

ABSTRACT

Recently, the demands for wireless multimedia communication services are drastically increasing from the fact that it can be used at anytime, anywhere and for any multimedia services by end users. To realize wireless multimedia communication services, it is strongly required to achieve higher transmission data rate with keeping higher signal quality under the limited frequency bandwidth and lower carrier to noise power ratio (C/N). However, the signal quality would be degraded relatively in wireless communications due to the occurrence of multipath fading distortion which is usually experienced in the received signal. To overcome this problem, orthogonal frequency division multiplexing (OFDM) has been proposed as one of efficient transmission techniques for wireless communications systems because of its efficient usage of frequency bandwidth and robustness to multipath fading distortion. The salient features of OFDM technique are to divide wide-band data information into a group of narrowband subcarriers and adding a cyclic prefix (CP) at the start of every data symbol which enables an employment of simple one-tap frequency domain equalization with keeping the orthogonality among narrowband OFDM subcarriers even in multipath fading channels. From these advantages, OFDM has been already adopted as the standard transmission technique in advanced wireless communications systems such as the 4th generation mobile phone (LTE: Long Term Evolution), digital video broadcasting (DVB), wireless local area networks (WLANs) and worldwide interoperability for microwave access networks (WiMAX).

When assuming lower time-varying fading channels, the channel impulse responses (CIRs) can be considered as a constant during one OFDM symbol period. Accordingly, the channel frequency responses (CFRs) which are converted from the CIRs at any sampling points during one OFDM symbol period are also constant. From this fact, the received OFDM signal can be equalized precisely at the receiver by using simple one-tap frequency domain equalization. However in higher time-varying fading channels, the CIRs are changing during one symbol period and the corresponding CFRs are also changing during one OFDM symbol. From this fact, the signal quality would be degraded relatively in higher time-varying fading channels accompanying with the Doppler frequency shift in which the original property of orthogonality among OFDM subcarriers is no more satisfied due to the occurrence of inter-carrier interference (ICI). To solve the ICI problem in higher time-varying fading channels, various channel estimation and data equalization methods for CP-OFDM signal were proposed up to today.

In conventional CP-OFDM systems, the CIR is usually estimated by using scattered pilot subcarriers which are inserted into data subcarriers periodically both in the frequency and time domains. However, the CIR estimation accuracy would be degraded due to the occurrence of ICI in the received pilot subcarriers. To solve this problem, time domain training sequence (TS) inserted TS-OFDM was proposed in which the TS signal is employed in the estimation of CIR as well as the role of CP. The employment of TS signal can achieve higher estimation accuracy than that for using pilot subcarriers in higher time-varying fading channels from the reason that the period of TS is much shorter than the symbol period which could be assumed that the CIR is constant during the period of TS signal. However, the TS signal would cause the undesirable leakage of power spectrum density (PSD) at the outside of

allocated OFDM bandwidth due to the repetition of same data pattern of TS signal in the time domain which leads the serious adjacent channel interference problem to other systems.

From the above backgrounds, this thesis firstly proposes a channel estimation method by using a new design of TS signal. The features of proposed method are to employ the random data patterns of TS signal added to each data symbol over one frame and to employ a triangular window function as the waveform shaping both for reducing the leakage of PSD with keeping higher CIR estimation accuracy. In addition, this thesis conducts theoretical examinations for the effect of CIR estimation method of using the TS signal when the detected symbol timing at the receiver has an offset from the ideal symbol timing.

As for the ICI problem in higher time-varying fading channels, various frequency domain equalization (FDE) methods for CP-OFDM signal were proposed up to today including a minimum mean square error-frequency domain equalization (MMSE-FDE) and successive interference cancellation (SIC) equalization methods. These methods employed the direct inverse matrix calculation for the channel frequency response (CFR) matrix to mitigate the ICI. However, the computation complexity for the inverse matrix calculation required at every symbol is relatively higher and unsuitable in the implementation of practical receiver. To reduce the complexity, a low-complexity MMSE-FDE method for CP-OFDM signal was proposed in which the full elements of CFR matrix are approximated by a banded matrix so as to enable the employment of the fast algorithm in the calculation of inverse matrix. However, the bit error rate (BER) performance would be degraded in higher time-varying fading channels due to the lower CIR estimation accuracy by using the scattered pilot subcarriers and the approximation for full elements of CFR matrix by the banded matrix. To solve the above problems, a low-complexity overlap and add (OLA) with MMSE-FDE (OLA-MMSE-FDE) and fast suboptimum with MMSE-FDE (FAST-MMSE-FDE) methods for TS-OFDM signals were proposed. In these methods, the CIR is assumed by changing linearly during one symbol period so as to employ the low complexity Maclaurin's expansion approximation technique in the calculation of inverse matrix. Although these methods can achieve lower complexity, the BER performance would be degraded in higher time-varying fading channels due to the assumption of linear changing of CIR and the approximation of first order Maclaurin's expansion. In the development of next generation wireless communication systems, it is strongly required to realize an efficient equalization method which can achieve higher transmission data rate with keeping higher signal quality even in higher time-varying fading channels. The realization of efficient equalization methods in higher time-varying fading channels is still challenging research topic and many researchers in worldwide has been investigating to solve this problem.

From above backgrounds, this thesis firstly proposes a new MMSE-FDE method for TS-OFDM signal in conjunction with the proposed CIR estimation method in higher mobile Rayleigh fading channels. The salient features of proposed method are to enable the acquisition of frequency diversity gain by using an enhanced CIR matrix and enable the reduction of complexity by using a fast algorithm for inverse matrix calculation. Although the proposed MMSE-FDE method can achieve better BER performance than the conventional MMSE-FDE methods with keeping lower complexity, the improvement of BER performance is insufficient especially under higher mobile environments. To solve this problem, this thesis secondly proposes a time domain equalization (TDE) method of using the enhanced CIR matrix in the time domain instead of using the CFR matrix for the MMSE-FDE method. The feature of proposed TDE method is to employ the partial differentiation for the received

signal in solving the maximum likelihood (ML) equation in which the CIR matrix becomes a symmetric banded matrix. This feature enables to employ the fast algorithm for inverse matrix calculation without any approximation which can achieve the same BER performance with much lower computation complexity as that for the direct inverse matrix calculation. These are completely different features from the conventional MMSE-FDE methods. The proposed TDE method can achieve much better BER performance with keeping lower complexity when employing in the wireless cellular phone systems under higher mobile Rayleigh fading environments.

To reduce further complexity, this thesis also proposes an iterative based TDE method for the TS inserted discrete Fourier transform spreading-OFDM (TS-DFTS-OFDM) signal in conjunction with the proposed CIR estimation method under higher mobile Rician environments. The salient features of proposed iterative based TDE method are to employ the enhanced CIR transfer matrix in the mitigation of ICI and to employ the preconditioned conjugate gradient squared (PCGS) algorithm as the iterative solution in the calculation of inverse matrix. The proposed iterative based TDE method can achieve better BER performance with keeping much lower computation complexity when employing in the intelligent transportation systems (ITS) under higher mobile Rician fading environments.

This thesis conducts numerous computer simulations to demonstrate the effectiveness of all proposed methods in higher time-varying fading channels. From the simulation results, it is confirmed that all methods including the CIR estimation method and equalization methods proposed in this thesis could be considered as the practical solutions in the development of OFDM based next generation wireless communication systems.

ACKNOWLEDGEMENTS

First and foremost I would like to express my special appreciation and thanks to my advisor Professor Dr. Hideo Kobayashi. It is great honor to be his last Ph.D. student in Mie University. He has taught me, both consciously and unconsciously, how good experimental in wireless communication engineering is done. I appreciate all his contributions of time, ideas, patience, and funding to make my Ph.D. experience productive and stimulating. The joy and enthusiasm he has for his research was contagious and motivational for me, even during tough times in the Ph.D. pursuit. I am also thankful for the excellent example he has provided as a successful engineer and professor.

An expression of gratitude is addressed to Professor Dr. Kazuo Mori. His invaluable advices inspire me to face any difficulties met during study and research. I would like to thank Associate Professor Dr. Katsuhiro Naito, Department of Information Science, Aichi Institute of Technology who gave me the valuable comments and recommendations during the discussions of research results. I also would like to thank to Assistant Professor Dr. Kousuke Sanada for his precious comments and recommendations during the discussions of research results. I would like to thank our laboratory technician Mr. Yoshiro Yamamoto for his permanent readiness to help on any technical troubles.

I would like to thank Professor Dr. Yoshikatsu Ohta for his important review opinions about the thesis and dedicated recommendations for the improvement of manuscript organization.

I am greatly thankful to Associate Professor Dr. Pisit Boonsrimuang, Broadband Wireless Access Research Laboratory, Department of Telecommunication Engineering, King Mongkut's Institute of Technology Ladkrabang (KMITL), Thailand who provides helps, advices, supports, ideas, and encouragements in various solutions during my study.

I am greatly indebted to the Japanese Government Monbukagakusho (MEXT) Scholarship for support me the immense chance to study at Mie University. A special thanks to all Japanese students in the communication laboratory and Thai students at Mie University for their friendship and assistances.

Lastly, I would like to thank my family for all their love and encouragement. For my parents who raise me with love of science and support me in all my pursuits. I would like to express my warmest thanks to my brother for his moral supports and patience for one year at Mie University during my study. And most of all for my loving, supportive, encouraging, and patient girlfriend whose faithful support during the final stages of this Ph.D. is so appreciated. Without their moral support, it would be impossible to concentrate on research and completed this Ph.D.

TABLE OF CONTENTS

TABLE OF CONTENTS	I
LIST OF TABLES	III
LIST OF FIGURES	IV
1 INTRODUCTION	1
1.1 Current Status of Wireless Communication Systems	2
1.1.1 Development of Wireless Local Area Networks	4
1.1.2 Development of Cellular Mobile Communications Systems	6
1.2 Models of Wireless Communication Channel	10
1.2.1 Time-invariant Channel Model	12
1.2.2 Time-variant Channel Model	14
1.3 Overview of OFDM System Model	18
1.3.1 OFDM Transmission Systems	18
1.3.2 Conventional FDE Method for OFDM Signal	19
1.4 Overview of DFTS-OFDM System Model	21
1.4.1 DFTS-OFDM Transmission Systems	22
1.4.2 Conventional MMSE-FDE Method for DFTS-OFDM Signal	23
1.5 Research Background	25
1.6 Thesis Structure	28
2 CHANNEL ESTIMATION METHOD FOR OFDM SYSTEMS UNDER HIGHER MOBILE ENVIRONMENTS	29
2.1 Introduction	30
2.2 Conventional Scattered Pilot based Channel Estimation Method	32
2.3 Proposed Time Domain TS based Channel Estimation Method	35
2.3.1 System Model for TS-OFDM Signal	35
2.3.2 Channel Estimation Method at Every Sampling Time	37
2.4 Performance Evaluation for Proposed Channel Estimation Method	39
2.5 Conclusions	43
3 THEORETICAL EXAMINATION OF CHANNEL ESTIMATION METHOD FOR TS-OFDM SIGNAL UNDER SYMBOL TIMEING OFFSET	44
3.1 Introduction	45
3.2 Design of TS-OFDM under Symbol Timing Offset	46
3.3 CFR Estimation Method for TS-OFDM under Symbol Timing Offset	47
3.4 Proof of Theoretical Analysis by Computer Simulation Results	51
3.5 Conclusions	54

4 FREQUENCY DOMAIN EQUALIZATION METHOD FOR TS-OFDM SIGNAL UNDER HIGHER MOBILE ENVIRONMENTS	55
4.1 Introduction	56
4.2 Conventional MMSE-FDE Methods under Higher Mobile Environments	58
4.2.1 MMSE-FDE Method for CP-OFDM Signal	58
4.2.2 FAST-MMSE-FDE Method for TS-OFDM Signal	59
4.3 Proposed MMSE-FDE Method for TS-OFDM Signal	61
4.3.1 System Structure for Proposed TS-OFDM Signal	61
4.3.2 Construction of Enhanced CIR Matrix	63
4.3.3 Low-Complexity Enhanced MMSE-FDE Method	64
4.3.4 Evaluation of Computation Complexity	65
4.4 Performance Evaluation for Proposed MMSE-FDE Method	66
4.5 Conclusions	69
5 TIME DOMAIN EQUALIZATION METHOD FOR TS-OFDM SIGNAL UNDER HIGHER MOBILE ENVIRONMENTS	70
5.1 Introduction	71
5.2 Proposal of Time Domain Equalization Method for TS-OFDM	73
5.2.1 System Model for Proposed TDE Method	73
5.2.2 Low-Complexity Time Domain Equalization Method	76
5.3 Evaluation of Computation Complexity	79
5.4 Performance Evaluations for Proposed TDE Method	81
5.5 Conclusions	86
6 ITERATIVE BASED TIME DOMAIN EQUALIZATION METHOD FOR DFTS-OFDM UNDER HIGHLY MOBILE ENVIRONMENTS	87
6.1 Introduction	88
6.2 System Structure for DFTS-OFDM Signal	91
6.2.1 TS inserted DFTS-OFDM System	91
6.2.2 CIR Estimation Method for TS inserted DFTS-OFDM Signal	93
6.3 Proposal of Time Domain Equalization Method	94
6.3.1 Proposed TDE with Direct Inverse Matrix Calculation	94
6.3.2 Proposed Iterative based TDE Method	97
6.4 Performance Evaluations	99
6.5 Conclusions	104
7 CONCLUSIONS	105
LIST OF PUBLICATIONS	107
BIBLIOGRAPHY	111

LIST OF TABLES

Table 1.1:	IEEE802.11 network physical layer standards.	4
Table 1.2:	Cellular mobile communication standards.	7
Table 2.1:	Simulation parameters.	39
Table 3.1:	Simulation parameters.	51
Table 4.1:	Order of complexities for proposed and conventional methods.	65
Table 4.2:	Simulation parameters.	66
Table 5.1:	Order of computation complexity for proposed TDE and conventional FDE methods.	80
Table 5.2:	Simulation parameters.	81
Table 6.1:	Simulation parameters.	99
Table 6.2:	Ratio of computation complexity for proposed iterative based TDE method	102

LIST OF FIGURES

Figure 1.1:	Applications of OFDM technique.	3
Figure 1.2:	Wireless access networks standardized by IEEE standards.	3
Figure 1.3:	Transmission data rate in IEEE802.11 standards.	5
Figure 1.4:	Present status and future trend for wireless communications systems.	6
Figure 1.5:	Increasing of transmission data rate in cellular mobile communications systems.	9
Figure 1.6:	Typical of radio propagation.	10
Figure 1.7:	Fading channel classifications.	11
Figure 1.8:	Block diagram of communication channel model.	12
Figure 1.9:	Wireless communications in time-variant channel model.	15
Figure 1.10:	Block diagram of conventional OFDM systems.	19
Figure 1.11:	Comparison of PAPR performance between OFDM and DFTS-OFDM signals.	21
Figure 1.12:	Block diagram of conventional DFTS-OFDM systems.	22
Figure 1.13:	Comparison of BER performance when changing operation C/N and normalized Doppler frequency (R_D).	24
Figure 2.1:	Relationships between CIR and CFR.	30
Figure 2.2:	Basic frame format of scattered pilot subcarrier using in CP-OFDM.	32
Figure 2.3:	Comparison of estimated CFR and actual CFR.	34
Figure 2.4:	Structure of TS-OFDM signal in multipath fading channels.	35
Figure 2.5:	Estimation of CIR at every sampling time by using cubic spline interpolation.	38
Figure 2.6:	Power spectrum density for proposed TS-OFDM signal with new design of TS, conventional TS-OFDM signal with PN sequence and conventional CP-OFDM signal.	40
Figure 2.7:	CIR estimation accuracy (NMSE) for proposed method when changing the number of zero padding at C/N=30dB.	41
Figure 2.8:	CIR estimation accuracy (NMSE) for proposed and conventional TS-OFDM when changing normalized Doppler frequency (R_D).	42
Figure 2.9:	CIR estimation accuracy (NMSE) for proposed and conventional TS-OFDM when changing C/N.	42
Figure 3.1:	Frame format for TS-OFDM signal under symbol timing offset.	46
Figure 3.2:	Amplitude of estimated CIR by using the time domain TS signal.	52
Figure 3.3:	BER performances for TS-OFDM signal when changing detected ST (η).	52
Figure 3.4:	BER performances when changing operation C/N.	53
Figure 4.1:	Basic Frame format of TS-OFDM signal at transmitter (a) and receiver (b).	61
Figure 4.2:	Structure of transceiver for proposed MMSE-FDE method.	62
Figure 4.3:	BER performance for proposed MMSE-FDE method when changing R_D at C/N=35dB.	67
Figure 4.4:	BER performance of proposed MMSE-FDE method when changing C/N at $R_D=5\%$.	68
Figure 5.1:	Structure of transceiver for proposed TDE method.	74

Figure 5.2:	Structure of TS-OFDM signal in multipath fading channels.	75
Figure 5.3:	BER performances versus the normalized Doppler frequency R_D when the modulation method is QPSK and C/N is 35dB.	83
Figure 5.4:	BER performances versus C/N when the modulation method is QPSK and normalized Doppler frequency R_D is 3%.	83
Figure 5.5:	BER performances versus C/N when the modulation method is QPSK and normalized Doppler frequency R_D is 10%.	84
Figure 5.6:	BER performances versus C/N when the modulation method is 16QAM and normalized Doppler frequency R_D is 6%.	85
Figure 5.7:	Comparisons of overall computation complexities for proposed TDE and conventional FDE methods when changing N .	85
Figure 6.1:	Relationships between CIR and CFR.	88
Figure 6.2:	Amplitude of CIR at every sampling time in high time-varying channel.	89
Figure 6.3:	Proposed frame format in the time domain.	92
Figure 6.4:	Structure of transceiver for DFTS-OFDM signal with proposed iterative based TDE method.	92
Figure 6.5:	Estimation of CIR at every sampling time by using cubic spline interpolation method.	93
Figure 6.6:	Received time domain signal in multipath fading channel.	94
Figure 6.7:	CIR estimation accuracy when changing R_D and operation C/N.	100
Figure 6.8:	BER performance for proposed iterative based TDE method when changing TOL and C/N at $R_D=15\%$.	101
Figure 6.9:	Average number of required iterations for proposed iterative based TDE method when changing R_D and C/N at TOL= 0.02.	101
Figure 6.10:	BER performance for proposed iterative based TDE method when changing R_D at C/N=20dB.	103
Figure 6.11:	BER performance for proposed iterative based TDE method when changing C/N at $R_D=15\%$.	103

CHAPTER 1

INTRODUCTION

This chapter firstly presents a current status of wireless communication systems focusing on wireless local area networks (WLANs) and cellular mobile communication systems which are currently used widely in the world. Section 1.2 presents the mathematical representation for wireless communication channel models including the time-invariant and time-variant fading channels which are used in this research. Section 1.3 introduces the overview and mathematical representation for orthogonal frequency division multiplexing (OFDM) system both for the transmitter and receiver. Section 1.4 introduces the discrete Fourier transform spreading-orthogonal frequency division multiplexing (DFTS-OFDM) system which is considered as the alternative technique to OFDM because of its lower peak to averaged power ratio (PAPR) in its time domain signal as compared with OFDM. This thesis proposes the channel estimation method and equalization methods both for OFDM and DFTS-OFDM techniques. Subsequently, this thesis identifies the problems which are still unsolved in the development of next generation wireless communication systems under higher mobile environments. From these backgrounds, all research topics proposed in this thesis under higher mobile environments are presented in Section 1.5. Finally, the organization of thesis structure is presented in Section 1.6.

1.1 Current Status of Wireless Communication Systems

Currently, wireless communications are considered as one of most active fields in which various new technology developments are conducted in the communications industry and research community. Wireless communications also have been received a lot of attentions from the end users who demand new multimedia services such as voice and video streaming, file transfer, and internet access. Wireless communications are defined by sending the information from one point to another point or multiple points without using wires. One of popular wireless communications is the wireless local area networks (WLANs) which are currently used widely to supplement or replace wired networks in such as the fields of businesses, public places and university campuses [1-3]. Wireless communications today covers a very wide areas of applications including wireless sensor networks, automated highways and factories, smart homes and appliances, and remote telemedicine all of which are emerging from research ideas to actual systems. The explosive growth of wireless communication systems coupled with the proliferation of laptop and palmtop computers indicate a bright future for wireless networks both as stand-alone systems and as part of the larger network infrastructures [4-6]. However, many technical challenges are still remaining in the development of advanced efficient wireless networks which can support emerging applications. Generally, various wireless communication technologies are supported by the transmission techniques such as the time-division multiple-access (TDMA), code-division multiple accesses (CDMA) and orthogonal frequency-division multiplexing (OFDM) both for multi-carrier systems and single-carrier systems. These transmission techniques are selected primarily taken into account the physical properties of wireless channels experienced in the multipath fading, dispersion, and interference [7-15].

Among various transmission techniques employed in the wireless communication systems, OFDM technique is considered as the most efficient transmission technique in the physical layer (PHY) which can achieve higher efficient usage of frequency bandwidth, robustness to multipath fading and simplicity systems structure. From these advantages, OFDM technique has been adopted widely as the standard transmission technique in wireless communication systems both for wired and wireless communications such as in the asymmetric digital subscriber line (ADSL) systems, power cable line (PCL) systems, terrestrial digital audio broadcasting and TV broadcasting systems (DAB and DVB) [16-17], wireless local area networks (WLANs) (IEEE802.11 standard) [18] and next generation mobile communication systems (LTE: Long term evaluation) [19-20] as shown in Figure 1.1.

Figure 1.2 shows various wireless access networks standardized by the Institute of Electrical and Electronics Engineers (IEEE) for serving from the small-area to the large area. The smallest one is the wireless personal area network (PAN) including sensor network interconnects devices within a relatively small area that covers only several meters around a user (IEEE802.15, Bluetooth and ZigBee). Operating in a larger area than wireless PAN, the wireless LAN (IEEE802.11 / Wi-Fi) is the most successful and prevalent wireless computer network standard. In wireless LAN, short-distance communications within several tens of meters and up to 100 meters are provided. The metropolitan area network (MAN) is the wireless network that connects several wireless LANs (IEEE802.16-2004 / WiMAX) which

1.1 Current Status of Wireless Communication Systems

extends its coverage area to several kilometers in urban areas. The wireless wide area network (WAN) is the wireless network that typically covers large areas such as towns and cities (IEEE802.16e, IEEE802.20 / Mobile Phone). The wireless WAN communications support the communications distance over up to 10 kilometers within hilly terrains and rural areas. The regional area network (RAN) is for wireless regional area network using white spaces in the television (TV) frequency spectrum (IEEE802.22) and its provide communication distance over up to 40 kilometers. With all these wireless networks, uninterrupted internet access can be made available whenever and wherever the end users desire.

This introduction section presents a brief reviewing for the wireless communication systems focusing on WLANs and cellular mobile communication systems which are the representative wireless communication systems from the past to today. This chapter also introduces the current status of wireless communication systems in operation today as well as emerging systems under the standardization.

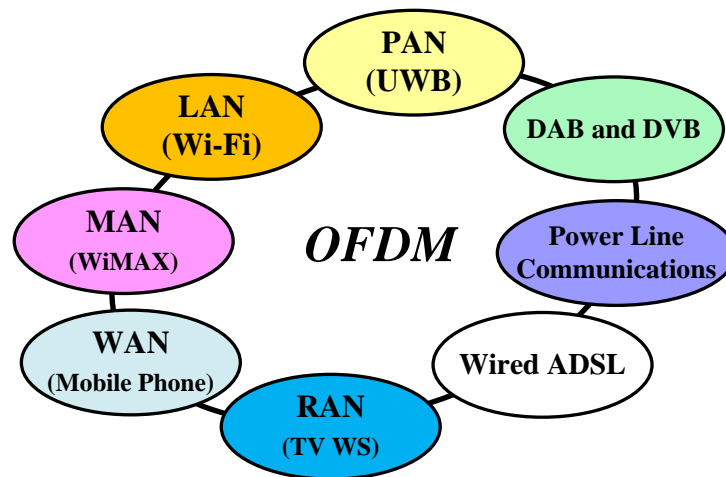


Figure 1.1: Applications of OFDM technique.

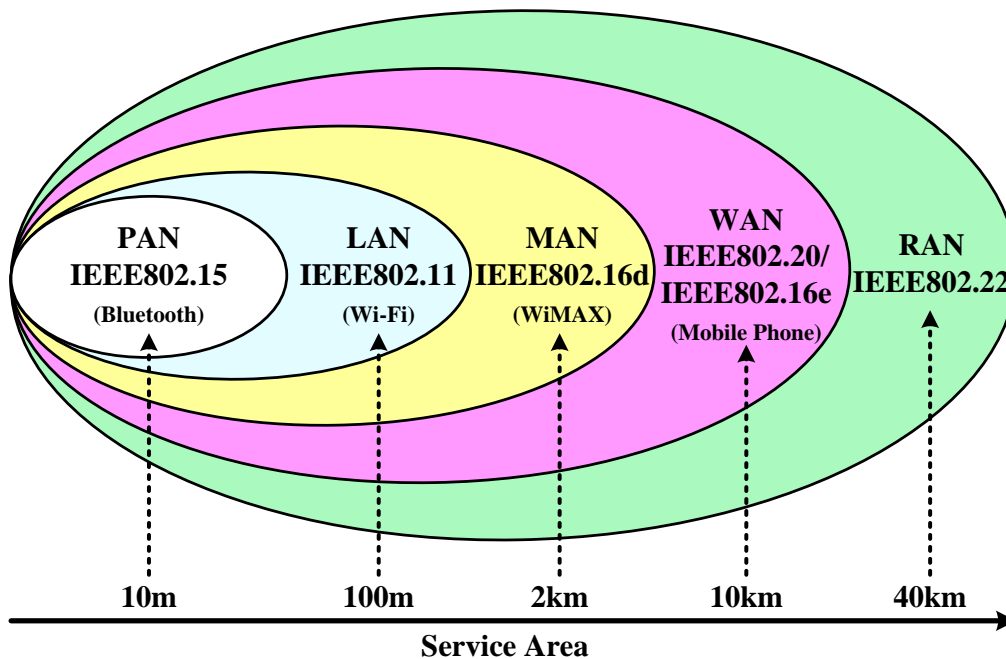


Figure 1.2: Wireless access networks standardized by IEEE standards.

1.1.1 Development of Wireless Local Area Networks

Wireless local area networks (WLANs) provide a high-speed data rate communication within a small service area (e.g. a campus or inside of building) as the users move from place to place. Wireless devices that access these LANs are typically stationary or moving at pedestrian speeds. Most of wireless LANs systems share the frequency band with the industrial, scientific and medical (ISM) frequency bands which are allocated originally at around 2.4GHz [21]. Recently the lack of frequency band due to the increasing of user demands, frequency band is expanded at 900 MHz and 5.8 GHz in which the license [22] is not required to operate in these bands. However, this advantage leads the serious problem of frequency congestions in these bands. Since many systems operate in these frequency bands from the fact of useful frequency bands, this would cause the interference problem among other systems. To solve this problem, many WLAN systems are standardized by IEEE. Table 1.1 shows the physical layer standards for IEEE802.11 [23] as shown in Table 1.1. The working group of IEEE 802.11 is also known as Wi-Fi which defines a series of wireless LAN standards. The 802.11 wireless LAN adopts cellular architecture using the access points (AP) to control the traffic to/from the subscriber station (SS) within their respective cells. The access points are usually connected to a wireline backbone to set up links to the internet. Based on the IEEE802.11 standards, various wireless LAN standards are developed commercially up to today.

The first IEEE 802.11 standard was released in 1997 using either frequency hopping (FH) spread spectrum (2.4 GHz) and direct sequence (DS) spread spectrum (2.4 GHz) as the transmission technology. The supported data rates are 1 and 2 Mbps. Two years later, IEEE 802.11b which employs a complementary code keying (CCK) modulation scheme, was ratified as an amendment to the previous systems. It extends the transmission rate up to 11 Mbps. From this fact, a data rate that is five times higher than the previous generation, IEEE 802.11b products become very popular in the market [24].

Table 1.1: IEEE802.11 network physical layer standards [23].

IEEE802.11		a	b	g	n	ac	ad
Number of Streams	1	1	1	1	4 (Max)	8 (Max)	1
Data Rate (Mbps)	2	54	11	54	65-600	290-6,900	4,600-6,800
Frequency (GHz)	2.4	5	2.4	2.4	2.4, 5	5	57-66
Bandwidth (MHz)	22	20	22	20	20/40	80/160	9000 (Max)
Transmission Technique	DS	OFDM	DS	OFDM	MIMO-OFDM	MIMO-OFDM	SC-OFDM
Modulation Technique	DS-FH	BPSK-64QAM	CCK	QPSK-64QAM	QPSK-64QAM	QPSK-256QAM	BPSK-16QAM
Release Year	1997	1999	1999	2003	2009	2013	2013

1.1 Current Status of Wireless Communication Systems

Simultaneously in 1999, another OFDM wireless LAN standard (IEEE 802.11a) was proposed and it increased the maximum data rate up to 54 Mbps. Since the 2.4 GHz ISM band is used by many users, IEEE 802.11a uses another band at around 5 GHz with a low level of interference. Unfortunately, a higher carrier frequency incurs more penetration loss and also increases the cost of radio-frequency components. As a result, IEEE 802.11g of using 2.4GHz was approved in 2003 which employs the same OFDM technique as in IEEE 802.11a and with the same data rate of up to 54 Mbps. In addition, IEEE 802.11g is backward compatible to IEEE 802.11b. It has so many conveniences and advantages that IEEE 802.11g or dual-band (2.4/5 GHz), tri-mode (11a/b/g) products are now produced commercially in the market.

In 2004, a new task group (IEEE 802.11n) was formed to increase the wireless LAN data rate further. A very aggressive spectral efficiency of OFDM wireless LAN standards (IEEE 802.11n/ac) were proposed in 2009 and 2013, respectively. The new IEEE 802.11n/ac standards can offer interoperability with existing 802.11a/b/g networks. The OFDM based wireless technologies including multi-input multi-output (MIMO) with up to eight antennas are adopted and it achieved the maximum data rate up to 1 Gbps. In the 802.11n/ac, the transmission data rate can be improved by using the higher code rate, low-density parity check code (LDPC), 20/40MHz channelization and reduction in guard interval overhead. The transmission data rate of IEEE802.11 standards up to today are shown in Figure 1.3.

Consequently in 2013, single carrier-OFDM based wireless communication standard (IEEE 802.11ad) was proposed which aimed at providing the transmission data rate up to 7 Gbps. To achieve these higher speeds, the 60 GHz ISM band is employed to achieve the enough wider frequency bandwidth and ensure reduced interference levels. Using frequencies in the millimeter range IEEE 802.11ad microwave Wi-Fi has a range that is measured of a few meters. The purpose of this standard is that it will be used for very short range and high volume of data transfers such as high-definition (HD) video transfers. When longer ranges are needed standards such as 802.11ac can be used. The next generation of OFDM based wireless communications are still under development which is not yet clear how and to what extent will be done.

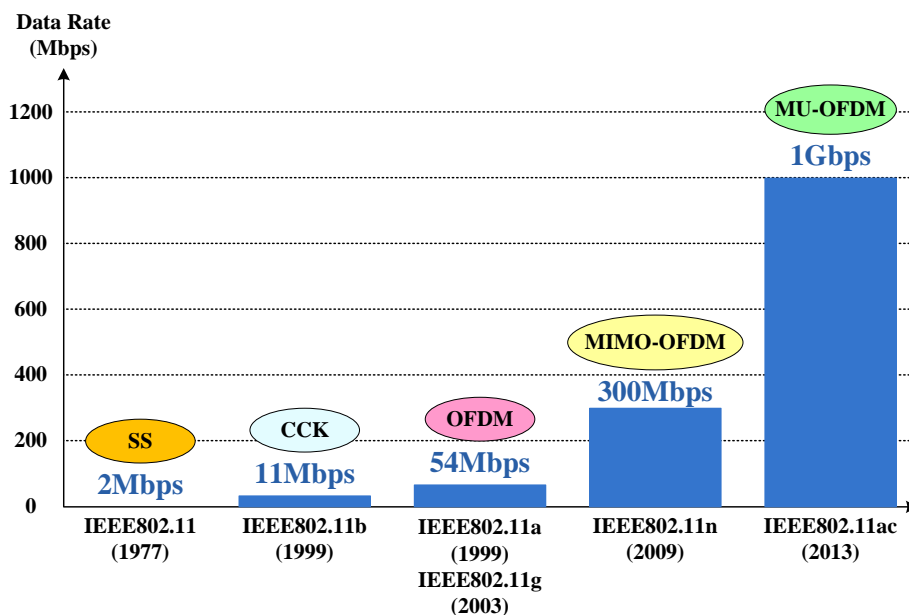


Figure 1.3: Evolution of transmission data rate in IEEE802.11 standards.

1.1.2 Development of Cellular Mobile Communications Systems

Cellular mobile communication systems have moved from analog to digital technologies because the digital technology has many advantages over analog technology in which the digital technology can develop the terminal by using the cheaper components, smaller devices with less power and also possible to achieve higher voice quality by using the forward error correction coding (FEC). Since the digital technology is not limited to the frequency division multiple accesses (FDMA) or time division multiple accesses (TDMA) techniques, it can achieve higher system capacity than analog technology by employing the advanced compression and encryption techniques with the voice activity factors. From these advantages, the using of the digital signals can be secured and against the eavesdropping. Figure 1.4 shows the development of cellular mobile communications systems from the first generation (1G) to the current fourth generation (4G) systems. Table 1.2 shows the cellular mobile communication standards for each generation systems. The digital cellular mobile communication systems have been developed from the second generation (2G) systems introduced in the early 1990's. From the introduction of 2G system, the new generation standards from the third generation (3G) to 4G have been introduced at every 10 years.

In the early 1980s, the first generation (1G) of wireless mobile communication technologies included the advanced mobile phone system (AMPS) introduced in the United States, total access communication system (TACS) in the United Kingdom, Nordic mobile telephone (NMT) system in the Scandinavian countries, Nippon Telephone & Telegraph (NTT) system in Japan. These technologies used analog frequency modulation (FM) for voice transmission and frequency shift keying (FSK) for signaling. The critical problems of the first generation (1G) included capacity and incompatible standards among these systems [25-27].

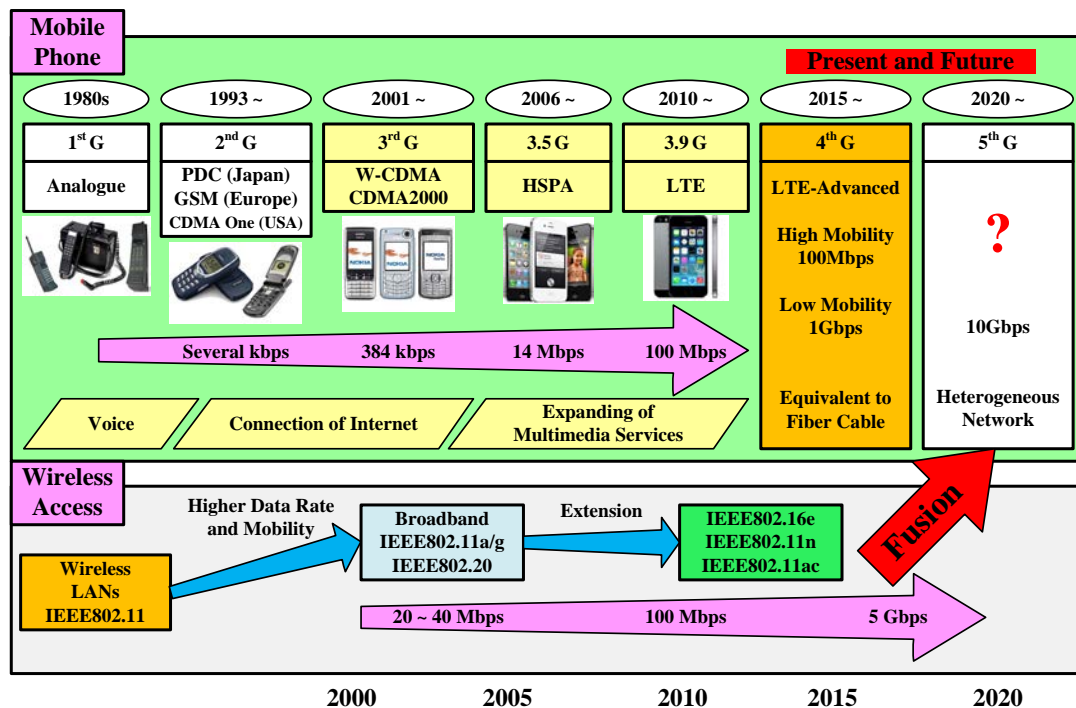


Figure 1.4: Present status and future trend for wireless communications systems.

1.1 Current Status of Wireless Communication Systems

Table 1.2: Cellular mobile communication standards.

Standards		
0G (Radio Telephone)	MTS, MTA, MTB, MTC, IMTS, MTD, AMTS, OLT, Autoradiopuhelin	
1G	AMPS family	AMPS (TIA/EIA/IS-3, ANSI/TIA/EIA-553), N-AMPS (TIA/EIA/IS-91), TACS, ETACS
	Other	NMT, Hicap, Mobitex, DataTAC
2G	GSM/3GPP family	GSM, CSD
	3GPP2 family	CDMA One (TIA/EIA/IS-95 and ANSI-J-STD 008)
	AMPS family	D-AMPS (IS-54 and IS-136)
	Other	CDPD, iDEN, PDC, PHS
2G Transitional (2.5G, 2.75G)	GSM/3GPP family	HSCSD, GPRS, EDGE/EGPRS (UWC-136)
	3GPP2 family	CDMA2000 1X (TIA/EIA/IS-2000), 1X Advanced
	Other	WiDEN
3G (IMT-2000)	3GPP family	UMTS (UTRAN), WCDMA-FDD, WCDMA-TDD, UTRA-TDD LCR (TD-SCDMA)
	3GPP2 family	CDMA2000 1xEV-DO Release 0 (TIA/IS-856)
3G Transitional (3.5G, 3.9G)	3GPP family	HSPA, HSPA+, LTE (E-UTRA)
	3GPP2 family	CDMA2000 1xEV-DO Revision A (TIA/EIA/IS-856-A), EV-DO Revision B (TIA/EIA/IS-856-B), DO Advanced
	IEEE family	Mobile WiMAX (IEEE 802.16e), Flash-OFDM, IEEE 802.20
4G (IMT-Advanced)	3GPP family	LTE Advanced (E-UTRA)
	IEEE family	WiMAX-Advanced (IEEE 802.16m)
5G	Research concept, not under formal development	

In 2G, the digital cellular systems are the nation or region based standards which includes several incompatible standards. In particular, there are two standards in the 900MHz (cellular: IS-54) frequency band of using the combination of TDMA and FDMA and using a semi-orthogonal CDMA (IS-95) [28-29]. The global system for mobile communications (GSM) system is standardized as the European standard which uses a combination of TDMA and slow frequency-hopping. The CDMA One (IS-95) is standardized in United States. The personal digital cellular (PDC) system is standardized in Japan which adopted the TDMA similar to IS-54 but different in the frequency band. The incompatible standard problem among European, United States and Japan makes the end users impossible to roam between systems nationwide or globally without using multiple phones. At the beginning, all of digital cellular systems offer digital voice services at around 10 Kbps. Afterwards, the general packet radio service (GPRS), enhanced data rate for global evolution (EDGE) and CDMA2000 1X systems are employed for the digital cellular systems and these technologies can increase the transmission data rates up to several hundreds of Kbps [30-31].

1.1 Current Status of Wireless Communication Systems

In 3G, the cellular mobile systems employed a wideband CDMA technique which is standardized by the international telecommunications union (ITU) [30]. Initially, the 3G standard was called international mobile telecommunications 2000 (IMT-2000) in which it provides the different data rates depending on mobility and location such as the transmission rate for the pedestrian use (384 Kbps), for vehicular use (144 Kbps), and for accommodation of multimedia applications use (2 Mbps). Since the 3G system is incompatible with any 2G systems, therefore the service providers must invest a new infrastructure before they can provide 3G service. The 3rd generation partnership project (3GPP) [32] started working on the radio, core network, and service architecture of a globally applicable 3G technology specification with the target of creating a collaboration entity among different telecommunications associations. Even though the data rates of 3G systems were already real in the theory, the initial systems like universal mobile telecommunications system (UMTS) did not immediately meet the IMT-2000 requirements in their practical deployments. Therefore, the 3G standards needed to be improved to meet or even exceed them. Two mainstream 3G standards are CDMA2000 3X and wideband-CDMA (W-CDMA). The enhanced version of W-CDMA has been standardized as high speed downlink packet access (HSDPA) in which it is regarded as the 3.5G and can achieve the transmission data rate up to 10 Mbps [33-34]. Motivated by the demand of end users for the new services with higher data rates and quality of service (QoS), the 3GPP long-term evolution (LTE) started working on two parallel projects as the long term evolution (LTE) and system architecture evolution (SAE) which are intended to define both the radio access network (RAN) and the network core of the system. These two technologies are included in 3GPP release 8. LTE/SAE and it's also known as the evolved packet system (EPS) which represents a radical step forward for the wireless industry that aims to provide a higher efficient, lower latency, packet-optimized and more secure service [35-36]. The main transmission technique design of this new system employed the OFDM technique in order to avoid the inter-symbol interference (ISI) with that typically limits the performance of high-speed systems and also employed the multiple input multiple output (MIMO) techniques to increase the transmission data rates. However, by the time of the 3.5G standard development started that the ITU-R framework for 4G systems was not in place and the measurements confirmed that the system did not fully comply with ITU 4G requirements. From this reason, the 3.9G has been introduced and widely used with the expectation of their evolving towards official 4G technology. Before 3GPP started working in the real 4G wireless technology, the minor changes were introduced in LTE through release 9 [37]. In particular, the femtocells, dual-layer beamforming and predecessors of future LTE-advanced technologies have been added to the standard. The formal definition of the 4G technology is known as the international mobile telecommunications advanced (IMT-advanced) project which was finally published by ITU-R through a circular letter in July 2008 with a call for candidate as the radio interface technologies (RITs) [38].

In 2009, six technologies were submitted seeking for approval as international 4G communications standard. The 3GPP's candidate standard is the LTE-Advanced in which the backward-compatible enhancements of LTE release 8 that will be fully specified in 3GPP release 10 [39]. The target of 3GPP LTE Advanced is to reach and surpass the ITU requirements. The LTE-advanced should be compatible with first release LTE equipment and should share the frequency bands with first release LTE. In the feasibility study for LTE-advanced, 3GPP determined that LTE-advanced would meet the ITU-R requirements for 4G standard. Other candidate technologies are IEEE 802.16m and China's ministry of industry

1.1 Current Status of Wireless Communication Systems

and information technology TD-LTE-advanced (LTE-advanced TDD specification) [40-42]. One of the important LTE-advanced benefits is the ability to take advantage of advanced topology networks such as the optimized heterogeneous networks with a mix of macrocells with low power nodes such as picocells, femtocells and new relay nodes. In addition, LTE-advanced further improves the capacity and coverage and ensures user fairness. Currently, the trialed LTE-Advanced is now deploys in Japan with Chinese vendor Huawei in which Softbank operator used the 3.5 GHz spectrum band and can achieve the transmission data rate up to 770 Mbps.

The next generation is so-called fifth generation (5G) systems which is now considers for the next major phase of cellular mobile telecommunications standards beyond the current 4G/IMT-Advanced standards. The 5G systems are aim to include the internet connection speeds faster than the current 4G and other improvements. From this fact, the efficient cellular mobile system designs are interference-limited as the interference dominates the noise floor so as to add more users to the systems. As a result, many techniques are now proposed to reduce interference in cellular mobile communication systems leads directly to increase the system capacity and performance. Some methods for interference reduction in use today or proposed for future systems including cell optimization [43-44], directional and smart antennas [45-47], multiuser detection [48-50] and dynamic resource allocation [51-52].

Figure 1.5 shows the increasing of transmission data rate in cellular mobile communications systems ranging from 1G to 5G systems. From the Figure, it can be seen that the transmission data rate is increased by 10,000 times during 30 years. At the present time, the 3GPP LTE-advance standard supports the data rate possibly approaching 1 Gbps. Here, the current wireless communication standards now exist, under development and adopt or consider adopting OFDM as the transmission technique. It is clear that OFDM technique has become the definitive transmission technique in current and next generation of wireless communication systems.

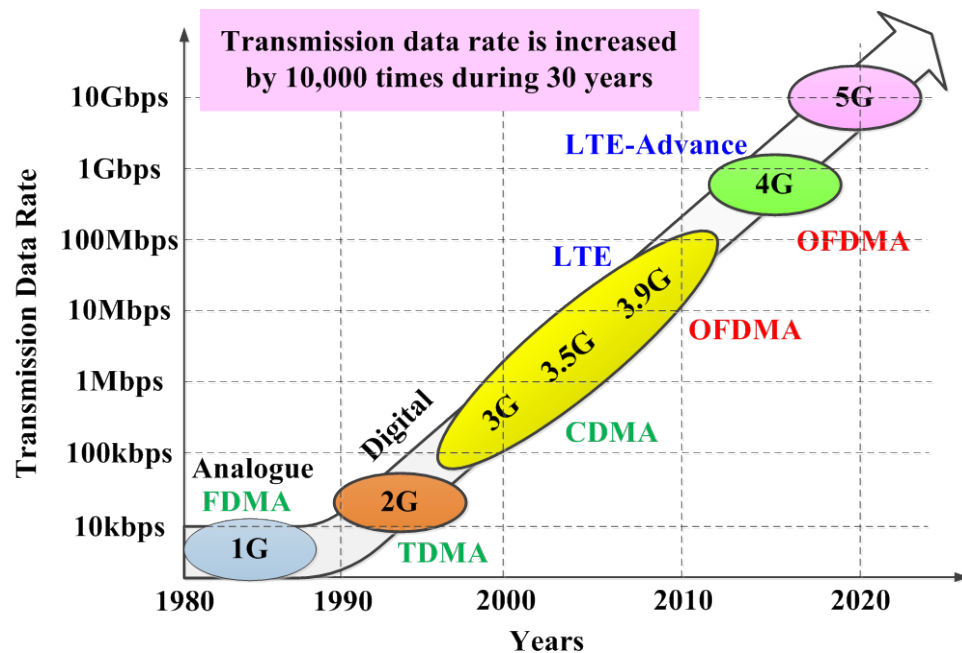


Figure 1.5: Increasing of transmission data rate in cellular mobile communications systems.

1.2 Models of Wireless Communication Channel

The basic structure of any communication system is modeled by transmitter, channel and receiver. The channel can be categorized by wired and wireless. In this thesis, the wireless communications is mainly focused. In the fixed line of sight (LOS) transmission, the receiver has only a single attenuated received signal when the directional antennas are employed both at the transmitter and receiver. However in real wireless communication channel, the received signal includes multiple reflected signals with or without LOS component at the receiver. The propagation channel with the LOS component is modeled by a Rice distribution while propagation channel without LOS is modeled by a Rayleigh distribution.

The propagation of an electromagnetic wave in a radio channel undergoes diverse physical phenomenon. The three major mechanisms that impact this propagation are the reflection, diffraction and scattering. The reflection occurs when a propagating wave impinges upon a smooth surface with very large dimensions relative to its wavelength. The diffraction is produced when the propagation path between the transmitter and the receiver is obstructed by a dense body with dimensions that are large relative to the wavelength of signal which causing secondary waves to be formed behind the obstructing body. It is often referred to as shadowing because the diffraction field can reach the receiver even when shadowed by an impenetrable obstacle. Finally, scattering is produced when the radio wave falls on a surface whose dimensions are less than the wavelength of signal which causing the energy to scatter in all directions. Those above mechanisms lead the reception of multiple copies of the transmitted signal at the receiver. Therefore, the received signal is made up from the superposition of attenuated and delayed signals of transmitted signal. Figure 1.6 shows the schematic figure of typical these radio propagations. The multiple paths characterize as a multipath propagation and cause fluctuations in the received signal's amplitude, phase and arrival angle which produces the multipath fading.

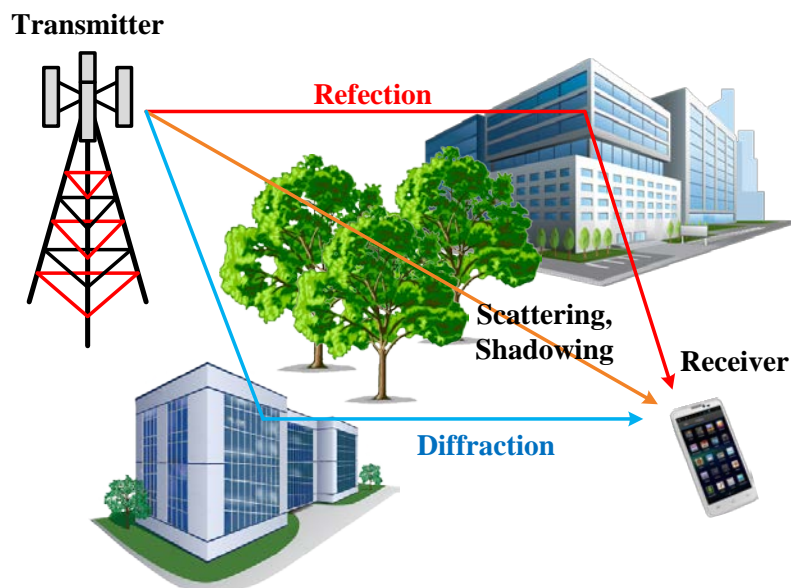


Figure 1.6: Typical radio propagation in wireless communications.

1.2 Models of Wireless Communication Channel

In the multipath fading channels, there exist two types of fading [53] as a large-scale fading and a small-scale fading. The large-scale fading represents the average signal power attenuation or path-loss due to the motion over large areas (e.g. Hills, forests, and buildings). Practically, this fading is characterized by statistics which provides a way of computing the estimation of the path-loss as a function of the distance. Precisely, the path-loss is proportional to $1/d^\alpha$, where d is the distance between the transmitter and the receiver, and α is the path-loss component varying from 2 (free-space) to 6 (urban environments). It is normally described in terms of mean path-loss and a log-normally distributed variation about the mean. Figure 1.7 shows the classifications of fading channel. A small-scale fading refers to the dramatic change in signal amplitude and phase that can be experienced as a result of small changes in the spatial positioning between a receiver and a transmitter. In order to better understand this phenomenon, this section introduces the parameters which characterize it. In particular, those are related to the time spreading of the signal and the time variation of the channels. The delay spread τ_m is the difference between the arrival of the first and the last signal. The coherence bandwidth $B_c \approx 1/\tau_m$ is the range of frequencies over which the channel is considered as the flat. Here, the Doppler spread is the spectral broadening caused by the relative motion of the receiver and transmitter which equals to the maximum Doppler frequency (f_d). The coherence time ($T_c \approx 1/f_d$) is the time over which the channel is considered constant. The variations of those parameters determine the channel classification. In the frequency domain, when $B_c > B$, where B is the signal bandwidth, the channel undergoes flat or frequency non-selective fading. Its equivalent in the time-delay domain is observed when the delay spread is much smaller than the signal symbol period τ_s as $\tau_m < \tau_s$. The frequency selective channel is produced when the inverse scenario occurs, either $B > B_c$ in the frequency domain representation or $\tau_m > \tau_s$ in the time-delay representation. The fading can also be slow or fast. A fast fading scenario occurs when the coherence time of the channel is less than the symbol duration $T_c < \tau_s$ as seen in the time domain or equivalently when the Doppler spread is greater than the signal bandwidth $f_d > B$ in the frequency domain. The slow fading is produced when $T_c > \tau_s$ or $f_d < B$ as shown in Figure 1.7.

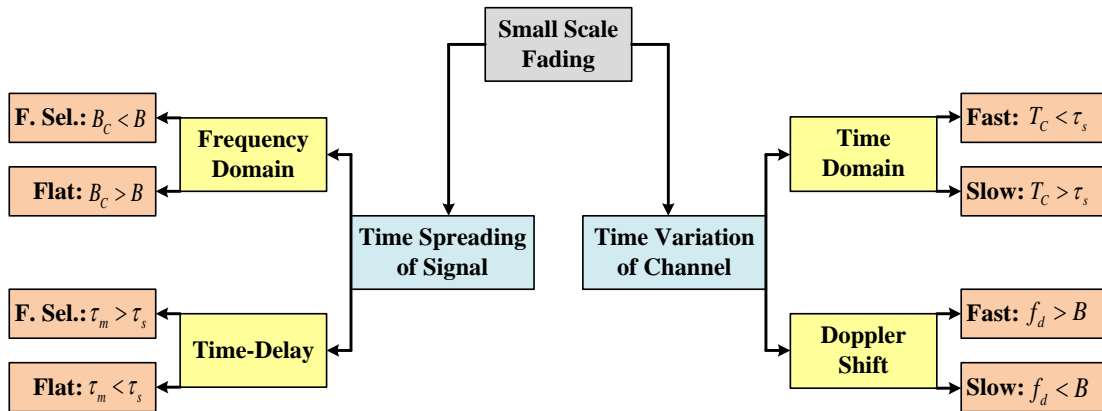


Figure 1.7: Fading channel classifications.

1.2.1 Time-Invariant Channel Model

The small scale fading is characterized by the radio propagation resulting from the presence of reflectors and scattering because of the multiple versions of the transmitted signal is arrived at the receiver including the distorted in amplitude, phase and arrival angle. All common communication channels can be characterized by the transfer function of $f(\cdot, \cdot, \cdot)$ and the maximum memory duration τ_{\max} in which the received signal $y(t)$ at the time t for the certain of transmitted signal $x(t)$ is given by,

$$y(t) = \int_{\tau_{\max}}^0 f(x(t-\tau), t, \tau) d\tau \quad (1.1)$$

The channel transfer function $f(\cdot, \cdot, \cdot)$ is actually depend on the unlimited number of parameters such as the temperature, conductivity of material and also the cosmic radiation of the propagation medium. Since it is impossible to concern all the propagation of channel's parameters, therefore, the simplified mathematical is described in this thesis. By assuming that the power amplifier has a linear characteristic and the transmitter or receiver is considered as moving slow or fast during the transmission, the transfer function for the wireless channel model can be categorized by

1) Time-invariant channel model.

$$f(x(t-\tau), t, \tau) \equiv x(t-\tau) \cdot h(\tau) \Rightarrow y(t) = \int_{\tau_{\max}}^0 x(t-\tau) \cdot h(\tau) d\tau \quad (1.2)$$

2) Time-variant channel model.

$$f(x(t-\tau), t, \tau) \equiv x(t-\tau) \cdot h(t, \tau) \Rightarrow y(t) = \int_{\tau_{\max}}^0 x(t-\tau) \cdot h(t, \tau) d\tau \quad (1.3)$$

Figure 1.8 shows the block diagram of communication channel model by assuming that the summation in (1.3) including with L terms, where L is the number of delay path and $w(t)$ is the additive noise.

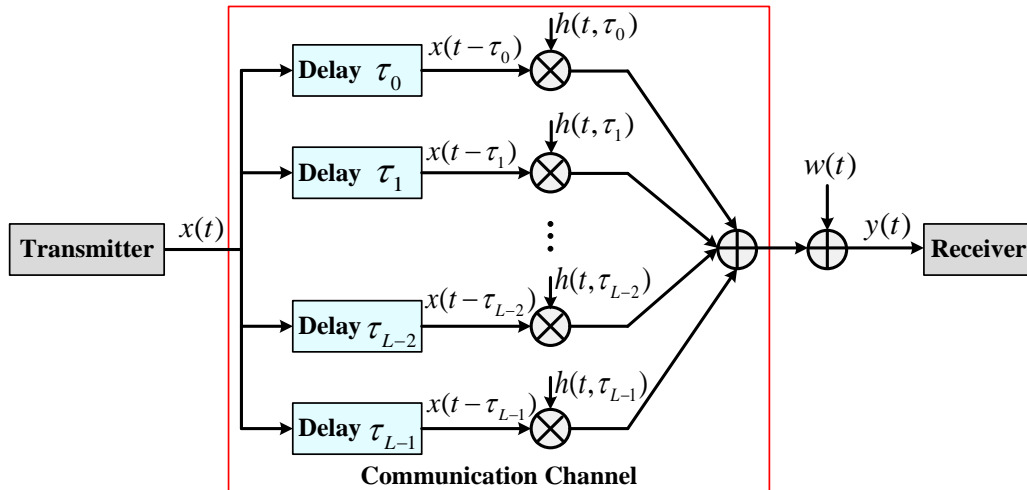


Figure 1.8: Block diagram of communication channel model.

1.2 Models of Wireless Communication Channel

In general, the wireless channel communication is considered as time-variant, however under the certain condition, it is possible to assume the channel is time-invariant during the limitation of the time period. The duration of the invariance time is depending on the frequency of the signal and transmitter or receiver movement. The estimation of an upper limit of the invariance time duration can be calculated based on the first Fresnel zone radius crossing time interval Δt_{Fren} [54] which is given by,

$$\Delta t \ll \Delta t_{Fren} = \frac{c}{2 \cdot f_0 \cdot v} \quad (1.4)$$

where c is the speed of light ($\approx 3 \times 10^8 m/s$), f_0 is the central carrier frequency of the signal and v is the relative velocity between transmitter and receiver. Most of wireless communication systems, the signal propagation channel are modeled as time-variant because the transmitter and receiver are mobile. However in some cases, when the transmitter or receiver is moving at pedestrian speeds such as in wireless LANs, then it is possible to assuming the channel is nearly time-invariant.

Here, assuming that the channel is time-invariant, the value of channel impulse response $h(\tau)$ is treated as a random variable and it constants during the single realization but changed randomly between the realizations. Similar to any random variable, the impulse response can be characterized by its probability density function as the following,

$$\begin{aligned} p(u, \tau) &= \lim_{\Delta u \rightarrow 0} \frac{P(u \leq h(\tau) \leq u + \Delta u)}{\Delta u} \\ p(u_1, u_2, \tau_1, \tau_2) &= \lim_{\Delta u_1, \Delta u_2 \rightarrow 0} \frac{P(u_1 \leq h(\tau_1) \leq u_1 + \Delta u_1, u_2 \leq h(\tau_2) \leq u_2 + \Delta u_2)}{\Delta u_1 \cdot \Delta u_2} \\ p(u_1, \dots, u_n, \tau_1, \dots, \tau_n) &= \lim_{\Delta u_1, \dots, \Delta u_n \rightarrow 0} \frac{P(u_1 \leq h(\tau_1) \leq u_1 + \Delta u_1, \dots, u_n \leq h(\tau_n) \leq u_n + \Delta u_n)}{\Delta u_1 \cdot \dots \cdot \Delta u_n} \end{aligned} \quad (1.5)$$

And its mean, variance and auto-correlation function can be given by,

$$\begin{aligned} \text{mean}(\tau) &= \{h(\tau)\} = \int_{-\infty}^{+\infty} u \cdot p(u, \tau) du \\ \text{power}(\tau) &= \{|h(\tau)|^2\} = \int_{-\infty}^{+\infty} |u|^2 \cdot p(u, \tau) du \\ \text{var}(\tau) &= \{|h(\tau) - \{h(\tau)\}|\} = \int_{-\infty}^{+\infty} |u - \{h(\tau)\}|^2 \cdot p(u, \tau) du \\ \text{cor}(\tau_1, \tau_2) &= \{h(\tau_1) \cdot h^*(\tau_2)\} = \int_{-\infty}^{+\infty} \int_{-\infty}^{+\infty} u_1 \cdot u_2^* \cdot p(u_1, u_2^*, \tau_1, \tau_2) du_1 du_2^* \end{aligned} \quad (1.6)$$

where $P(u \leq x \leq v)$ and $P(u_1 \leq x_1 \leq v_1, u_2 \leq x_2 \leq v_2)$ are the separate and joint probabilities of x_1 and x_2 , X^* is the complex conjugate of $|X|^2 = X^* \cdot X$.

Consider the situation that when there is a line-of-sight (LOS) component in the received signal, the wireless communication channel is usually modeled as a Rician fading channel [55-56] which is common modeled in the microcellular systems. The probability distribution for the envelope of the received signal is can be given by,

1.2 Models of Wireless Communication Channel

$$p(u) = \frac{2u \cdot (K+1)}{P_r} \cdot e^{-\left[K \frac{(K+1) \cdot u^2}{P_r}\right]} \cdot J_0\left(2u \cdot \sqrt{\frac{K \cdot (K+1)}{P_r}}\right), \quad u \geq 0 \quad (1.7)$$

where P_r is the average received power in fading channel, K is the Rician factor which represents the ratio of the dominant LOS path's power and $J_0(\cdot)$ is the Bessel's function of the zero-th order. It should be noted that when LOS path is not exist which correspond to $K=0$, then the probability distribution of the channel impulse response model in (1.7) transforms into the Rayleigh fading distribution as

$$p(u) = \frac{2u}{P_r} \cdot e^{-\frac{u^2}{P_r}}, \quad u \geq 0 \quad (1.8)$$

As discussed in the proceeding section when $K=\infty$, this probability distribution would transform it into a simple additive white Gaussian noise (AWGN) distribution with no fading. In some of the practical wireless communication applications, such as the mobile communication, the assumption of the time-invariant channel can be introduced. However, the irreducible channel estimation error result would bring the strong performance degradation. In such the situations, the communication channel must be modeled as a random process with some limited number of the initially unknown random parameters which can be theoretically calculated or empirically approximated for the certain signal propagation conditions.

1.2.2 Time-Variant Channel Model

Consider the situation that when the transmitter or receiver is moving during the transmission, and then the wireless communication channel is time-variant. This case makes the channel communication analysis is more complicated and required more advanced techniques for compensation of the performance degradation. The channel impulse response in time-variant channel is a stochastic process and can be characterized by its n -th order probability density function as the following,

$$p(u_1, \dots, u_n, \tau, t_1, \dots, t_n) = \frac{\partial^n P(u_1 \leq h(\tau, t_1) \leq u_1 + \Delta u_1, \dots, u_n \leq h(\tau, t_n) \leq u_n + \Delta u_n)}{\partial u_1 \cdot \dots \cdot \partial u_n} \quad (1.9)$$

In most of practical communication systems, the probability density function of order higher than 2-nd order are unknown and only the first and second order probability density functions with correspond to the first and second order statistics are considered as given by,

$$\begin{aligned} p(u, \tau, t) &= \frac{\partial P(u \leq h(\tau, t) \leq u + \Delta u)}{\partial u} \\ p(u_1, u_2, \tau, t_1, t_2) &= \frac{\partial^2 P(u_1 \leq h(\tau, t_1) \leq u_1 + \Delta u_1, u_2 \leq h(\tau, t_2) \leq u_2 + \Delta u_2)}{\partial u_1 \cdot \partial u_2} \end{aligned} \quad (1.10)$$

And its mean, variance and auto-correlation function can be given by,

1.2 Models of Wireless Communication Channel

$$\begin{aligned}
\text{mean}(\tau, t) &= \{h(\tau, t)\} = \int_{-\infty}^{+\infty} u \cdot p(u, \tau, t) du \\
\text{power}(\tau, t) &= \{|h(\tau, t)|^2\} = \int_{-\infty}^{+\infty} |u|^2 \cdot p(u, \tau, t) du \\
\text{var}(\tau, t) &= \{|h(\tau, t) - \{h(\tau, t)\}|^2\} = \int_{-\infty}^{+\infty} |u - \{h(\tau, t)\}|^2 \cdot p(u, \tau, t) du \\
\text{cor}(\tau, t_2, t_2) &= \{h(\tau, t_1) \cdot h^*(\tau, t_2)\} = \int_{-\infty}^{+\infty} \int_{-\infty}^{+\infty} u_1 \cdot u_2 \cdot p(u_1, u_2, \tau, t_1, t_2) du_1 du_2
\end{aligned} \tag{1.11}$$

Figure 1.9 shows the schematic diagram of wireless communications in time-variant channel model. In the figure, each propagation path has some arrival angle and delay components in which some delay would consist from multiple sub-paths of different arrival angles. Due to the receiver is moving in the certain direction of motion, the electromagnetic wave that propagate with arrival angle φ would occurs the frequency shift which can be given by,

$$\Delta f = f_d \cos(\varphi) \quad \text{and} \quad f_d = f_0 \frac{v}{c} \tag{1.12}$$

where φ is the arrival angle of signal propagation path, f_d is the maximum Doppler frequency shift value and v is the relative velocity between transmitter and receiver. The Doppler frequency shift causes the wireless communication channel become time-variant which would change in accordance to the scattering angular distribution and spatial correlation. The impulse response with the certain delay path can be expressed by,

$$h(\tau, t) = \int_0^{2\pi} \xi(\tau, \varphi) \cdot e^{j2\pi f_d \cdot \cos(\varphi) t} d\varphi \tag{1.13}$$

where $\xi(\tau, \varphi)$ is the random amplitude of the propagation path with delay τ and arrival angle φ . The random amplitude of the propagation path can be characterized by probability distribution which is given by,

$$p(\varsigma, \tau, \varphi) = \frac{\partial P(\varsigma \leq \xi(\tau, \varphi) \leq \varsigma + \Delta\varsigma)}{\partial \varsigma} \tag{1.14}$$

In the probability distribution function of impulse response given in (1.14), the random scattering can be classified into two types as

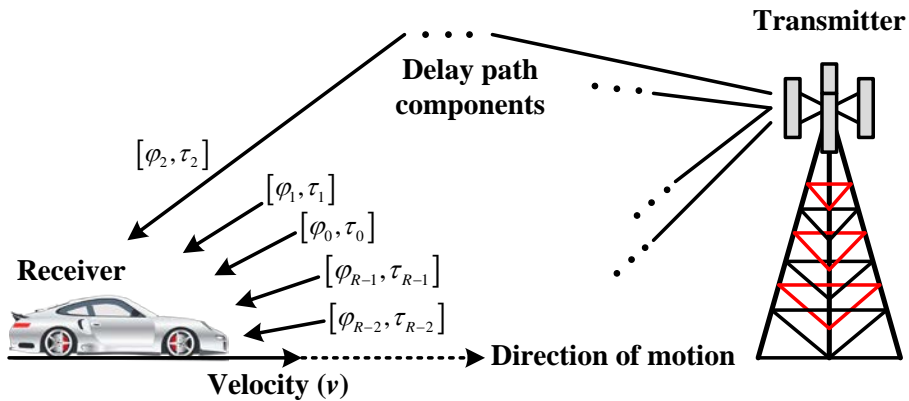


Figure 1.9: Wireless communications in time-variant channel model.

1.2 Models of Wireless Communication Channel

- 1) Wide sense stationary (WSS) which indicates that each delay path has isotropic scattering.
- 2) Wide sense stationary uncorrelated scatters (WSSUS) which indicates that each delay path has non-isotropic scattering.

In WSS model, a stochastic process whose joint probability distribution does not change when shifted in time. Consequently, the parameters such as mean and variance also do not change over time which is known as a Jake's model [57]. This model applicable only for the urban channel communications with the scattering is nearly symmetric distribution. The Jake's model probability distribution function can be given by,

$$p(\varsigma, \tau, \varphi) = \frac{1}{2\pi} \cdot p(\varsigma, \tau) \quad (1.15)$$

Similarly, the Jake's model description is given by means of the Doppler frequency distribution which expresses that the probability distribution of the signal would obtain by the frequency shift.

$$p(\varsigma, \tau, \varphi) = \begin{cases} \frac{p(\varsigma, \tau)}{2\pi} \cdot \frac{1}{\sqrt{f_d^2 - f^2}}, & |f| \leq f_d \\ 0, & \text{otherwise} \end{cases} \quad (1.16)$$

As for the WSSUS model, the probability distribution function of the arrival angle is non-isotropic scattering. In actual wireless communication systems are non-isotropic and only some cases of scatters with symmetric spatial distribution, the communication channel can be assumed to be isotropic scattering. Commonly in rural and urban areas, the communication channel is limited with the number of strong scatters which is assumed by non-isotropic scattering. The propagation paths in these cases are clustered and the path angular distribution function is concentrated in some spatial angles. This means that the paths inside each cluster can be strongly correlated which can be created the non-stationary of the time-variant channel impulse response as given by,

$$h(\tau, t) = \sum_{q=0}^{Q-1} \oint_{\Omega_q} \xi(\tau, \Omega) \cdot e^{j2\pi f_d \cdot \cos(\varphi(\tau, \Omega))t} d\Omega \quad (1.17)$$

where Q is the number of all scattering clusters at the q -th index of each cluster, Ω_q is the spatial angle at the q -th index of each cluster, $\varphi(\tau, \Omega)$ is the arrival angle of the certain spatial angle. The channel impulse response in time-variant given in (1.17) can be represented by the summation of the limited number of delay path groups with some central Doppler frequency shifts. The random amplitudes of channel impulse response are relative slowly changing during the time which is expressed by,

$$h(\tau, t) = \sum_{q=0}^{Q-1} \eta_q(\tau, t) \cdot e^{j2\pi f_{d,q}(\tau)t} \quad (1.18)$$

where $f_{d,q}(\tau)$ is the central Doppler frequency shift at the q -th group of delay paths and $\eta_q(\tau)$ is the random relative slowly changing amplitude of the q -th group of delay paths. The central Doppler frequency shift at the q -th group of delay paths can be estimated as

$$f_{d,q}(\tau) = \frac{f_d (\cos(\varphi_{\min}(\tau, \Omega_q)) + \cos(\varphi_{\max}(\tau, \Omega_q)))}{2} \quad (1.19)$$

1.2 Models of Wireless Communication Channel

where $\varphi_{\min}(\tau, \Omega_q)$ and $\varphi_{\max}(\tau, \Omega_q)$ are the minimum and maximum arrival angles of the spatial angle Ω_q at the q -th group, respectively. The random amplitudes $\eta_q(\tau, t)$ are the stochastic processes with the limited frequency spectrum which depending on the size of the spatial angle and it can be expressed by,

$$F(\eta_q(\tau, t)) = \frac{f_d (\cos(\varphi_{\min}(\tau, \Omega_q)) - \cos(\varphi_{\max}(\tau, \Omega_q)))}{2} \quad (1.20)$$

This random stochastic processes with non-isotropic introduces the behavior of the communication channel and makes its estimation with much more complex as comparing with the isotopic scattering channel. However, it is still possible to provide the discrete version of (1.18) by the sampling of the signal delay path as given by,

$$h_l(t) = \sum_{q=0}^{Q-1} \eta_{l,q}(t) \cdot e^{j2\pi f_{d,l,q} t} \quad (1.21)$$

In the contrast of the isotopic scattering channel, the quantization of angular would introduce quite large an error due to the distribution of arrival angle path is burst [58].

From (1.21), the discrete version of channel impulse response (CIR) at every sampling time for transmitted signal can be expressed by,

$$h_l(m, n) = \sum_{q=0}^{Q-1} \eta_{l,q} \cdot e^{j2\pi f_{d,l,q} \cos(\varphi_{l,q})(mT_s + n\Delta t)} \quad (1.22)$$

where T_s is the sampling time period of OFDM symbol, m is the m -th of OFDM symbol and n is the n -th of OFDM sampling time.

In general, the term fading describes the variations with time of received signal strength. The fading distortions due to the combination effects of multipath propagation and the relative motion between transmitter and receiver are generate time-variant attenuations and delays. These fading distortions may significantly degrade the performance of the wireless communication systems.

1.3 Overview of OFDM System Model

Orthogonal frequency division multiplexing (OFDM) is reputed for its ability to mitigate multipath fading and enhance the spectral efficiency from its orthogonal subcarriers. This paved the way towards its presence in several standards today, ranging from wired technologies such as the asynchronous digital subscriber line (ADSL) [59] to wireless technologies such as the long term evolution (LTE) in its downlink. The basic idea behind OFDM is to transform a frequency-selective channel into N parallel sub-channels that undergo at fading. In fact, one can directly anticipate that the favorable scenario for transmission is to have slow at fading channel conditions [13-15]. This is guaranteed when $f_d < B < B_C$. However, this is only possible when $f_d \cdot \tau_m \ll 1$. Then, the symbol duration is chosen such that $\tau_m < \tau_s < T_c$. Thus, in order to achieve high data rates, one would send a large number of narrowband signals over relatively close frequencies. This is the exact rational behind multi-carrier transmission, which consequently facilitates channel equalization at the receiver.

1.3.1 OFDM Transmission Systems

Figure 1.10 shows the block diagram of wireless OFDM transceiver. The conventional OFDM system is implemented with the fast Fourier transform (FFT) as the digital signal processing (DSP) circuits. At the transmitter, the input data information is obtained after the processing of the binary data which are modulated the quadrature-phase shift keying (QPSK) or quadrature-amplitude modulation (QAM) method and then passed through a serial to parallel (S/P) converter. The modulated frequency domain signal $X(m, k)$ at k -th subcarrier of m -th symbol is converted to the time domain signal by inverse FFT which is given by,

$$x(m, n) = \frac{1}{\sqrt{N}} \sum_{k=0}^{N-1} X(m, k) \cdot e^{j \frac{2\pi n k}{N}}, \quad 0 \leq n \leq N-1 \quad (1.23)$$

where $x(m, n)$ is the transmitted time domain OFDM signal at the n -th sample time of m -th symbol. The cyclic prefix (CP) with the length of N_g sample is added at the start of OFDM data symbol which can be given by,

$$x^T(m, n_t) = \begin{cases} x(m, N - N_g - n_t), & 0 \leq n_t \leq N_g - 1 \\ x(m, n_t - N_g), & N_g \leq n_t \leq N_t - 1 \end{cases} \quad (1.24)$$

where $x^T(m, n_t)$ is the transmitted time domain signal including CP at the n_t -th sample time of m -th symbol and N_t is the length of $x^T(m, n_t)$ signal. Typically, the length of CP is chosen to be larger than τ_m to avoid the inter-symbol interference (ISI). Here, the total number of sample time is $N_t = N + N_g$ and the total duration of each OFDM symbol is $T_t = N_t \cdot T_s$, where T_s is the sampling time. Then, the time domain including CP is again converted to from parallel to serial (P/S). The signal is then passed through a digital to analog (D/A) converter which contains low-pass filters with bandwidth $1/T_s$. Then the signal is transmitted through the multipath fading channel where an additive white Gaussian noise (AWGN) $w(n)$ with a covariance of σ^2 is added into the received signal. The propagation channel is assumed to be a multipath fading channel model with consist of arrival delay path L sampling time. The channel impulse response $h(\tau)$ can be given by,

1.3 Overview of OFDM System Model

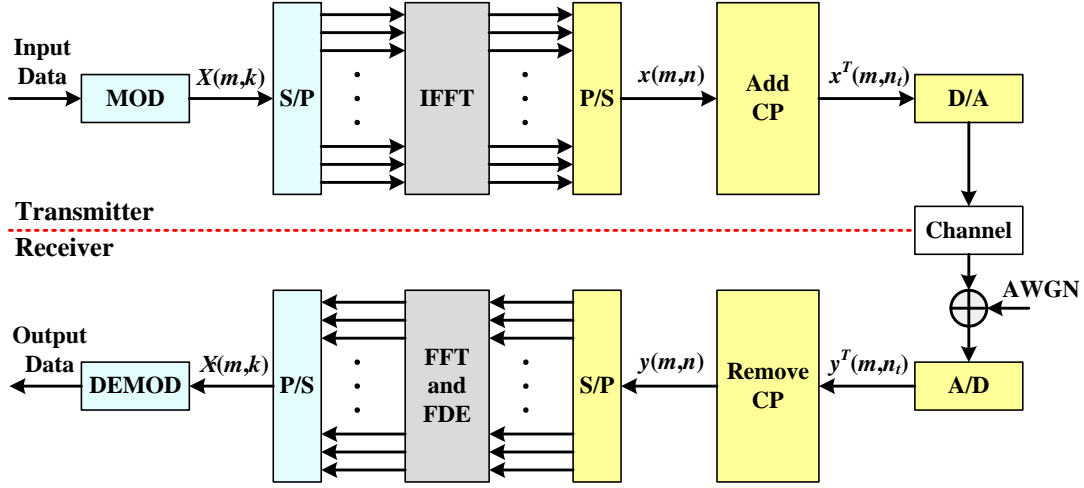


Figure 1.10: Block diagram of conventional OFDM systems.

$$h(\tau) = \sum_{l=0}^{L-1} h_l(\tau) \cdot \delta(\tau - \tau_l) \quad (1.25)$$

where $\delta(\cdot)$ is the Dirac delta function, h_l is the complex amplitude at the l -th delay path, and τ_l is the time delay at l -th delay path. Assuming that the l -th delay path has the time delay of the l samples (i.e. $\tau_l = l$). At the receiver, the inverse operations of the transmitter are performed. After the (A/D) converter and removing of CP, the received time domain signal can be expressed by,

$$y(m,n) = \sum_{l=0}^{L-1} h_l(m,n) \cdot x(m,n-l) + w(m,n), \quad 0 \leq n \leq N-1 \quad (1.26)$$

where $y(m,n)$ is the received time domain signal after remove CP at the n -th sample time of m -th symbol.

1.3.2 Conventional FDE Method for OFDM Signal

Consider the received time domain signal given in (1.26), this received signal can be formed to the matrix operation which is expressed by,

$$\mathbf{y} = \mathbf{h}\mathbf{x} + \mathbf{w} \quad (1.27)$$

where

$$\mathbf{h} = \begin{bmatrix} h_0 & & & h_{L-1} & \cdots & h_1 \\ h_1 & h_0 & & 0 & & \vdots \\ \vdots & h_1 & \ddots & & & h_{L-1} \\ h_{L-1} & & \ddots & \ddots & & \\ & h_{L-1} & & \ddots & \ddots & \\ & & \ddots & \ddots & \ddots & \\ 0 & & & h_{L-1} & \cdots & h_1 & h_0 \end{bmatrix}_{N \times N} \quad (1.28)$$

where \mathbf{y} is the received time domain vector with size of $N \times 1$, \mathbf{x} is the transmitted time domain vector with size of $N \times 1$, \mathbf{w} is the noise vector with size of $N \times 1$, and \mathbf{h} is the channel impulse

1.3 Overview of OFDM System Model

response matrix with size of $N \times N$, respectively. In (1.27), the m -th index is omitted for brevity because the frequency domain equalization is operated for every symbol. The received frequency domain signal can be obtained from converting the received time domain signal by N -point FFT with can be expressed by,

$$\begin{aligned} \mathbf{Y} &= \mathbf{F}\mathbf{y} \\ &= \mathbf{F}\mathbf{h}\mathbf{F}^H\mathbf{F}\mathbf{x} + \mathbf{F}\mathbf{w} \\ &= \mathbf{H}\mathbf{X} + \mathbf{W} \end{aligned} \quad (1.29)$$

where $(\cdot)^H$ is the Hermitian transposition, \mathbf{F} and \mathbf{F}^H are the FFT and its inverse FFT matrix with size of $N \times N$, respectively. \mathbf{Y} is the received frequency domain signal with size of $N \times 1$, \mathbf{X} is the transmitted frequency domain signal with size of $N \times 1$, \mathbf{W} is the noise components infrequency domain with size of $N \times 1$, and $\mathbf{H} = \mathbf{F}\mathbf{h}\mathbf{F}^H$ is the channel frequency response matrix with size of $N \times N$. In conventional OFDM systems, the channel impulse response is assumed to be constant during one OFDM symbol. With this assumption, the channel matrix \mathbf{h} given in (1.28) has the circulant property which leads the construction of matrix \mathbf{H} is diagonal matrix. The k -th diagonal element of channel matrix \mathbf{H} can be given by,

$$H(k) = \sum_{l=0}^{L-1} h_l \cdot e^{-j\frac{2\pi l k}{N}}, \quad 0 \leq k \leq N-1 \quad (1.30)$$

The equation given in (1.30) is based on the fact that in time-invariant channels, the complex amplitudes of channel impulse response $h_l(\tau)$ are constant from one realization of the channel to the other. This allows the construction of channel frequency response \mathbf{H} with size of $N \times 1$. Then, the frequency domain equalization (FDE) can be performed to detect the transmitted frequency domain signal which can be expressed by,

$$\hat{X}(m, k) = \frac{Y(m, k)}{H(m, k)}, \quad 0 \leq k \leq N-1 \quad (1.31)$$

where $\hat{X}(m, k)$ is the estimated frequency domain signal at k -th subcarrier of m -th symbol. Then, the output data information can be obtained by the demodulator as shown in Figure 1.10. Consequently, this FDE method is so called simple one-tap equalization with a coefficient equal to the inverse of the channel frequency response at that subcarrier can effectively mitigate the channel fading effect. From this fact, the subcarrier spacing in OFDM systems must be carefully designed so that each subcarrier suffers only flat fading. Usually, the extent of channel coherence determines the maximum subcarrier spacing. On the other hand, due to parallel transmission on numerous subcarriers, the OFDM symbol period is made longer than that of the single-carrier symbols. Unfortunately, time-selective fading compromises the long OFDM symbols. In the case in which the channel response varies significantly within an OFDM symbol, the inter-carrier interference (ICI) will arise and degrade the system performance. The OFDM symbol period is thus the upper bounded by the length of the interval that the channel stays stationary. As the symbol period is the inverse of the subcarrier spacing, the minimum subcarrier spacing is thus determined by how fast the channel is changing.

1.4 Overview of DFTS-OFDM System Model

Discrete Fourier transform spreading-orthogonal frequency division multiplexing (DFTS-OFDM) is a promising air interface for high data rate transmission in frequency-selective fading channels. Essentially, the DFTS-OFDM system has a similar transceiver structure to the OFDM systems except that the data information is pre-coded in frequency domain via the discrete Fourier transform (DFT) operation. Thus, it shares the two main advantages of both single-carrier and multi-carrier transmission schemes. The first advantage is its low peak-to-average ratio (PAPR) and it is suitable for uplink multiple access because the issue of battery life represents a key concern at the user terminal in the next generation wireless communication systems. Second, it preserves the orthogonal property among users by converting the received signal into frequency domain and allows for a simple one-tap equalization to compensate the channel distortion in multipath channels. Currently, the DFTS-OFDM has been selected as the multiple access schemes for uplink transmission in the long term evolution (LTE) specifications by the 3GPP community [19-20].

Consider the time domain OFDM signal $x(m,n)$ given in (1.23) is defined as the ratio of the maximum peak power divided by the average power of its signal which is expressed by,

$$PAPR \triangleq \frac{\max \left[|x(m,n)|^2 \right]}{\text{mean} \left[|x(m,n)|^2 \right]}, \quad 0 \leq n \leq N-1 \quad (1.32)$$

In the statistical points of view, the PAPR performance is evaluated by using the complementary cumulative distribution function (CCDF) which using to represent the probability of exceeding threshold $PAPR_0$ [60-62].

$$CCDF(PAPR_0) = \Pr[PAPR(x(m,n)) > PAPR_0] \quad (1.33)$$

Figure 1.11 shows the comparison of PAPR performance between OFDM and DFTS-OFDM signals with QPSK modulation when changing the number of data subcarriers.

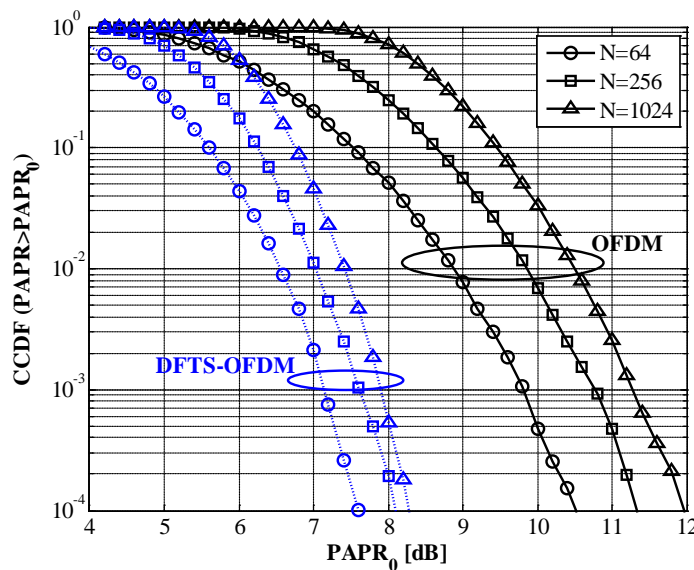


Figure 1.11: Comparison of PAPR performance between OFDM and DFTS-OFDM signals.

1.4.1 DFTS-OFDM Transmission Systems

Figure 1.12 shows the block diagram of wireless DFTS-OFDM transceiver. At the transmitter, the input information data is modulated by QPSK or QAM method. The modulated signal in time domain $x_D(m,n)$ at the n -th sampling time of m -th symbol is converted to the frequency domain signal $X_D(m,k)$ by the K -point discrete Fourier transform (DFT) operation which is given by the following equation.

$$X_D(m,k) = \frac{1}{\sqrt{K}} \sum_{n=0}^{K-1} x_D(m,n) \cdot e^{-j\frac{2\pi nk}{K}}, \quad 0 \leq n \leq K-1 \quad (1.34)$$

The K subcarriers of $X_D(m,k)$ given in (1.34) are mapped into the certain frequency band within the frequency bandwidth with N subcarriers continuously from the subcarrier number N_{Z1} to N_{Z2} ($N_{Z2}-N_{Z1}+1=K$) and the null subcarriers (zero padding) are added at the both ends of K data subcarriers. After the subcarrier mapping, the frequency domain signal $X(m,k_1)$ over N subcarriers can be given by,

$$X(m,k_1) = \begin{cases} 0 \text{ (zero padding)}, & 0 \leq k_1 \leq N_{Z1}-1 \\ X_D(m,k_1 - N_{Z1}), & N_{Z1} \leq k_1 \leq N_{Z2} \\ 0 \text{ (zero padding)}, & N_{Z2}+1 \leq k_1 \leq N-1 \end{cases} \quad (1.35)$$

where $(N-K)$ is the number of zero padding (N_Z) added at the both ends of K data subcarriers in the frequency domain. The frequency domain signal $X(m,k_1)$ including the zero padding given in (1.35) is converted to the time domain signal as similar to the conventional OFDM signal by the N -point IFFT which can be given by,

$$x(m,n_1) = \frac{1}{\sqrt{N}} \sum_{k_1=N_{Z1}}^{N_{Z2}} X(m,k_1) \cdot e^{j\frac{2\pi n_1 k_1}{N}}, \quad 0 \leq n_1 \leq N-1 \quad (1.36)$$

where $x(m,n_1)$ is the transmitted DFTS-OFDM signal in the time domain. Then adding the CP with the length of N_g sample at the start of DFTS-OFDM symbol as the same condition as OFDM signal. The DFTS-OFDM signal is passed through D/A converter and then is transmitted through the multipath fading channel.

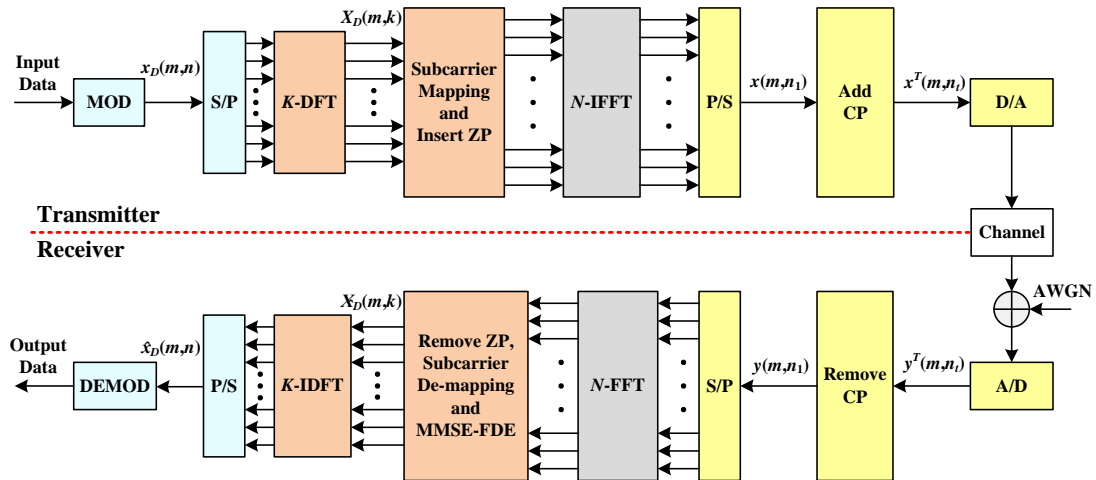


Figure 1.12: Block diagram of conventional DFTS-OFDM systems.

1.4.2 Conventional MMSE-FDE Method for DFTS-OFDM Signal

At the receiver, the received signal is passed through the A/D converter and then removing of CP. The received time domain signal can be expressed by,

$$y(m, n_1) = \sum_{l=0}^{L-1} h_l(m, n_1) \cdot x(m, n_1 - l) + w(m, n_1), \quad 0 \leq n_1 \leq N-1 \quad (1.37)$$

where $y(m, n_1)$ is the received time domain signal after remove CP at the n_1 -th sample time of m -th symbol. The received time domain signal $y(m, n_1)$ is converted to the frequency domain signal $Y(m, k_1)$ by N -point FFT which can be given by,

$$\begin{aligned} Y(m, k_1) &= \frac{1}{\sqrt{N}} \sum_{n_1=0}^{N-1} y(m, n_1) \cdot e^{-j \frac{2\pi n_1 k_1}{N}}, \quad 0 \leq k_1 \leq N-1 \\ &= H(m, k_1) X(m, k_1) + W(m, k_1) \end{aligned} \quad (1.38)$$

where $X(m, k_1)$ is the frequency domain signal over N subcarriers, $W(m, k_1)$ is the noise components in frequency domain, and $H(m, k_1)$ is the channel frequency response. Then the received frequency domain signal $Y_D(m, k)$ over K subcarriers can be obtained by de-mapping operation. In conventional DFTS-OFDM, the minimum mean square error-frequency domain equalization (MMSE-FDE) method is employed because it can obtain the frequency diversity gain. The MMSE-FDE method [63-65] can be given by,

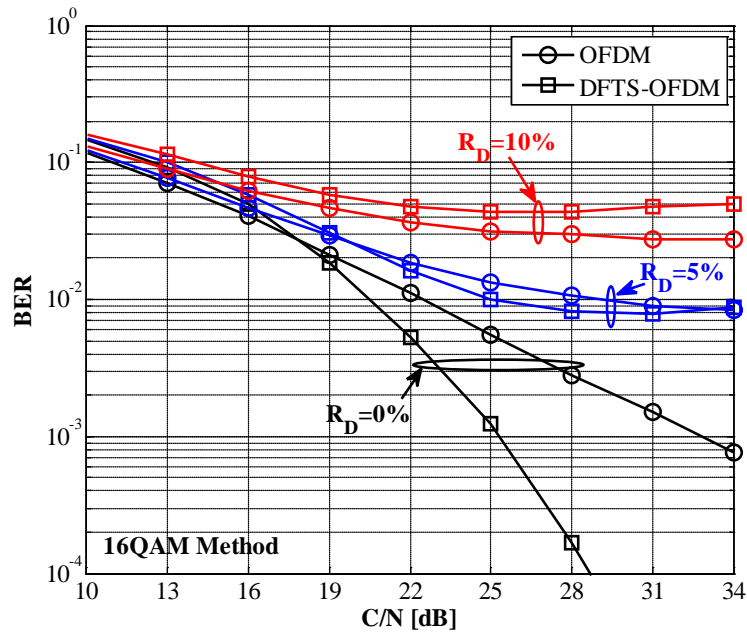
$$\hat{X}_D(m, k) = \left(\frac{H_D^*(m, k)}{|H_D(m, k)|^2 + \sigma_k^2} \right) Y_D(m, k), \quad 0 \leq k \leq K-1 \quad (1.39)$$

where $(\cdot)^*$ is the complex conjugate operation, $\hat{X}_D(m, k)$ is the estimated frequency domain signal over K subcarriers, and σ is the covariance of AWGN noise. Then the estimated frequency domain signal $\hat{X}_D(m, k)$ is converted to the time domain signal $\hat{x}_D(m, n)$ by K -point IDFT. Consequently, the data information can be obtained by demodulation of $\hat{x}_D(m, n)$ as shown in Figure 1.12. Similar to OFDM signal, the DFTS-OFDM signal can compensate the channel distortion of multipath fading channels precisely and allows employing simple one-tap equalization. This one-tap equalization can work very well when assuming that the wireless channel is time-invariant fading channel. However in time-variant fading channel, the bit error rate (BER) performance of both OFDM and DFTS-OFDM signals would be degraded relatively due to the concurrent of inter-carrier interference (ICI).

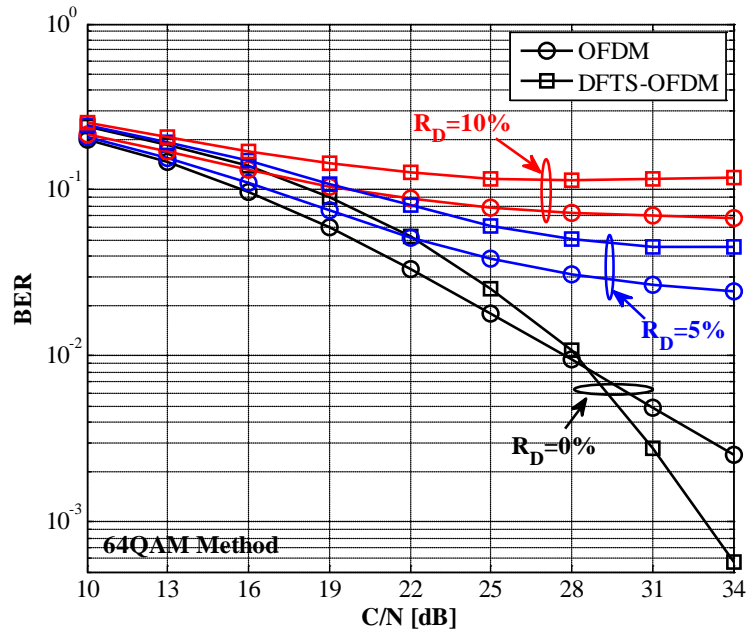
Figure 1.13 shows the comparison of BER performance between OFDM and DFTS-OFDM signal when changing C/N operation at various normalized Doppler frequency (R_D). In the computer simulation, the modulation methods are 16 and 64QAM. The OFDM bandwidth is 5MHz, radio frequency is 5GHz, number of data subcarriers is $K=96$, the number of N -point FFT is 128 and length of CP is taken by $N_g=16$. The time-varying fading channel is modeled by the exponential power delay profile having the power decay constant -1dB with the length of delay path $L=14$. The normalized Doppler frequency $R_D=f_{\text{dmax}}/\Delta f$ is employed as the measure of mobile environments in which f_{dmax} is the maximum Doppler frequency and Δf is the subcarrier spacing. From the figure, it can be observed that the both for OFDM and DFTS-OFDM can achieve better BER performances when the mobile channel

1.4 Overview of DFTS-OFDM System Model

is assumed to be time-invariant ($R_D=0$). However in higher time-varying fading channels, the BER performance for both OFDM and DFTS-OFDM are degraded relatively as the increasing ICI level caused from Doppler frequency spread.



(a) BER performance for 16QAM method.



(b) BER performance for 64QAM method.

Figure 1.13: Comparison of BER performance when changing operation C/N and normalized Doppler frequency (R_D).

1.5 Research Background

Recently, the demands for wireless multimedia communication services are drastically increasing from the fact that it can be used at anytime, anywhere and for any multimedia services by end users. To realize wireless multimedia communication services, it is strongly required to achieve higher transmission data rate with keeping higher signal quality under the limited frequency bandwidth and lower carrier to noise power ratio (C/N). However, the signal quality would be degraded relatively in wireless communications due to the occurrence of multipath fading distortion which is usually experienced in the received signal. To overcome this problem, orthogonal frequency division multiplexing (OFDM) has been proposed as one of efficient transmission techniques for wireless communications systems because of its efficient usage of frequency bandwidth and robustness to multipath fading distortion. The salient features of OFDM technique are to divide wide-band data information into a group of narrowband subcarriers and adding a cyclic prefix (CP) at the start of every data symbol which enables an employment of simple one-tap frequency domain equalization with keeping the orthogonality among narrowband OFDM subcarriers even in multipath fading channels. From these advantages, OFDM has been already adopted as the standard transmission technique in advanced wireless communications systems such as the 4th generation mobile phone (LTE: Long Term Evolution), digital video broadcasting (DVB), wireless local area networks (WLANs) and worldwide interoperability for microwave access networks (WiMAX).

When assuming lower time-varying fading channels, the channel impulse responses (CIRs) can be considered as a constant during one OFDM symbol period. Accordingly, the channel frequency responses (CFRs) which are converted from the CIRs at any sampling points during one OFDM symbol period are also constant. From this fact, the received OFDM signal can be equalized precisely at the receiver by using simple one-tap frequency domain equalization. However in higher time-varying fading channels, the CIRs are changing during one symbol period and the corresponding CFRs are also changing during one OFDM symbol. From this fact, the signal quality would be degraded relatively in higher time-varying fading channels accompanying with the Doppler frequency shift in which the original property of orthogonality among OFDM subcarriers is no more satisfied due to the occurrence of inter-carrier interference (ICI). To solve the ICI problem in higher time-varying fading channels, various channel estimation and data equalization methods for CP-OFDM signal were proposed up to today.

In conventional CP-OFDM systems, the CIR is usually estimated by using scattered pilot subcarriers which are inserted into data subcarriers periodically both in the frequency and time domains. However, the CIR estimation accuracy would be degraded due to the occurrence of ICI in the received pilot subcarriers. To solve this problem, time domain training sequence (TS) inserted TS-OFDM was proposed in which the TS signal is employed in the estimation of CIR as well as the role of CP. The employment of TS signal can achieve higher estimation accuracy than that for using pilot subcarriers in higher time-varying fading channels from the reason that the period of TS is much shorter than the symbol period which could be assumed that the CIR is constant during the period of TS signal. However, the TS signal would cause the undesirable leakage of power spectrum density (PSD) at the outside of

1.5 Research Background

allocated OFDM bandwidth due to the repetition of same data pattern of TS signal in the time domain which leads the serious adjacent channel interference problem to other systems.

From the above backgrounds, this thesis firstly proposes a channel estimation method by using a new design of TS signal. The features of proposed method are to employ the random data patterns of TS signal added to each data symbol over one frame and to employ a triangular window function as the waveform shaping both for reducing the leakage of PSD with keeping higher CIR estimation accuracy. In addition, this thesis conducts theoretical examinations for the effect of CIR estimation method of using the TS signal when the detected symbol timing at the receiver has an offset from the ideal symbol timing.

As for the ICI problem in higher time-varying fading channels, various frequency domain equalization (FDE) methods for CP-OFDM signal were proposed up to today including a minimum mean square error-frequency domain equalization (MMSE-FDE) and successive interference cancellation (SIC) equalization methods. These methods employed the direct inverse matrix calculation for the channel frequency response (CFR) matrix to mitigate the ICI. However, the computation complexity for the inverse matrix calculation required at every symbol is relatively higher and unsuitable in the implementation of practical receiver. To reduce the complexity, a low-complexity MMSE-FDE method for CP-OFDM signal was proposed in which the full elements of CFR matrix are approximated by a banded matrix so as to enable the employment of the fast algorithm in the calculation of inverse matrix. However, the bit error rate (BER) performance would be degraded in higher time-varying fading channels due to the lower CIR estimation accuracy by using the scattered pilot subcarriers and the approximation for full elements of CFR matrix by the banded matrix. To solve the above problems, a low-complexity overlap and add (OLA) with MMSE-FDE (OLA-MMSE-FDE) and fast suboptimum with MMSE-FDE (FAST-MMSE-FDE) methods for TS-OFDM signals were proposed. In these methods, the CIR is assumed by changing linearly during one symbol period so as to employ the low complexity Maclaurin's expansion approximation technique in the calculation of inverse matrix. Although these methods can achieve lower complexity, the BER performance would be degraded in higher time-varying fading channels due to the assumption of linear changing of CIR and the approximation of first order Maclaurin's expansion. In the development of next generation wireless communication systems, it is strongly required to realize an efficient equalization method which can achieve higher transmission data rate with keeping higher signal quality even in higher time-varying fading channels. The realization of efficient equalization methods in higher time-varying fading channels is still challenging research topic and many researchers in worldwide has been investigating to solve this problem.

From above backgrounds, this thesis firstly proposes a new MMSE-FDE method for TS-OFDM signal in conjunction with the proposed CIR estimation method in higher mobile Rayleigh fading channels. The salient features of proposed method are to enable the acquisition of frequency diversity gain by using an enhanced CIR matrix and enable the reduction of complexity by using a fast algorithm for inverse matrix calculation. Although the proposed MMSE-FDE method can achieve better BER performance than the conventional MMSE-FDE methods with keeping lower complexity, the improvement of BER performance is insufficient especially under higher mobile environments. To solve this problem, this thesis secondly proposes a time domain equalization (TDE) method of using the enhanced CIR matrix in the time domain instead of using the CFR matrix for the MMSE-FDE method. The feature of proposed TDE method is to employ the partial differentiation for the received

1.5 Research Background

signal in solving the maximum likelihood (ML) equation in which the CIR matrix becomes a symmetric banded matrix. This feature enables to employ the fast algorithm for inverse matrix calculation without any approximation which can achieve the same BER performance with much lower computation complexity as that for the direct inverse matrix calculation. These are completely different features from the conventional MMSE-FDE methods. The proposed TDE method can achieve much better BER performance with keeping lower complexity when employing in the wireless cellular phone systems under higher mobile Rayleigh fading environments.

To reduce further complexity, this thesis also proposes an iterative based TDE method for the TS inserted discrete Fourier transform spreading-OFDM (TS-DFTS-OFDM) signal in conjunction with the proposed CIR estimation method under higher mobile Rician environments. The salient features of proposed iterative based TDE method are to employ the enhanced CIR transfer matrix in the mitigation of ICI and to employ the preconditioned conjugate gradient squared (PCGS) algorithm as the iterative solution in the calculation of inverse matrix. The proposed iterative based TDE method can achieve better BER performance with keeping much lower computation complexity when employing in the intelligent transportation systems (ITS) under higher mobile Rician fading environments.

This thesis conducts numerous computer simulations to demonstrate the effectiveness of all proposed methods in higher time-varying fading channels. From the simulation results, it is confirmed that all methods including the CIR estimation method and equalization methods proposed in this thesis could be considered as the practical solutions in the development of OFDM based next generation wireless communication systems.

1.6 Thesis Structure

The reminder of this thesis is organized as follows.

Chapter 2 presents a time domain TS based channel estimation method under higher mobile environments. Section 2.1 introduces the description of research background. Section 2.2 presents a conventional scattered pilot based channel estimation method. Section 2.3 presents a proposed TS based channel estimation method under higher time-varying channels. Section 2.4 presents various computer simulation results to verify the effectiveness of proposed method as comparing with the conventional method. Finally, Section 2.5 draws some conclusions.

Chapter 3 presents the theoretical examinations for the effect of channel estimation method of using the TS method under symbol timing offset. Section 3.1 introduces the effect of symbol timing offset for pilot subcarrier method. Section 3.2 introduces the frame format for TS-OFDM signal under symbol timing offset. Section 3.3 presents the channel frequency response (CFR) estimation method with the TS signal under symbol timing offset. Section 3.4 presents various computer simulation results to demonstrate the effectiveness of the channel estimation method by using the time domain TS signal as comparing with the conventional pilot method under the symbol timing offset, and Section 3.5 draws some conclusions.

Chapter 4 presents a low-complexity frequency domain equalization (FDE) method for TS-OFDM signal under higher mobile environments. Section 4.1 introduces the problem of conventional OFDM in higher time-varying fading channels. Section 4.2 presents the problem of conventional MMSE-FDE methods both for CP-OFDM and TS-OFDM signals. Section 4.3 proposes the transceiver structure for TS-OFDM signal including the construction of enhanced CIR matrix by using the estimated CIR at every sampling time and low-complexity MMSE-FDE method by using the fast algorithm for inverse matrix calculation. Section 4.4 presents various computer simulation results to verify the effectiveness of proposed MMSE-FDE method for TS-OFDM as comparing with the conventional MMSE-FDE methods both for CP-OFDM and TS-OFDM signals. Finally, Section 4.5 draws some conclusions.

Chapter 5 presents a time domain equalization (TDE) method for TS-OFDM signal under higher mobile environments. Section 5.1 introduces the problem of conventional frequency domain equalization methods. Section 5.2 proposes the TDE method with the fast algorithm for inverse matrix calculation for the TS-OFDM signal. Section 5.3 evaluates the overall computation complexity for the proposed TDE method as comparing with conventional FDE methods. Section 5.4 presents various simulation results to verify the effectiveness of proposed TDE method as comparing with various conventional FDE methods both for the CP-OFDM and TS-OFDM signals. Finally, Section 5.5 draws some conclusions.

Chapter 6 presents an Iterative based TDE for DFTS-OFDM signal under highly mobile environments. Section 6.1 introduces the problem of conventional FDE method for DFTS-OFDM signal under highly mobile environments. Section 6.2 presents the structure of proposed transceiver for proposed DFTS-OFDM signal. Section 6.3 proposes a low-complexity iterative based TDE with a time domain CIR estimation method for the DFTS-OFDM signal. Section 6.4 presents various computer simulation results to verify the effectiveness of proposed iterative based TDE method as comparing with the conventional methods, and Section 6.5 draws some conclusions.

Finally, the overall conclusion of this thesis is given in Chapter 7.

CHAPTER 2

CHANNEL ESTIMATION METHOD FOR OFDM SYSTEMS UNDER HIGHER MOBILE ENVIRONMENTS

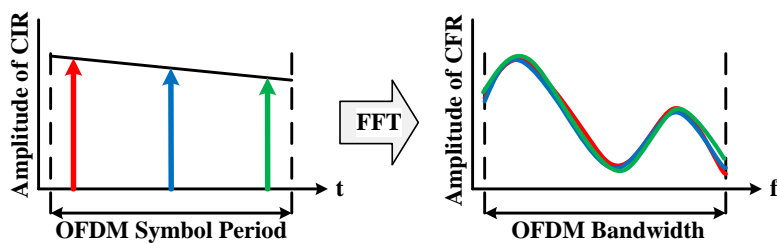
A loss of subcarrier orthogonality in orthogonal frequency division multiplexing (OFDM) signal due to time-varying multipath fading channel causes an inter-carrier interference (ICI) which would lead the fatal degradation of the channel estimation accuracy. To solve this problem, this chapter proposes a new design of time domain training sequence (TS) signal in the estimation of channel impulse response (CIR) for the training sequence inserted OFDM (TS-OFDM) signal. The proposed new design of TS signal can reduce the leakage of power spectrum density (PSD) at the outside of OFDM allocated frequency bandwidth with keeping higher CIR estimation accuracy. This chapter presents various computer simulation results to demonstrate the effectiveness of proposed CIR estimation method for the TS-OFDM signal as comparing with the conventional scattered pilot subcarrier method for CP-OFDM signal and pseudo noise (PN) sequence method for TS-OFDM signal under higher mobile environments.

2.1 Introduction

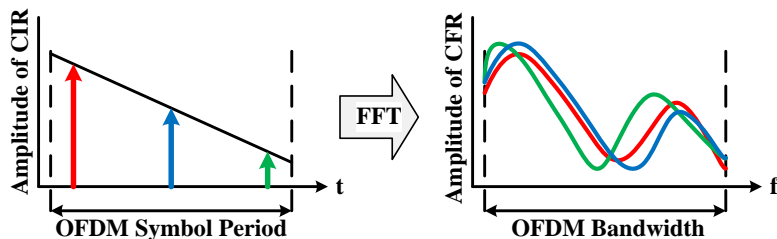
Orthogonal frequency division multiplexing (OFDM) technique has been received a lot of attentions especially in field of wireless communications from its efficient usage of frequency bandwidth and robustness to multipath fading channels. From these advantages, the OFDM has already been adopted as standard transmission techniques in various wireless communications systems such as the digital video broadcasting (DVB), wireless local area networks (WLANs) and fourth generation (4G) cellular systems [59].

A simple one-tap frequency domain equalization (one-tap FDE) method is usually employed in the cyclic prefix OFDM (CP-OFDM) signal to compensate the fading distortion occurred in the quasi-static multipath fading channels. Figure 2.1 shows a schematic diagram for the relationships between the CIR in the time domain and the CFR in the frequency domain. In the figure, the CFR in the frequency domain is obtained by converting the time domain CIR at the certain sampling time. Figure 2.1(a) shows the CIR and CFR in the quasi-static channel. From the figure, it can be seen that the CIR at the three sampling times are almost the same and their corresponding CFRs are also almost the same. From this fact, the distortion of multipath fading can be compensated precisely by the conventional one-tap FDE method of using any CFR obtained at any sampling time. However, the CIR would be no more constant even during one OFDM symbol period in higher time-varying fading channels which causes inter-carrier interference (ICI) due to the loss of orthogonality among subcarriers [66]. Figure 2.2(b) shows the CIR and CFR in higher time-varying fading channel. From the figure, the CFR is changing according to the CIR at the different sampling time. From this fact, it is difficult to compensate the time-varying distortion of fading by the conventional one-tap FDE method of using one of the CFRs during one symbol period which leads the degradation of bit error rate (BER) performance under higher mobile environments.

To solve the ICI problem, many equalization methods were proposed for CP-OFDM signal to mitigate the ICI by using the CIR at every sampling time [67-70]. These equalization methods require the higher CIR estimation accuracy at every sampling time so as to detect the



(a) Quasi-static environments.



(b) High time-varying environments.

Figure 2.1: Relationships between CIR and CFR.

2.1 Introduction

transmitted data signal at every symbol. The CIR estimation method usually employs scattered pilot subcarriers which are inserted into data subcarriers periodically in the frequency axis. The scattered pilot subcarriers method can achieve higher CIR estimation accuracy only when the number of FFT points is equal to the number of data subcarriers which corresponds to the Nyquist sampling [71]. However in the actual OFDM transmitter, a certain number of null subcarriers (zero padding) are added at both ends of OFDM data subcarriers to reject the aliasing occurring at the output of digital to analogue (D/A) converter. Since the actual CIR is occurred based on the overall bandwidth including zero padding, the estimated CIR by using the scattered pilot subcarriers inserted within the OFDM allocated bandwidth is different from the actual CIR especially when increasing the number of zero padding. Furthermore, the estimation accuracy of CIR by using the scattered pilot subcarriers method would be degraded due to the occurrence of ICI in the received pilot subcarriers under high mobile environments [72].

To solve the above problem on the channel estimation of using the pilot subcarriers method for the CP-OFDM signal in higher time-varying fading channels, a pseudo noise (PN) sequence or Chu sequence is employed as the training sequence (TS) in the estimation of CIR as well as the role of CP for the TS-OFDM signal [73-74]. The employment of TS-OFDM signal with the time domain PN or Chu sequence can achieve higher CFR estimation accuracy than the CP-OFDM signal of using the scattered pilot subcarriers method in higher time-varying fading channels. However, the employment of PN or Chu sequence as the TS signal would causes the undesirable leakage of power spectrum density (PSD) at the outside of allocated OFDM frequency bandwidth. Because the occupied frequency bandwidth of TS signal would be much wider than the allocated OFDM frequency bandwidth when the TS signal is employed so as to keep the good property of autocorrelation for the PN and Chu sequences which leads the serious adjacent channel interference problem to other systems [75]. Furthermore, when the same data pattern of PN or Chu sequence is added at every data symbol over one frame, higher power spurious components would be occurred at the outside of allocated OFDM frequency bandwidth due to the repetition of same data pattern of TS signal in the time domain. The leakage of PSD at the outside of OFDM allocated bandwidth would cause the difficulty in the design of transmitter so as to meet the spectral mask requirement for the adjacent channel interference. From this fact, the leakage of PSD must be suppressed when using the TS-OFDM signal.

From the above backgrounds, this chapter proposes the channel estimation method by using a new design of TS signal. The feature of proposed channel estimation method are to employ a different data pattern of TS signal added to each data symbol over one frame and to employ the triangular window function for the TS signal as the waveform shaping. The proposed TS signal can achieve higher CIR estimation accuracy with keeping the lower leakage of PSD at the outside of OFDM allocated frequency bandwidth. This chapter presents various simulation results to demonstrate the effectiveness of proposed channel estimation method as comparing with the conventional channel estimation methods.

The remainder of this chapter is organized as follows. Section 2.2 presents a conventional scattered pilot based channel estimation method. Section 2.3 presents a proposed TS based channel estimation method under higher time-varying channels. Section 2.4 presents various computer simulation results to verify the effectiveness of proposed method as comparing with the conventional method. Finally, Section 2.5 draws some conclusions.

2.2 Conventional Scattered Pilot based Channel Estimation Method

Figure 2.2 shows the basic frame format of conventional CP-OFDM signal of using scattered pilot subcarriers in the CIR estimation. At the transmitter, the input information data is modulated by quadrature-phase shift keying (QPSK) or quadrature-amplitude modulation (QAM) method. Then, the scattered pilot subcarriers are periodically inserted into the modulated frequency domain signal both for frequency axis with an interval of FIP and the time axis with an interval of TIP , respectively. After that the K subcarriers of the modulated frequency domain signal including scattered pilot subcarriers $X_p(m, k)$ at the k -th subcarriers of m -th symbol is mapped into the certain frequency band within the frequency bandwidth with N subcarriers continuously from the subcarrier number N_{Z1} to N_{Z2} and the null subcarriers (zero padding) are added at the both ends of K data subcarriers. After subcarrier mapping, the frequency domain signal $X(m, k_1)$ over N subcarriers is given by,

$$X(m, k_1) = \begin{cases} 0 \text{ (zero padding)}, & 0 \leq k_1 \leq N_{Z1} - 1 \\ X_p(m, k_1 - N_{Z1}), & N_{Z1} \leq k_1 \leq N_{Z2} \\ 0 \text{ (zero padding)}, & N_{Z2} + 1 \leq k_1 \leq N - 1 \end{cases} \quad (2.1)$$

where $(N-K)$ is the number of zero padding (N_Z) added at the both ends of K data subcarriers in the frequency domain. The frequency domain signal $X(m, k_1)$ including the zero padding given in (2.1) is converted to time domain signal by the N -point IFFT which can be given by,

$$x(m, n) = \frac{1}{\sqrt{N}} \sum_{k_1=N_{Z1}}^{N_{Z2}} X(m, k_1) \cdot e^{j \frac{2\pi n k_1}{N}}, \quad 0 \leq n \leq N - 1 \quad (2.2)$$

where $x(m, n)$ is the transmitted OFDM signal in the time domain. Then the CP with the length of N_g sample is added at the start of OFDM symbol. The OFDM signal is passed through digital to analog (D/A) converter and transmitted through the multipath fading channel.

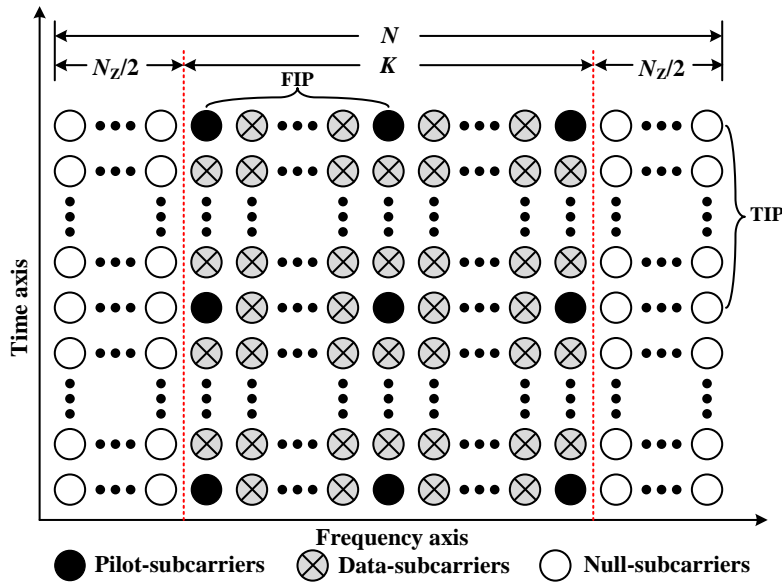


Figure 2.2: Basic frame format of scattered pilot subcarrier using in CP-OFDM.

2.2 Conventional Scattered Pilot based Channel Estimation Method

At the receiver, the received time domain signal $y(m,n)$ is removed the CP and then converted to the frequency domain signal by N -point FFT. After that the subcarrier remapping is used and then the received frequency domain signal which can be given by,

$$Y_p(m,k) = H_p(m,k) \cdot X_p(m,k) + W_p(m,k), \quad 0 \leq k \leq K-1 \quad (2.3)$$

where $Y_p(m,k)$ is the received frequency domain at k -th subcarriers of m -th symbol, $H_p(m,k)$ is the channel frequency response (CFR), $X_p(m,k)$ is the modulated frequency domain signal including scattered pilot subcarriers, and $W_p(m,k)$ is the additive white Gaussian noise (AWGN) with variance of σ^2 . Here, the CFR at k_p -th pilot subcarriers of m_p -th pilot symbols which is periodically inserted into the data signal can be estimated by,

$$\hat{H}_p(m_p, k_p) = \frac{Y_p(m_p, k_p)}{X_p(m_p, k_p)}, \quad 0 \leq p \leq K_p - 1 \quad (2.4)$$

where K_p is the number of scattered pilot subcarriers in the frequency axis in which k_p is expressed by $k_p = p \times FIP$, $0 \leq p \leq K_p - 1$. $X_p(m_p, k_p)$ is the known data patterns of scattered pilot subcarriers at k_p -th pilot subcarriers of m_p -th data symbol including pilot subcarriers and $\hat{H}_p(m_p, k_p)$ is the estimated CFR at subcarriers at k_p -th pilot subcarriers of m_p -th data symbol including pilot subcarriers. By using (2.4) under the assumption that the channel impulse response $h_l(m_p)$ at the l -th delay path of m_p -th data symbol including pilot subcarriers is the unknown parameter, the channel frequency response $H_p(m_p, k_p)$ can be given by,

$$H_p(m_p, k_p) = \sum_{l=0}^{L-1} h_l(m_p) \cdot e^{-j \frac{2\pi \cdot l \cdot (k_p + N_{Z1})}{N}} \quad (2.5)$$

By using (2.4) and (2.5), the time channel impulse response $h_l(m_p)$ at the l -th delay path of m_p -th data symbol including pilot subcarriers including pilot subcarriers can be estimated by solving the following maximum likelihood (ML) equation under the constraint condition in which the error between the estimated CFR given in (2.4) and the CFR by using the unknown parameter of $h_l(m_p)$ given in (2.5) is minimized [76].

$$\Upsilon \{h_1 h_2 \dots h_{N_g}\} = \arg \min \left[\sum_{p=0}^{K_p-1} \left| \hat{H}(m_p, k_p) - \sum_{l=0}^{N_g-1} h_l(m_p) \cdot e^{-j \frac{2\pi \cdot l \cdot (k_p + N_{Z1})}{N}} \right|^2 \right] \quad (2.6)$$

where N_g is the length of CP. Here, it should be noted that the number of delay paths to be estimated is assumed by N_g of which length is taken by longer than the number of delay paths L because the actual number of delay paths L is unknown at the receiver. From (2.6), the CIR for all delay paths $h_l(m_p)$ can be estimated at the data symbol with pilot subcarriers by solving the following simultaneous equations.

$$[\hat{h}_l(m_p)]_{N_g \times 1} = \dagger [Z_{m_p}(k_p, l)]_{N_g \times K_p} [\hat{H}(m_p, k_p)]_{K_p \times 1} \quad (2.7)$$

where $\dagger[\cdot]$ is the Moore-Penrose inverse matrix and the element of $[Z(k_p, l)]$ is given by,

$$Z(k_p, l) = e^{-j \frac{2\pi \cdot l \cdot (k_p - N_{Z1})}{N}} \quad (2.8)$$

where $\hat{h}_l(m_p)$ is the estimated time domain CIR at l -th delay path of m_p -th data symbol including pilot subcarriers. Since all elements of $[Z(k_p, l)]$ given in (2.8) are known at the receiver, the inverse matrix in (2.7) can be calculated in advance for all different data patterns

of scattered pilot subcarriers inserted over one frame which enables the considerable reduction of computation complexity in the estimation of CIR at every symbol. By using the estimated CIR $\hat{h}_l(m_p)$ at m_p -th data symbol including pilot subcarriers, the CIR at every sampling time $\hat{h}_l(m, n)$ can be estimated by using the cubic spline interpolation method over one OFDM frame. From Figure 2.2 and equation (2.6), there is a serious problem in the CIR estimation accuracy of using scattered pilot subcarriers method due to the zero padding inserted both ends of OFDM subcarriers. The estimated CIR at every sampling time $\hat{h}_l(m, n)$ are much different from actual time domain CIR at every sampling time $h_l(m, n)$ because the obtained CIR is estimated from the received OFDM signal within N_{Z1} to N_{Z2} period which it represents only for the OFDM allocated frequency bandwidth (not includes the bandwidth of zero padding). Figure 2.3 shows the comparison of estimated CFR and actual CFR. The CFR can be obtained by performing FFT processing to the CIR at the certain sampling time during one OFDM symbol period. From the figure, it can be observed that the estimated CFR by using the scattered pilot subcarriers can be estimated the CFR precisely within OFDM bandwidth. However the actual CFR in the actual channel is completely different from the estimated CFR as shown in Figure 2.3. From this fact, the actual CIR is also completely different from the estimated CIR when the number of N -points FFT/IFFT is not equal to the number of K data subcarriers which corresponds to non-Nyquist sampling. Here, it should be noted that the CFR can be estimated precisely within the OFDM allocated frequency bandwidth even when the estimated CIR is much different from the actual CIR.

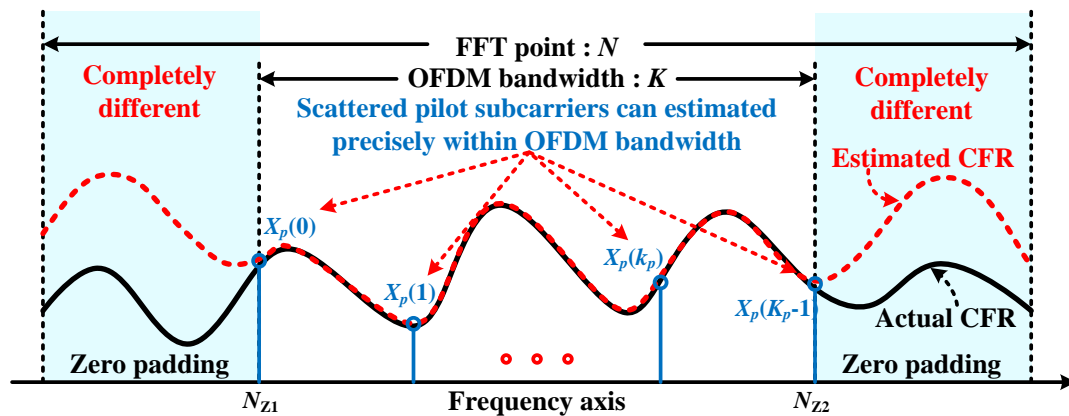


Figure 2.3: Comparison of estimated CFR and actual CFR.

This section presents the frame format for the proposed new design of TS signal based channel estimation method by using a time domain triangular window function for the TS-OFDM signal. The proposed new design of TS signal can reduce the leakage of power spectrum density (PSD) with keeping higher channel estimation accuracy even under higher mobile environments.

Figure 2.4(a) shows the frame format for the proposed TS-OFDM signal with the time domain triangular window function. In the proposed frame format, the time domain TS1 and TS2 with the length of S samples are inserted at the start of every data symbol in which the length of S should be taken longer than the number of delay paths (L). The time domain TS signal would be used in the estimation of CIR at every sampling time and also used as the role of CP to avoid the inter-symbol interference (ISI) occurred in the multipath fading channel.

Figure 3(a) illustrates the frame format for the proposed TS-OFDM signal at the transmitter. The frame is divided into two main sections: the m -th Symbol and the $(m+1)$ -th Symbol. Each symbol section contains a Training Symbol (TS) and a Data Symbol. The Training Symbol is further divided into two parts: TS1 (yellow) and TS2 (blue). The duration of each Training Symbol is S , and the duration of each Data Symbol is N . The frame format is shown for the m -th and $(m+1)$ -th symbols.

Figure 3(b) illustrates the proposed TS-OFDM signal in multipath fading channels. The signal is received at the receiver, and the frame format is shown for the m -th and $(m+1)$ -th symbols. The received signal is divided into two main sections: the m -th Symbol and the $(m+1)$ -th Symbol. Each symbol section contains a Training Symbol (TS) and a Data Symbol. The Training Symbol is further divided into two parts: TS1 (yellow) and TS2 (blue). The duration of each Training Symbol is S , and the duration of each Data Symbol is N . The frame format is shown for the m -th and $(m+1)$ -th symbols. The received signal is divided into two main sections: the m -th Symbol and the $(m+1)$ -th Symbol. Each symbol section contains a Training Symbol (TS) and a Data Symbol. The Training Symbol is further divided into two parts: TS1 (yellow) and TS2 (blue). The duration of each Training Symbol is S , and the duration of each Data Symbol is N . The frame format is shown for the m -th and $(m+1)$ -th symbols. The received signal is divided into two main sections: the m -th Symbol and the $(m+1)$ -th Symbol. Each symbol section contains a Training Symbol (TS) and a Data Symbol. The Training Symbol is further divided into two parts: TS1 (yellow) and TS2 (blue). The duration of each Training Symbol is S , and the duration of each Data Symbol is N . The frame format is shown for the m -th and $(m+1)$ -th symbols.

Figure 2.4: Structure of TS-OFDM signal in multipath fading channels.

2.3 Proposed Time Domain TS based Channel Estimation Method

The different data patterns of TS signals which can achieve higher CIR estimation accuracy in the multipath fading channels are selected by using the computer simulation results. In the computer simulations, the TS data patterns having higher CIR estimation accuracy are selected by changing the randomly generated data patterns of OFDM symbols which are independent from the data pattern of transmission information data symbols. It should be noted that the selected data patterns of TS signals can achieve higher CIR estimation accuracy even when these TS signals are added at the start of random information data symbols. In the implementation of practical systems, all system parameters including the number of data symbols in one frame are known in advance. From this fact, it is possible to prepare the required number of TS data patterns in advance which can achieve higher CIR estimation accuracy by using the computer simulation results.

As for the discontinuities at the both ends of TS signal in the time domain, this chapter employs the time domain triangular window function for the TS signal as the waveform shaping. The window function is commonly used in the digital processing to reduce the leakage of PSD. The triangular window function is one of window functions such as the Hamming, Hann (Raised cosine) and Blackman windows. It is well known that these window functions can improve the leakage of power spectrum density (PSD) by shaping the time domain signal with taking zero at both ends of signal of which various window functions are discussed theoretically in [77]. In this chapter, the triangular window function is employed for the TS signal because of its simpler waveform. By using the proposed TS signals having the different data patterns over one frame in conjunction with the time domain triangular window function, the leakage of power spectrum density could be suppressed relatively.

In this chapter, the data pattern for the proposed TS1 and TS2 signals at the m -th symbol employs the same data pattern which is represented by $c(m, s)$. Furthermore, the TS1 and TS2 signals at the m -th data symbol are multiplied by the time domain triangular window function of $\Gamma(s)$ to suppress the leakage of PSD as shown in Figure 2.4(a). The time domain triangular window function $\Gamma(s)$ with the length of $2S$ samples is given by,

$$\Gamma(s) = \begin{cases} (s+1)/S, & 0 \leq s \leq S-1 \\ 2-s/S, & S \leq s \leq 2S-1 \end{cases} \quad (2.9)$$

The proposed TS1 and TS2 signals at the m -th data symbol after multiplying $\Gamma(s)$ can be expressed by,

$$C(m, s) = \begin{cases} d_1(m, s) = c(m, s) \cdot \Gamma(s), & 0 \leq s \leq S-1 \\ d_2(m, s) = c(m, s-S) \cdot \Gamma(s), & S \leq s \leq 2S-1 \end{cases} \quad (2.10)$$

where $C(m, s)$ with the length of $2S$ samples is the sequential data pattern of TS1 and TS2 from 0 to $2S-1$ in the time domain. Then, $C(m, s)$ is inserted at the start of every OFDM data symbol which is represented by,

$$x_T(m, n_1) = \begin{cases} C(m, n_1), & 0 \leq n_1 \leq 2S-1 \\ x(m, n_1-2S), & 2S \leq n_1 \leq N+2S-1 \end{cases} \quad (2.11)$$

where $x_T(m, n_1)$ is the transmission signal including the TS signal at the n_1 -th sample of m -th symbol with the length of $N+2S$ samples. Assuming that the synchronization of symbol timing at the receiver is perfect, the received time domain OFDM signal $y(m, n_2)$ at the n_2 -th sampling time of m -th symbol after passing through the multipath fading channels as shown in Figure 2.4(b) can be expressed by,

2.3 Proposed Time Domain TS based Channel Estimation Method

$$y(m, n_2) = \sum_{l=0}^{L-1} h_l(m, n_2) \cdot x_T(m, n_2 - l) + w(m, n_2), \quad 0 \leq n_2 \leq N + 2S - 1 \quad (2.12)$$

where $h_l(m, n_2)$ is the CIR at the n_2 -th time sample of m -th data symbol for the l -th delay path occurred in the actual time-varying fading channels, $w(m, n_2)$ is the additive white Gaussian noise (AWGN) with the variance of σ^2 , and L is the number of delay paths. As shown in Figure 2.4(b), the received signal $y(m, n_2)$ can be divided into two parts which consist of the observation period for the CIR estimation $y_E(m, n_2)$ with the length of S samples and for the data demodulation period $y_R(m, n_2)$ with the length of $P=N+S$ samples, respectively.

2.3.2 Channel Estimation at Every Sampling Time

The received time domain TS2 signal $y_E(m, n_2)$ which be used in the estimation of CIR at every symbol can be expressed by,

$$y_E(m, n_2) = \sum_{l=0}^{L-1} h_l(m, n_2) \cdot d_2(m, n_2 - l) + w(m, n_2), \quad 0 \leq n_2 \leq S - 1 \quad (2.13)$$

where $d_2(m, n_2)$ is the TS2 signal with the triangular window function given in (2.10). Here it should be noted that the CIR is assumed to be constant during the short time period of TS1 and TS2 even in higher time-varying fading channels. Assuming $\hat{h}_l(m)$ is unknown parameters for the CIR at the m -th symbol, the expected received time domain TS2 signal $\hat{y}_E(m, n_2)$ can be given by,

$$\hat{y}_E(m, n_2) = \sum_{l=0}^{S-1} \hat{h}_l(m) d_2(m, n_2 - l), \quad 0 \leq n_2 \leq S - 1 \quad (2.14)$$

Here it should be noted that $d_2(m, n_2)$ given in (2.10) is known at the receiver and the number of delay paths to be estimated is assumed by S of which length is taken by longer than the number of delay paths L because the actual number of delay paths L is unknown at the receiver. The unknown parameter of CIR $\hat{h}_l(m)$ at the m -th symbol can be estimated by solving the following maximum likelihood (ML) equation under the constraint for minimizing the difference between the actual received TS signal $y_E(m, n_2)$ in (2.13) and the expected received TS signal $\hat{y}_E(m, n_2)$ in (2.14) [78].

$$\Upsilon = \arg \min_{\hat{h}_l(m)} \left[\sum_{n_2=0}^{S-1} \|y_E(m, n_2) - \hat{y}_E(m, n_2)\|^2 \right] \quad (2.15)$$

The ML equation in (2.15) can be simple solved by the following equations.

$$y_E(m, n_2) - \hat{y}_E(m, n_2) = 0, \quad 0 \leq n_2 \leq S - 1 \quad (2.16)$$

The result of (2.16), by minimizing the difference of actual received time domain TS signal and expected received time domain TS signal can be expressed by,

$$y_E(m, n_2) = \sum_{l=0}^{S-1} \hat{h}_l(m) \cdot d_2(m, n_2 - l), \quad 0 \leq n_2 \leq S - 1 \quad (2.17)$$

Finally, (2.17) results on the following simultaneous equations.

$$[y_E(m, n_2)]_{S \times 1} = [d_2(m, n_2 - l)]_{S \times S} [\hat{h}_l(m)]_{S \times 1} \quad (2.18)$$

2.3 Proposed Time Domain TS based Channel Estimation Method

where

$$[d_2(m, n_2 - l)]_{S \times S} = \begin{bmatrix} d_2(m, 0) & d_1(m, S-1) & \cdots & d_1(m, 2) & d_1(m, 1) \\ d_2(m, 1) & d_2(m, 0) & \ddots & \vdots & d_1(m, 2) \\ \vdots & d_2(m, 1) & \ddots & \ddots & \vdots \\ \vdots & \vdots & \ddots & \ddots & d_1(m, S-1) \\ d_2(m, S-1) & d_2(m, S-2) & \cdots & d_2(m, 1) & d_2(m, 0) \end{bmatrix} \quad (2.19)$$

The unknown parameter of CIR $\hat{h}_l(m)$ at the m -th symbol can be solved by the following matrix calculation of using the inverse matrix of $[d_2(m, n_2 - l)]_{S \times S}$.

$$[\hat{h}_l(m)]_{S \times 1} = [d_2(m, n_2 - l)]_{S \times S}^{-1} [y_E(m, n_2)]_{S \times 1} \quad (2.20)$$

where $[\cdot]^{-1}$ represents the matrix inversion. Since all elements of $[d_2(m, n_2 - l)]$ given in (2.18) are known at the receiver, the inverse matrix in (2.20) can be calculated in advance for all different data patterns of TS signals inserted over one frame which enables the considerable reduction of computation complexity in the estimation of CIR at every symbol. By using the estimated $\hat{h}_l(m)$ at every symbol, the CIR at every sampling time $\hat{h}_l(m, n_2)$ can be estimated by using the cubic spline interpolation method over one frame. The power spectrum density (PSD) at the output of transmitter and CIR estimation accuracy at every sampling time $\hat{h}_l(m, n_2)$ for the proposed TS-OFDM signal are evaluated in Section 2.4.

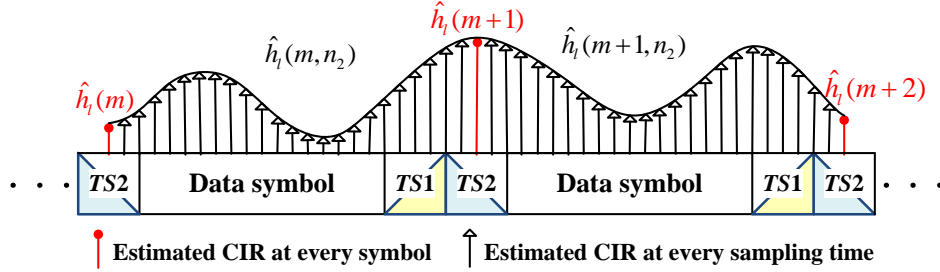


Figure 2.5: Estimation of CIR at every sampling time by using cubic spline interpolation.

2.4 Performance Evaluation for Proposed Channel Estimation Method

This section presents various simulation results to verify the effectiveness of proposed new design of TS based channel estimation method as comparing with conventional scattered pilot and PN sequence based channel estimation methods. The simulation parameters to be used in the following evaluations are listed in Table 2.1. The number of subcarriers is $K=96$, the number of zero padding is $N_z=32$ and the number of FFT/IFFT points is $N=128$. The conventional CP-OFDM employs the scattered pilot subcarriers in the estimation of CIR. The interval of pilot subcarriers in the frequency axis is $FIP=6$ and the pilot symbol including the data subcarriers is added at every symbol in the time axis ($TIP=1$). The length of TS for the proposed CIR estimation method for TS-OFDM signal is $S=16$ which is the same as the length of CP in the CP-OFDM signal. In the following evaluations, the normalized Doppler frequency $R_D=f_{\text{dmax}}/\Delta f$ is employed in which f_{dmax} is the maximum Doppler frequency and Δf is the OFDM subcarrier spacing. The estimation accuracy for the CIR at every sampling time is evaluated by normalized mean square error (NMSE) which is given by,

$$NMSE = \frac{\sum_{l=0}^{L-1} \sum_{m=0}^{M-1} \sum_{n_2=0}^{N+2S-1} |\hat{h}_l(m, n_2) - h_l(m, n_2)|^2}{\sum_{l=0}^{L-1} \sum_{m=0}^{M-1} \sum_{n_2=0}^{N+2S-1} |h_l(m, n_2)|^2} \quad (2.21)$$

where $\hat{h}_l(m, n_2)$ and $h_l(m, n_2)$ are the estimated and actual CIR, respectively.

Table 2.1: Simulation parameters.

Parameter		Value
Number of FFT points (N)		128
Number of subcarriers (K)		96~128
Number of Zero padding (N_z)		0~32
Conventional CP-OFDM	Modulation for Pilot	QPSK
	Pilot interval (FIP, TIP)	(6,1)
	Number of sampled CP (N_g)	16
Proposed TS-OFDM	Modulation for TS	16QAM
	TS interval (TIP)	1
	Number of sampled TS (S)	16
Modulation for data subcarrier		16QAM
Number of data symbol (M)		65
Allocated bandwidth		2MHz
Radio carrier frequency		5GHz
Rayleigh multipath fading channel model		
Delay profile		Exponential
Decay constant		-1
Number of delay paths (L)		14
Number of Arriving Rays Angle		20

2.4 Performance Evaluation for Proposed Channel Estimation Method

Figure 2.6 shows the comparison of power spectrum density (PSD) at the output of transmitter for the conventional CP-OFDM with pilot subcarrier, the TS-OFDM with the PN sequence and the proposed TS-OFDM with the new design of TS signal when the modulation method for data subcarriers is 16QAM and the oversampling ratio of OFDM transmission signal is taken by four times. From the figure, it can be seen that the PSD for the conventional TS-OFDM with the PN sequence has high power spurious components at the outside of allocated OFDM frequency bandwidth. This is the reason that the same data pattern of PN sequence is used for all data symbols over one frame and the time domain PN sequence itself has wider frequency bandwidth as compared with that for the conventional CP-OFDM signal. While the PSD for the proposed TS-OFDM of using different patterns of TS signals with the triangular window function shows almost the same PSD as that for the conventional CP-OFDM signal. From the figure, it can be concluded that the proposed TS-OFDM with the new design of TS signal can be used in the CIR estimation with keeping lower PSD at the outside of allocated OFDM frequency bandwidth.

Figure 2.7 shows the CIR estimation accuracy at every sampling time evaluated by the normalized mean square error (NMSE) given in (2.21) for the conventional pilot subcarriers method in the frequency domain and the proposed new design of time domain TS based CIR estimation method when changing the number of zero padding (N_z) and the normalized Doppler frequency R_D at $C/N=30\text{dB}$. From the figure, it can be observed that the proposed method can keep the higher estimation accuracy with regardless of N_z . While the estimation accuracy for the conventional pilot subcarriers method is getting worse when increasing N_z and the normalized Doppler frequency R_D . From these results, it can be confirmed that the proposed CIR estimation method of using the TS can achieve higher estimation accuracy even when the time domain OFDM signal is sampled with non-Nyquist sampling.

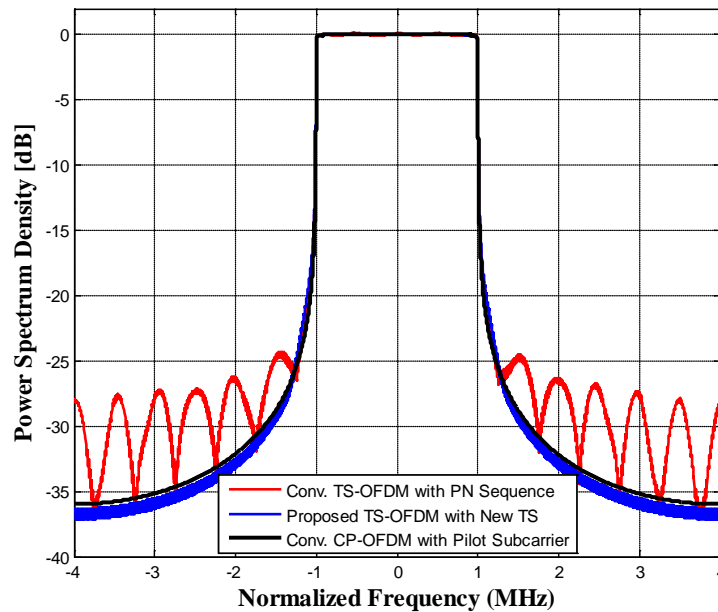


Figure 2.6: Power spectrum density for proposed TS-OFDM signal with new design of TS, conventional TS-OFDM signal with PN sequence and conventional CP-OFDM signal.

2.4 Performance Evaluation for Proposed Channel Estimation Method

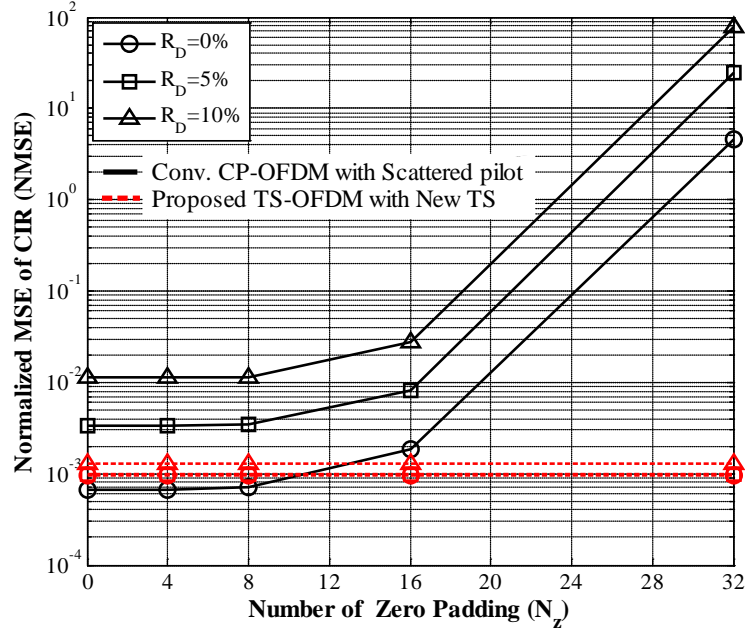


Figure 2.7: CIR estimation accuracy (NMSE) for proposed method when changing the number of zero padding at $C/N=30\text{dB}$.

Figure 2.8 shows the CIR estimation accuracy at every sampling time for the conventional TS-OFDM with the PN sequence and the proposed TS-OFDM with the new design of TS signal when changing the normalized Doppler frequency (R_D). The CIR estimation accuracy is evaluated by the normalized mean square error (NMSE) given in (2.21). Here it should be noted that the estimated CIR at every sampling time is obtained by using the cubic interpolation method for the estimated CIR at every symbol. From the figure, it can be observed that the accuracy of estimated CIR at every sampling time for the proposed TS signal is almost the same performance as that for the PN sequence even when increasing the normalized Doppler frequency (R_D) up to 10%.

Figure 2.9 shows the CIR estimation accuracy at every sampling time for the conventional TS-OFDM with the PN sequence and the proposed TS-OFDM with the new design of TS signal when changing the operation C/N . From the figure, it can be observed that the accuracy of estimated CIR at every sampling time for the proposed TS signal is almost the same performance as that for the PN sequence. From Figure 2.6 to Figure 2.9, it can be concluded that the estimated CIR of using the proposed new design of TS signal can achieve higher channel estimation accuracy with keeping lower leakage of PSD at the outside of OFDM allocated bandwidth even in higher time-varying fading channels.

2.4 Performance Evaluation for Proposed Channel Estimation Method

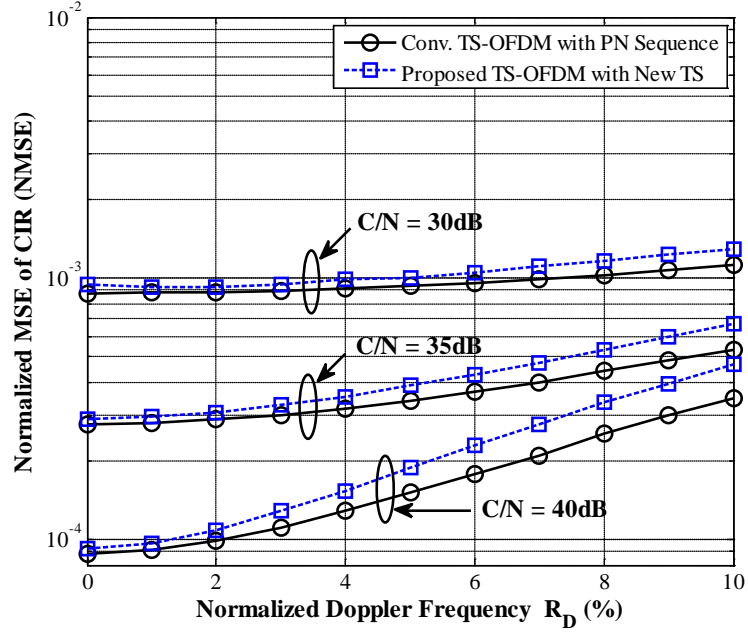


Figure 2.8: CIR estimation accuracy (NMSE) for proposed and conventional TS-OFDM when changing normalized Doppler frequency (R_D).

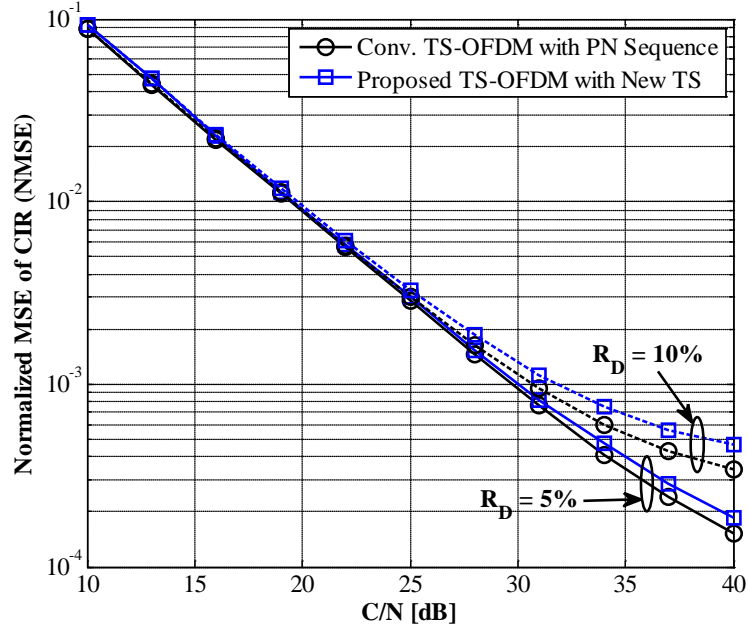


Figure 2.9: CIR estimation accuracy (NMSE) for proposed and conventional TS-OFDM when changing C/N.

2.5 Conclusions

This chapter proposed the channel estimation method for the TS-OFDM signal in higher time-varying fading channels. The salient features of proposed method are to employ the new design of TS signal in the estimation of CIR at every sampling time and to employ the triangular window function for the TS signal as the waveform shaping. The proposed TS can achieve higher CIR estimation accuracy with keeping the lower leakage of PSD at the outside of OFDM allocated frequency bandwidth. To demonstrate the effectiveness of proposed channel estimation method, this chapter conducted various computer simulations. From the simulation results, this chapter confirmed that the proposed new TS signal can achieve lower leakage of power spectrum density at the outside of allocated OFDM frequency bandwidth with keeping higher CIR estimation accuracy even under higher mobile environments.

CHAPTER 3

THEORETICAL EXAMINATION OF CHANNEL ESTIMATION METHOD FOR TS-OFDM SIGNAL UNDER SYMBOL TIMEING OFFSET

Recently the channel estimation method of using a time domain training sequence (TS) signal for the time domain training sequence inserted-orthogonal frequency division multiplexing (TS-OFDM) has been considered actively by many researchers as an alternative method of using scattered pilot subcarriers signals in the frequency domain. However most of them were investigated by assuming the ideal symbol timing. This chapter conducts the theoretical examinations for the effect of channel estimation method of using the TS method when the detected symbol timing has an offset from the ideal symbol timing. This chapter also verifies the theoretical analysis by computer simulation results.

3.1 Introduction

Orthogonal frequency division multiplexing (OFDM) system is an effective transmission technique for combating inter-symbol interference (ISI) caused by the multipath fading environments. However, the frequency mismatch between transmitter and receiver oscillator violates the orthogonality of subcarriers and results in the inter-carrier interference (ICI). Before performing the channel estimation, equalization and demodulation, the correct timing for the OFDM symbol has to be acquired. The perfect synchronization is achieved if the data symbol selected for the fast Fourier transform (FFT) processing corresponds exactly to the transmitted inverse FFT symbol. The most important effect of a timing misalignment is the violation of the cyclic prefix (CP) condition, as well as addition noise due to the estimation of a shortened channel. Any misalignment of the FFT window at the receiver within the useful CP of the OFDM symbol results in a phase rotation of the subcarrier. Furthermore if the FFT window extends over a symbol boundary, both ISI and ICI are occurred and lead the fatal degradation of system performance [79].

In the employment of cyclic prefix-orthogonal frequency division multiplexing (CP-OFDM) in multipath fading channels, the channel frequency response (CFR) is usually estimated by using scattered pilot signals in which the scattered pilot signals are inserted into data symbols periodically in the frequency domain. As an alternative method of using scattered pilot signals, a CFR estimation method of using a time domain training signal (TS) was proposed for the TS-OFDM [74, 80-82]. In [82], the authors demonstrated that the TS aided method can achieve higher CFR estimation accuracy than the pilot aided method especially under higher mobile environments. However these papers in [74, 80-82] assume the ideal symbol timing (ST) and as far as we know there was no detailed investigation under the symbol timing offset (STO). In this chapter, we perform theoretical examinations for the effect of CFR estimation method for the TS-OFDM under the STO. This chapter also verifies the theoretical analysis by computer simulation results.

The rest of this chapter is organized as follows. Section 3.2 introduces the frame format for TS-OFDM signal under symbol timing offset. Section 3.3 presents the channel frequency response (CFR) estimation method with the time domain TS signal under symbol timing offset. Section 3.4 presents various computer simulation results to demonstrate the effectiveness of the channel estimation method by using the time domain TS signal as comparing with the conventional pilot method under the symbol timing offset, and Section 3.5 draws some conclusions.

3.2 Design of TS-OFDM under Symbol Timing Offset

At the CP-OFDM receiver, a ST must be firstly established to discard the CP from the received signal and to decide the FFT window for the data symbol. The ST is usually detected by taking an auto-correlation between the transmitted and received signals [83]. However, this method would establish the ST at the delay path with the maximum amplitude among the multiple delay paths which leads the inter-symbol interference (ISI) in earlier received delay paths than the detected ST after removing the CP. To solve this problem, [83] proposed the early gate FFT window method for the CP-OFDM in which the ST for FFT window is established by adding a pre-advanced offset to the detected ST to avoid the ISI.

Based on the early gate FFT window method for the CP-OFDM, this chapter employs a frame format for the TS-OFDM as shown in Figure 3.1. In the figure, the ideal ST is defined at the start of TS1, L is the number of delay paths in the real channel, S is the length of TS1 and TS2 with the same data pattern which are added at the both ends of data symbol, η is the firstly detected ST and β is the pre-advanced offset. When assuming η is detected at the delay path with the maximum amplitude, η is existed within $0 \leq \eta \leq L-1$ and the ST for the FFT window is established at $\eta_e = -\beta + \eta$. The required length of S can be decided by considering two cases $\eta = 0$ and $\eta = L-1$ as shown in Figure 3.1 which correspond to the established ST $\eta_e = -\beta$ and $\eta_e = -\beta + L-1$, respectively. Hence the following conditions are required to satisfy the ISI free for both cases.

$$\begin{cases} \beta + L \leq S & \text{when } \eta = 0 \\ -\beta + L - 1 \leq 0 & \text{when } \eta = L - 1 \end{cases} \quad (3.1)$$

From (3.1), the required length of S is given by $S \geq 2L-1$ which satisfies the ISI free if η is detected within $0 \leq \eta \leq L-1$. Here the length of S could be reduced from the fact that the amplitude of longer delay path is stochastically smaller than the shorter delay path in the real channel. However since the purpose of this chapter is to evaluate the effect of estimated CFR under the STO, the conditions of $0 \leq \eta \leq L-1$, $S = 2L-1$ and $\beta = L-1$ under the ISI free are assumed in the following theoretical analysis. In the following, the sub-indexes Id , So , TS and D represent the ideal ST, ST with offset, training and data signals, respectively.

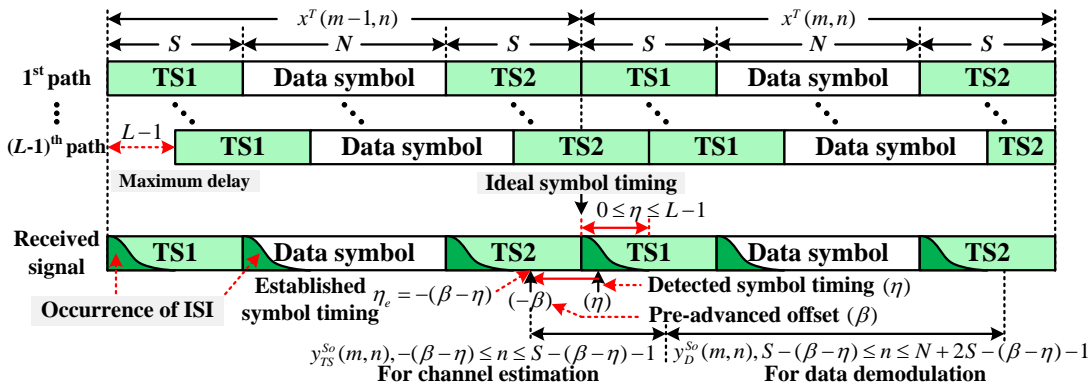


Figure 3.1: Frame format for TS-OFDM signal under symbol timing offset.

3.3 CFR Estimation Method with TS under Symbol Timing Offset

This section firstly presents a CFR estimation method for the TS-OFDM under the ideal ST in which the ST is established at $\eta_e = 0$ ($\beta = \eta$). The transmission time domain signal $x^T(m, n)$ at the n -th sample of m -th symbol is given by,

$$x^T(m, n) = \begin{cases} TS1 : b_n, & 0 \leq n \leq S-1 \\ Data : x(m, n-S), & S \leq n \leq N+S-1 \\ TS2 : b_{n-N-S}, & N+S \leq n \leq N+2S-1 \end{cases} \quad (3.2)$$

From Figure 3.1, the received TS1 $y_{TS}^{ld}(m, n)$ under the ideal ST can be expressed by,

$$y_{TS}^{ld}(m, n) = \sum_{l=0}^{S-1} h_l(m) \cdot b_{\text{mod}[n-l, S]} + w_{TS}^{ld}(m, n), \quad 0 \leq n \leq S-1 \quad (3.3)$$

where $\text{mod}[n, S]$ represents n modulo S , $w_{TS}^{ld}(m, n)$ is an additive white Gaussian noise and $h_l(m)$ is the channel impulse response (CIR) for the l -th delay path at the m -th symbol in the real channel. Since the number of delay paths L in the real channel is unknown at the receiver, the length of TS ($=S$) which be taken by larger than L is employed in (3.3). Assuming that $\hat{h}_l^{ld}(m)$ is the unknown parameters to be estimated, the expected received TS1 $\hat{y}_{TS}^{ld}(m, n)$ can be given by,

$$\hat{y}_{TS}^{ld}(m, n) = \sum_{l=0}^{S-1} \hat{h}_l^{ld}(m) \cdot b_{\text{mod}[n-l, S]}, \quad 0 \leq n \leq S-1 \quad (3.4)$$

By using (3.3) and (3.4), the unknown parameters $\hat{h}_l^{ld}(m)$ under the ideal ST can be estimated by solving the following maximum likelihood (ML) equation [82].

$$\Gamma = \arg \min_{\hat{h}_l^{ld}(m)} \left[\sum_{n=0}^{S-1} \|y_{TS}^{ld}(m, n) - \hat{y}_{TS}^{ld}(m, n)\|^2 \right] \quad (3.5)$$

The simple solution for (3.5) can be given by assuming $y_{TS}^{ld}(m, n) = \hat{y}_{TS}^{ld}(m, n)$ and it is expressed by the following simultaneous equations.

$$[y_{TS}^{ld}(m, n)]_{S \times 1} = [b_{\text{mod}[n-l, S]}]_{S \times S} [\hat{h}_l^{ld}(m)]_{S \times 1} \quad (3.6)$$

where $[b_{\text{mod}[n-l, S]}]$ is the circulant matrix with the size of $(S \times S)$. By using the property of circulant matrix, its inverse matrix is also the circulant matrix [84]. Let $[c_{\text{mod}[n-l, S]}]$ is the inverse matrix of $[b_{\text{mod}[n-l, S]}]$, the unknown parameter $\hat{h}_l^{ld}(m)$ in (3.6) can be estimated by,

$$\begin{aligned} [\hat{h}_l^{ld}(m)]_{S \times 1} &= [b_{\text{mod}[n-l, S]}]_{S \times S}^{-1} [y_{TS}^{ld}(m, n)]_{S \times 1} \\ &= [c_{\text{mod}[n-l, S]}]_{S \times S} [y_{TS}^{ld}(m, n)]_{S \times 1} \end{aligned} \quad (3.7)$$

Here it should be noted that $[c_{\text{mod}[n-l, S]}]$ can be calculated in advance because all elements of $[b_{\text{mod}[n-l, S]}]$ are known at the receiver which leads the considerable reduction of computation complexity in the estimation of CIR at every symbol under mobile environments. From (3.7),

3.3 CFR Estimation Method with TS under Symbol Timing Offset

$\hat{h}_l^{Id}(m)$ can be given by,

$$\begin{aligned}
 \hat{h}_l^{Id}(m) &= \sum_{n=0}^{S-1} y_{TS}^{Id}(m, n) \cdot c_{\text{mod}[n-l, S]} \\
 &= \sum_{n=0}^{S-1} \left\{ \sum_{l=0}^{S-1} h_l(m) \cdot b_{\text{mod}[n-l, S]} + w_{TS}^{Id}(m, n) \right\} \cdot c_{\text{mod}[n-l, S]} \\
 &= h_l(m) + \sum_{n=0}^{S-1} w_{TS}^{Id}(m, n) \cdot c_{\text{mod}[n-l, S]} \\
 &= h_l(m) + z_{TS}^{Id}(m, l)
 \end{aligned} \tag{3.8}$$

where $z_{TS}^{Id}(m, l)$ is the noise component at the l -th delay path under the ideal ST. From (3.8), it can be observed that the estimated $\hat{h}_l^{Id}(m)$ under the ideal ST can be expressed by $h_l(m)$ in the real channel although it includes the noise component.

When the ST is established at $\eta_e \neq 0$ ($\beta > \eta$) which includes $(-\eta_e)$ offset from the ideal ST as shown in Figure 3.1, the received TS $y_{TS}^{So}(m, n)$ can be expressed by,

$$\begin{aligned}
 y_{TS}^{So}(m, n) &= y_{TS}^{Id}(m, n), \quad \text{for } -(\beta - \eta) \leq n \leq S - (\beta - \eta) - 1 \\
 &= y_{TS}^{Id}(m, n - (\beta - \eta)), \quad \text{for } 0 \leq n \leq S - 1
 \end{aligned} \tag{3.9}$$

The CIR $\hat{h}_l^{So}(m)$ under the STO must be estimated by using the inverse matrix $[c_{\text{mod}[n-l, S]}]$ given in (3.7) because the Ideal ST is unknown at the receiver. From (3.3) and (3.9), $\hat{h}_l^{So}(m)$ under the STO can be estimated by,

$$\begin{aligned}
 \hat{h}_l^{So}(m) &= \sum_{n=0}^{S-1} y_{TS}^{Id}(m, n - (\beta - \eta)) \cdot c_{\text{mod}[n-l, S]} \\
 &= \sum_{n=0}^{S-1} \left[\sum_{l=0}^{S-1} h_l(m) \cdot b_{\text{mod}[n-(\beta-\eta)-l, S]} + w_{TS}^{Id}(m, n - (\beta - \eta)) \right] \cdot c_{\text{mod}[n-l, S]} \\
 &= h_{\text{mod}[l-(\beta-\eta), S]}(m) + z_{TS}^{So}(m, l)
 \end{aligned} \tag{3.10}$$

where $z_{TS}^{So}(m, l)$ is the noise component under the STO. From Eq.(3.10), it can be concluded that $\hat{h}_l^{So}(m)$ under the STO can be given by $h_{\text{mod}[l-(\beta-\eta), S]}(m)$ in the real channel although it includes the noise component $z_{TS}^{So}(m, l)$.

In this chapter, we employ the MMSE-FDE method for the TS-OFDM which can obtain the frequency diversity gain by decomposing the received time domain signal by $(N+S)$ -point FFT/IFFT [74]. Then CFR under the STO can be given by,

$$\begin{aligned}
 \hat{H}^{So}(m, k) &= \sum_{l=0}^{N+S-1} \hat{h}_l^{So}(m) \cdot e^{-j \frac{2\pi l k}{(N+S)}} \\
 &= \sum_{l=0}^{S-1} \left\{ h_{\text{mod}[l-(\beta-\eta), S]}(m) + z_{TS}^{So}(m, l) \right\} \cdot e^{-j \frac{2\pi l k}{(N+S)}}
 \end{aligned} \tag{3.11}$$

When $\eta_e \neq \beta - \eta$, the CIR in (3.11) can be split into three terms as given by,

$$\begin{aligned}
 \hat{H}^{So}(m, k) &= \sum_{l=0}^{(\beta-\eta)-1} h_{\text{mod}[l-(\beta-\eta), S]}(m) \cdot e^{-j \frac{2\pi l k}{(N+S)}} + \sum_{l=(\beta-\eta)}^{L+(\beta-\eta)-1} h_{\text{mod}[l-(\beta-\eta), S]}(m) \cdot e^{-j \frac{2\pi l k}{(N+S)}} \\
 &+ \sum_{l=L+(\beta-\eta)}^{S-1} h_{\text{mod}[l-(\beta-\eta), S]}(m) \cdot e^{-j \frac{2\pi l k}{(N+S)}} + Z_{TS}^{So}(m, k), \quad 0 \leq k \leq N + S - 1
 \end{aligned} \tag{3.12}$$

3.3 CFR Estimation Method with TS under Symbol Timing Offset

As for the 1st and 3rd terms in (3.12), $h_{\text{mod}[l-(\beta-\eta),S]}(m)$ for $0 \leq l \leq (\beta-\eta)-1$ and $L+(\beta-\eta) \leq l \leq S-1$ are given by $h_l(m)$ for $S-(\beta-\eta) \leq l \leq S-1$ and $L \leq l \leq S-1-(\beta-\eta)$, respectively. Since $h_l(m)$ is the CIR in the real channel which exists only within $0 \leq l \leq L-1$. From this fact, the 1st and 3rd terms can be assumed to be zero and (3.12) can be expressed by,

$$\begin{aligned}\hat{H}^{So}(m,k) &= \sum_{l=(\beta-\eta)}^{L+(\beta-\eta)-1} h_{\text{mod}[l-(\beta-\eta),S]}(m) e^{-j\frac{2\pi lk}{(N+S)}} + Z_{TS}^{So}(m,k) \\ &= e^{-j\frac{2\pi(\beta-\eta)k}{(N+S)}} \cdot \sum_{l=0}^{L-1} h_l(m) e^{-j\frac{2\pi lk}{(N+S)}} + Z_{TS}^{So}(m,k) \\ &= e^{-j\frac{2\pi(\beta-\eta)k}{(N+S)}} \cdot H(m,k) + Z_{TS}^{So}(m,k), \quad 0 \leq k \leq N+S-1\end{aligned}\quad (3.13)$$

where $Z_{TS}^{So}(m,k)$ is the noise component in the frequency domain and $H(m,k)$ is the CFR in the real channel. From (3.13), it can be concluded that the estimated $\hat{H}^{So}(m,k)$ under the STO is affected by the phase rotation as the function of detected ST $\eta_e (= -\beta + \eta)$ from the ideal ST to the $H(m,k)$ in the real channel. However it should be noted that the estimated $\hat{H}^{So}(m,k)$ includes the noise components $Z_{TS}^{So}(m,k)$ over $(N+S)$ samples which are caused from the noise component added to the estimated CIR $\hat{h}_l^{So}(m)$ within S samples even when $\hat{h}_l^{So}(m)$ is only existed at L samples within S samples.

In the data demodulation with the MMSE-FDE method [74], the received signal with the length of $(N+S)$ samples after discarding the length of S from the established ST η_e as shown in Figure 3.1 can be given by,

$$\begin{aligned}y_D^{So}(m,n) &= y_D^{ld}(m,n), \quad \text{for } S-(\beta-\eta) \leq n \leq N+2S-(\beta-\eta)-1 \\ &= \sum_{l=0}^{S-1} h_l(m) \cdot x^T(m, n-(\beta-\eta)-l) + w_D^{ld}(m, n-(\beta-\eta)) \\ &\quad , \quad \text{for } S \leq n \leq N+2S-1\end{aligned}\quad (3.14)$$

where $x^T(m, n-(\beta-\eta)-l)$ is the transmitted time domain signal in (3.2) including the data with the length of N and some parts of TS1 and TS2 with the total length of S which are added at the start and end of data symbol. Let $X^T(m,i)$ is the frequency domain signal converted from the time domain signal $x^T(m,n)$ given in (3.2), $x^T(m, n-(\beta-\eta)-l)$ in (3.14) is given by,

$$x^T(m, n-(\beta-\eta)) = \frac{1}{\sqrt{N+S}} \sum_{i=0}^{N+S-1} X^T(m,i) \cdot e^{j\frac{2\pi i(n-(\beta-\eta)-S)}{(N+S)}}, \quad S \leq n \leq N+2S-1 \quad (3.15)$$

By using (3.15), the received frequency domain signal which is converted from the time domain signal in (3.14) by $(N+S)$ -point FFT, can be given by,

$$\begin{aligned}Y_D^{So}(m,k) &= \frac{1}{\sqrt{N+S}} \sum_{n=S}^{N+2S-1} y_D^{So}(m,n) \cdot e^{-j\frac{2\pi(n-S)k}{(N+S)}} \\ &= \frac{1}{(N+S)} \sum_{i=0}^{N+S-1} X^T(m,i) \cdot e^{-j\frac{2\pi i(\beta-\eta)}{(N+S)}} \sum_{l=0}^{S-1} h_l(m) \cdot e^{-j\frac{2\pi il}{(N+S)}} \sum_{n=S}^{N+2S-1} e^{j\frac{2\pi(i-k)(n-S)}{(N+S)}} \\ &\quad + \frac{1}{\sqrt{N+S}} \sum_{n=S}^{N+2S-1} w_D^{ld}(m, n-(\beta-\eta)) \cdot e^{-j\frac{2\pi(n-S)k}{(N+S)}} \\ &= e^{-j\frac{2\pi(\beta-\eta)k}{(N+S)}} X^T(m,k) \cdot H(m,k) + Z_D^{So}(m,k), \quad 0 \leq k \leq N+S-1\end{aligned}\quad (3.16)$$

3.3 CFR Estimation Method with TS under Symbol Timing Offset

In the derivation of (3.16), the following relationship is used.

$$\sum_{n=S}^{N+2S-1} e^{j \frac{2\pi(i-k)(n-S)}{(N+S)}} = \begin{cases} N+S & \text{when } i=k \\ 0 & \text{when } i \neq k \end{cases} \quad (3.17)$$

From (3.16), it can be observed that frequency domain received data signal $Y_D^{So}(m, k)$ under the STO is affected by the phase rotation to the transmitted frequency domain data symbol $X^T(m, k)$ which is completely the same phase rotation as the estimated CFR $\hat{H}^{So}(m, k)$ in (3.13). From this fact, the phase rotation of $Y_D^{So}(m, k)$ in (3.16) due to the STO can be compensated by the MMSE-FDE method of using the estimated $\hat{H}^{So}(m, k)$ in (3.13) which is expressed by,

$$\begin{aligned} \hat{X}^T(m, k) &= \left\{ \frac{[H^{So}(m, k)]^*}{|H^{So}(m, k)|^2 + \sigma_k^2} \right\} \cdot Y_D^{So}(m, k) \\ &= \left\{ \frac{\left[e^{-j \frac{2\pi(\beta-\eta)k}{(N+S)}} \cdot H(m, k) + Z_{TS}^{So}(m, k) \right]^*}{\left[e^{-j \frac{2\pi(\beta-\eta)k}{(N+S)}} \cdot H(m, k) + Z_{TS}^{So}(m, k) \right]^2 + \sigma_k^2} \right\} \cdot e^{-j \frac{2\pi(\beta-\eta)k}{(N+S)}} X^T(m, k) \cdot H(m, k) + Z_D^{So}(m, k) \\ &= X^T(m, k) + Z(m, k) \end{aligned} \quad (3.18)$$

where $(\cdot)^*$ is the complex conjugate operation and $\hat{X}^T(m, k)$ is the estimated frequency domain signal with the length of $(N+S)$.

In the demodulation of frequency domain data information $X(m, k)$, the estimated $\hat{X}^T(m, k)$ after the MMSE-FDE is converted to the time domain signal $\hat{x}^T(m, n)$ by $(N+S)$ -points IFFT. Here it should be noted that the frequency domain $\hat{X}^T(m, k)$ corresponds to the time domain $\hat{x}^T(m, n)$ from $n=S$ to $N+2S-1$ as given in (3.2). From this fact, the data information $\hat{X}(m, k)$ in the frequency domain can be demodulated by converting $\hat{x}^T(m, n)$ from $n=S$ to $S+N-1$ which corresponds to the time domain data information $x(m, n)$ in (3.2) by N -points FFT [74].

3.4 Proof of Theoretical Analysis by Computer Simulation Results

To verify the theoretical analysis derived in Section 3.3, this chapter conducts the computer simulations. The simulation parameters to be used in the following evaluations are listed in Table 3.1. In the simulation, the modulation method is quadrature phase shift keying (QPSK), TS-OFDM bandwidth is 5MHz, radio frequency is 2GHz, the number of data subcarriers is $K=96$ and the number of IFFT points at the transmitter is $N=128$. The channel is the time-varying multipath fading channel with $L=10$ delay paths which are modeled by the exponential power delay profile with -1dB decay constant. The normalized Doppler frequency are $f_d T_s=0.001$ and 0.006 where f_d is maximum Doppler frequency and T_s is the symbol duration. To satisfy the ISI free conditions given in (3.1), the length of TS is $S=19$ and the pre-advance offset is $\beta=9$. In the demodulation of data symbol, the MMSE-FDE method with the observation period of $(N+S)$ samples is employed.

Table 3.1: Simulation parameters.

Parameter		Value
Number of FFT points (N)		128
Number of subcarriers (K)		96
Number of Zero padding ($N-K$)		32
Conventional CP-OFDM	Modulation for Pilot	QPSK
	Pilot interval (FIP, TIP)	(6,1)
	Number of sampled CP (N_g)	19
Proposed TS-OFDM	Modulation for TS	QPSK
	TS interval (TIP)	1
	Number of sampled TS (S)	19
Modulation for data subcarrier		QPSK
Number of data symbol (M)		65
Allocated bandwidth		5MHz
Radio carrier frequency		2GHz
Rayleigh multipath fading channel model		
Delay profile		Exponential
Decay constant		-1
Number of delay paths (L)		10
Number of Arriving Rays Angle		20

Figure 3.2 shows an example of simulation result for the estimated channel impulse response (CIR) of using TS signal to verify the equation (3.12) when the symbol timing is detected at the delay path $l=2$ ($\eta=2$) with the maximum amplitude. From the figure, it can be observed that the estimated CIR $\hat{h}_l^{so}(m)$ is existed from $l = \beta - \eta$ ($=7$) to $l = L + \beta - \eta - 1$ ($=16$) which correspond to the real CIR $h_{\text{mod}[l-(\beta-\eta), S]}(m)$ within $0 \leq l \leq L-1$ ($0 \leq l \leq 9$) as given in equation (3.12). From the results, the theoretical analysis in

3.4 Proof of Theoretical Analysis by Computer Simulation Results

equation (3.12) under the STO is proved by the computer simulation results.

Figure 3.3 shows the bit error rate (BER) performances with the MMSE-FDE method for the TS-OFDM signal when changing the detected symbol timing η from 0 to $L-1$. From the figure, it can be observed that the channel estimation based TS method can keep better BER performance when the ST is detected within $0 \leq \eta \leq L-1 (=9)$. From these results, it is concluded that the theoretical analysis under the STO presented in this chapter is proved by the computer simulation results.

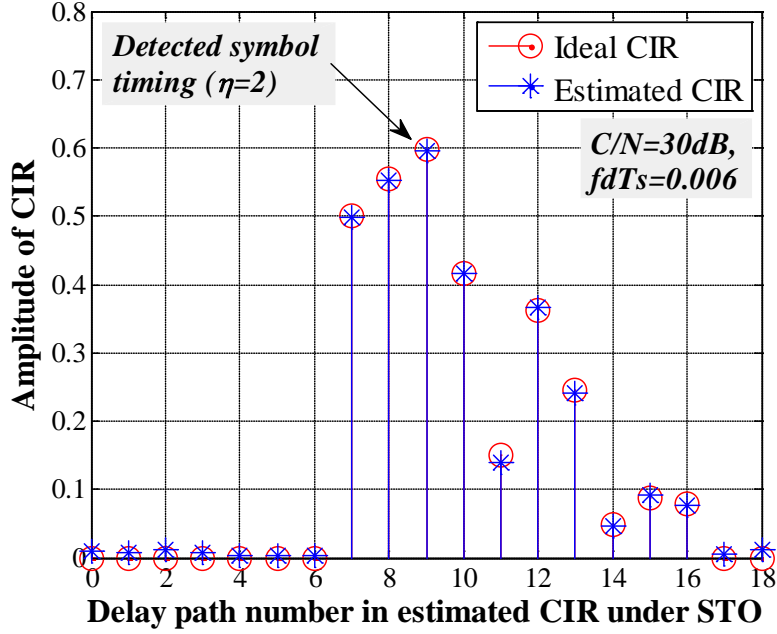


Figure 3.2: Amplitude of estimated CIR by using the time domain TS signal.

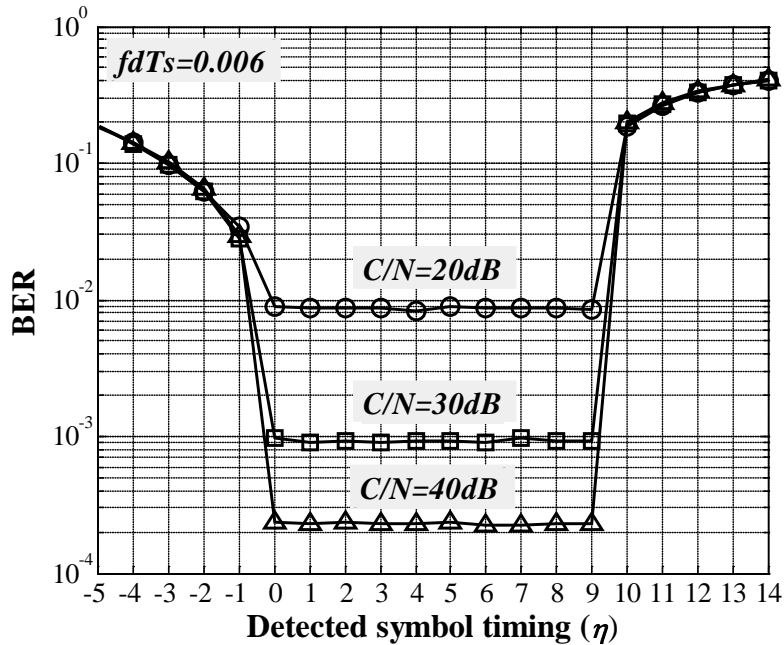


Figure 3.3: BER performances for TS-OFDM signal when changing detected ST (η).

3.4 Proof of Theoretical Analysis by Computer Simulation Results

Figure 3.4 shows the BER performances of the TS-OFDM with TS signal based channel estimation method when changing operation C/N. In the Figure, the BER performances of the conventional CP-OFDM signal with pilot subcarrier based channel estimation method is also shown. In the computer simulations, the symbol timing is detected from the randomly maximum amplitude of CIR. From the figure, it can be observed that the both TS-OFDM and CP-OFDM can keep better BER performance even ST is detected from the unknown maximum amplitude of CIR. Consequently, it also can be observed that the TS-OFDM signal shows the better BER performance than the conventional CP-OFDM signal because of it can be obtained the frequency diversity gain.

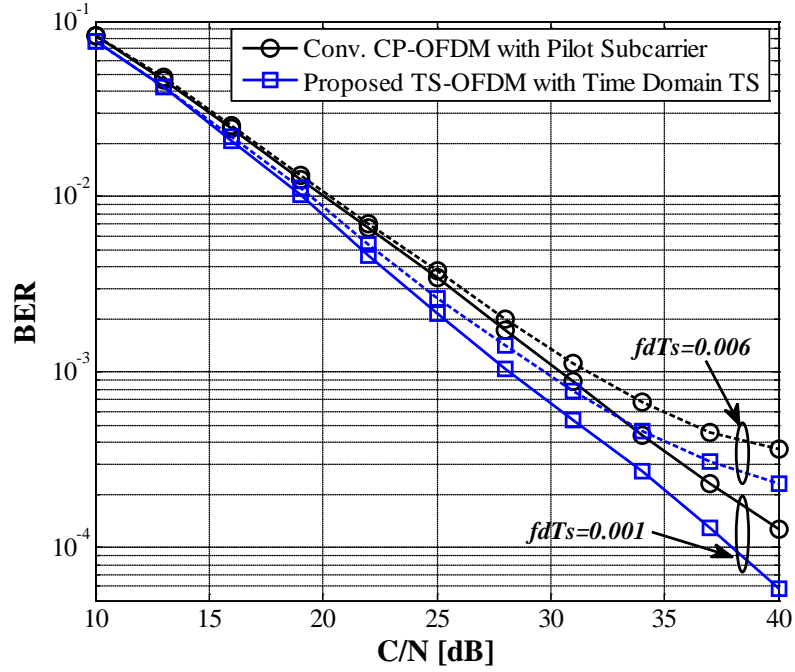


Figure 3.4: BER performances when changing operation C/N.

3.5 Conclusions

This chapter presented the theoretical examinations for the CFR estimation method of using TS signal under the symbol timing offset. From the theoretical analysis, it was confirmed that the symbol timing offset causes the same phase rotation both to the estimated CFR and the received data in frequency domain signal. This phase rotation can be canceled completely by using the MMSE-FDE method. This chapter also verified the theoretical analysis presented in this chapter by computer simulation results under both for symbol timing offset and time-varying fading channels.

CHAPTER 4

FREQUENCY DOMAIN EQUALIZATION METHOD FOR TS-OFDM SIGNAL UNDER HIGHER MOBILE ENVIRONMENTS

This chapter proposes a minimum mean square error-frequency domain equalization (MMSE-FDE) method for training sequence inserted orthogonal frequency division multiplexing (TS-OFDM) signal under higher mobile environments. The salient features of proposed method are to enable the acquisition of frequency diversity gain by using an enhanced channel impulse response (CIR) matrix and to enable the reduction of complexity by using a fast algorithm for inverse matrix calculation. From the simulation results, this chapter confirms that the proposed MMSE-FDE method can achieve better bit error rate (BER) performance than the conventional MMSE-FDE methods with keeping lower complexity under higher mobile environments.

4.1 Introduction

Orthogonal frequency division multiplexing (OFDM) is considered as one of efficient transmission techniques for wireless communications. By inserting a cyclic prefix (CP) or time domain training sequence (TS) at the start of data symbol, a simple one-tap equalization can be employed to compensate the distortion of multipath fading [6]. From these advantages, OFDM has been adopted as the standard transmission technique in the 4th generation mobile phone, wireless local area networks (WLANs) and digital broadcasting systems [59]. However, signal quality of OFDM signal would be degraded relatively under higher mobile environments accompanying with the Doppler frequency shift in which the original property of orthogonality among OFDM subcarriers is no more satisfied due to the occurrence of inter-carrier interference (ICI) [67].

To solve ICI problem under higher mobile environments, various equalization methods have been proposed up to today both for CP-OFDM and TS-OFDM signals [67,81,85,86]. In [67], minimum mean square error-frequency domain equalization (MMSE-FDE) method was proposed for CP-OFDM signal. This method requires the direct inverse matrix calculation for the full-elements of channel frequency response (CFR) matrix at every symbol to compensate the ICI which leads significantly higher order of complexity $O[N^3]$, where N is the length of data subcarrier. To solve the above problem, [85] proposed a low-complexity MMSE-FDE method for CP-OFDM signal. In this method, the full element of CFR matrix which is converted from the channel impulse response (CIR) is approximated by a banded matrix so as to employ the fast algorithm for inverse matrix calculation [87]. However, the CIR matrix is constructed by using only data period which leads the degradation of bit error rate (BER) performance in deep fading channels. To solve this problem, [86] proposed an enhanced FDE method for CP-OFDM in which the CIR matrix is constructed by using both data and CP periods to acquire the frequency diversity gain. However, this method requires the Moore-Penrose inverse matrix calculation for the non-square CFR matrix at every data symbol which leads significantly higher complexity. Furthermore, above two methods [85,86] of using CP-OFDM are usually required to estimate the CIR by using pilot subcarriers in the frequency domain which leads the degradation of CIR estimation accuracy due to the occurrence of ICI in the received pilot subcarriers. To solve the above problems, [81] proposed a low-complexity FAST-MMSE-FDE method for TS-OFDM in which the TS is used in the estimation of CIR at every symbol and the enhanced CIR matrix at every sample time is constructed by using a linear interpolation between the CIRs estimated at two consecutive symbols. By assuming the linear changing of CIR within one symbol period, the low complexity Maclaurin's expansion approximation can be employed in the calculation of inverse matrix. Although this method can achieve the frequency diversity gain with lower complexity, the BER performance would be degraded in higher time-varying fading channels due to the assumption of linear changing of CIR and the approximation of first order Maclaurin's expansion.

To solve the above problems, this chapter proposes a new MMSE-FDE method for TS-OFDM signal which can achieve better BER performance with keeping lower computation complexity under high mobile environments. The salient features of proposed method are to enable the acquisition of frequency diversity gain by using the enhanced CIR matrix and reduction of complexity by using the fast algorithm for inverse matrix calculation.

4.1 Introduction

The remainder of this chapter is organized as follows. Section 4.2 presents the problem of conventional MMSE-FDE methods both for CP-OFDM and TS-OFDM signals. Section 4.3 proposes the transceiver structure for TS-OFDM signal including the construction of enhanced CIR matrix by using the estimated CIR at every sampling time and low-complexity MMSE-FDE method by using the fast algorithm for inverse matrix calculation. Section 4.4 presents various computer simulation results to verify the effectiveness of proposed MMSE-FDE method for TS-OFDM as comparing with the conventional MMSE-FDE methods both for CP-OFDM and TS-OFDM signals. Finally, Section 4.5 draws some conclusions.

4.2 Conventional MMSE-FDE Methods under Higher Mobile Environments

Recently, various low-complexity MMSE-FDE methods have been proposed up to today both for CP-OFDM and TS-OFDM signals to compensate ICI in high time-varying fading channels [67,81,85,86]. However, these methods can achieve lower complexity at the cost of degradation of BER performance.

4.2.1 MMSE-FDE Method for CP-OFDM Signal

In CP-OFDM signal, the input data information in frequency domain is modulated. Then, the modulated frequency domain signal is converted to time domain by N -point inverse fast Fourier transform (IFFT). After that the CP with the length longer than the length of delay path is inserted at front of every data time domain signal. Assuming the synchronization of symbol timing is perfect at the receiver, the received frequency domain signal can be expressed by,

$$\mathbf{Y}_{N \times 1} = \mathbf{H}_{N \times N} \mathbf{X}_{N \times 1} + \mathbf{W}_{N \times 1} \quad (4.1)$$

where \mathbf{X} is the transmitted frequency domain signal, \mathbf{W} is the additive white Gaussian noise (AWGN) with variance of σ^2 , and \mathbf{H} is the channel frequency response (CFR) matrix which can be expressed by,

$$\mathbf{H}_{N \times N} = \begin{bmatrix} H(0,0) & H(0,1) & \cdots & \cdots & H(0,N-2) & H(0,N-1) \\ H(1,0) & H(1,1) & \cdots & \cdots & H(1,N-2) & H(1,N-1) \\ \vdots & \vdots & \ddots & \ddots & \vdots & \vdots \\ \vdots & \vdots & \ddots & \ddots & \vdots & \vdots \\ H(N-2,0) & H(N-2,1) & \cdots & \cdots & H(N-2,N-2) & H(N-2,N-1) \\ H(N-1,0) & H(N-1,1) & \cdots & \cdots & H(N-1,N-2) & H(N-1,N-1) \end{bmatrix} \quad (4.2)$$

By using a minimum mean square error-frequency domain equalization (MMSE-FDE) method [67], the transmitted frequency domain signal can be estimated by,

$$\hat{\mathbf{X}}_{N \times 1} = [\mathbf{H}_{N \times N}^H \mathbf{H}_{N \times N} + \sigma_k^2 \mathbf{I}_N]^{-1} \mathbf{H}_{N \times N}^H \mathbf{Y}_{N \times 1} \quad (4.3)$$

From (4.3), the transmitted frequency domain signal can be estimated precisely by employing the direct inverse matrix calculation even in higher time-varying fading channels. However, this method require significantly higher complexity with order of $O[N^3]$. To reduce complexity, the MMSE-FDE method with fast algorithm for inverse matrix calculation [85] has been proposed with the assumption that the full element of CFR matrix is approximated by a banded matrix. Let \mathbf{B} is the band matrix which obtained by selecting the lower and upper bandwidth of Q_1 so as to employ the fast algorithm for inverse matrix calculation [87]. By using the banded matrix \mathbf{B} , (4.3) can be approximated by,

$$\hat{\mathbf{X}}_{N \times 1}^{Band} \approx [\mathbf{B}_{N \times N}^H \mathbf{B}_{N \times N} + \sigma_k^2 \mathbf{I}_N]^{-1} \mathbf{B}_{N \times N}^H \mathbf{Y}_{N \times 1} \quad (4.4)$$

4.2 Conventional MMSE-FDE Methods under Higher Mobile Environments

From (4.4), the inverse matrix $[\mathbf{B}^H \mathbf{B} + \sigma^2 \mathbf{I}]$ can be calculated by using fast algorithm for inverse matrix calculation which requires the complexity order of $O[3(Q_1+1)^2 N]$. However, the assumption of CFR matrix is approximated by band matrix and constructed by using only data symbol period would leads the degradation of bit error rate (BER) performance in higher time-varying fading channels. Furthermore, the MMSE-FDE method of using CP-OFDM are usually required to estimate the CIR by using pilot subcarriers in the frequency domain which leads the degradation of CIR estimation accuracy due to the occurrence of ICI in the received pilot subcarriers.

4.2.2 FAST-MMSE-FDE Method for TS-OFDM Signal

To solve the problem of CIR estimation accuracy in higher time-varying fading channels, a low-complexity FAST-MMSE-FDE method for TS-OFDM [81] has been proposed in which the TS signal is used in the estimation of CIR at every symbol and the CIR matrix at every sample time is constructed by using a linear interpolation between the CIRs estimated at two consecutives symbols with length of P subcarrier. The linear time-varying channel model to approximate the CIR matrix can be given by,

$$h_l[n] = h_l[\Theta] - \psi[n] \cdot h_l[\Delta], \quad 0 \leq n \leq P-1 \quad (4.5)$$

where $\psi[n]$ is given by $((P-1)/2 - n)/((P-1)/2)$ which represents the CIR at the n -th sample time when assuming the linear time-varying channels, $h_l[\Theta]$ is given by $(h_l[0] + h_l[P-1])/2$ which is the average of CIR at the start and end of sampling times for the l -th delay path and $h_l[\Delta]$ is given by $(h_l[P-1] - h_l[0])/2$ which is the slope of CIR between start and end of sampling times. By converting $h_l[\Theta]$ and $h_l[\Delta]$ to the frequency domain with P -point FFT which are given by $\mathbf{H}_A = [H_A(0), H_A(1), \dots, H_A(P-1)]^T$ and $\mathbf{H}_D = [H_D(0), H_D(1), \dots, H_D(P-1)]^T$, respectively. Let express the matrix $\boldsymbol{\Psi} = [\psi(0), \psi(1), \dots, \psi(P-1)]^T$, $\mathbf{A} = \text{diag}(\mathbf{H}_A)$, $\mathbf{C} = \text{diag}(\boldsymbol{\Psi})$, $\mathbf{E} = \text{diag}(\mathbf{H}_E)$, and $\mathbf{D} = \text{diag}(\mathbf{H}_D)$. Where $\text{diag}(\cdot)$ is the diagonal matrix and \mathbf{H}_B is given by,

$$\mathbf{H}_E = \left(\frac{H_D(0)}{H_A(0)}, \frac{H_D(1)}{H_A(1)}, \dots, \frac{H_D(P-1)}{H_A(P-1)} \right)^T \quad (4.6)$$

By using the Maclaurin's expansion algorithm, the CFR matrix \mathbf{H} can be approximated by $\mathbf{H} = (\mathbf{I} - \mathbf{T})\mathbf{A}$ under the assumption of linear time-varying channels. Where $\mathbf{T} = \mathbf{F}\mathbf{C}\mathbf{F}^H\mathbf{E}$, and \mathbf{I} is the $P \times P$ identity matrix. Based on this approximation, the transmitted frequency domain signal can be estimated by,

$$\begin{aligned} \hat{\mathbf{X}}^{FAST} &= \mathbf{A}^{-1}(\mathbf{I} - \mathbf{T})^{-1}\mathbf{Y}^{FAST} \\ &= \mathbf{A}^{-1} \sum_{i=0}^{\infty} \mathbf{T}^i \mathbf{Y}^{FAST} \end{aligned} \quad (4.7)$$

where \mathbf{Y}^{FAST} is the received frequency domain signal with P subcarrier. In (4.7), when assuming $\|\mathbf{T}\| \ll 1$, the term of $(\mathbf{I} - \mathbf{T})^{-1}$ can be approximated by the Maclaurin's series expansion with the Q_2 -th order which is given by,

$$\begin{aligned}
 (\mathbf{I} - \mathbf{T})^{-1} &= \sum_{i=0}^{\infty} \mathbf{T}^i \\
 &\approx \sum_{q=0}^{Q_2} \mathbf{T}^q
 \end{aligned} \tag{4.8}$$

Finally, by substituting (4.8) into (4.7), the frequency domain signal can be demodulated by,

$$\hat{\mathbf{X}}^{FAST} \approx \mathbf{A}^{-1} \left(\sum_{q=0}^{Q_2} \mathbf{T}^q \mathbf{Y}^{FAST} \right) \tag{4.9}$$

Since the order of complexity in (4.9) is highly dependent on the order of Q_2 , its order should be selected by not larger than $Q_2=1$ so as to keeping lower complexity. By using linear time-varying channel model to approximate the CIR matrix and Maclaurin's series expansion for inverse matrix calculation, the complexity order of $O[P^2]$ is required at every demodulation of data symbol. Although the assumption of linear changing of CIR and the approximation of first order Maclaurin's expansion can achieve lower complexity, the BER performance would be degraded in higher time-varying fading channels.

4.3 Proposed MMSE-FDE Method for TS-OFDM Signal

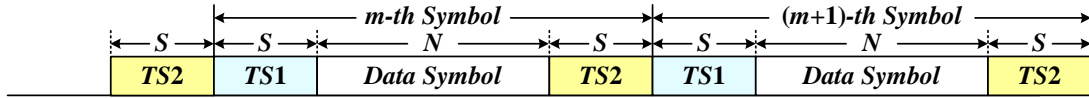
From above background, this thesis proposes a new MMSE-FDE method for TS-OFDM signal which can achieve better BER performance with keeping lower computation complexity under higher mobile environments.

4.3.1 System Structure for Proposed TS-OFDM Signal

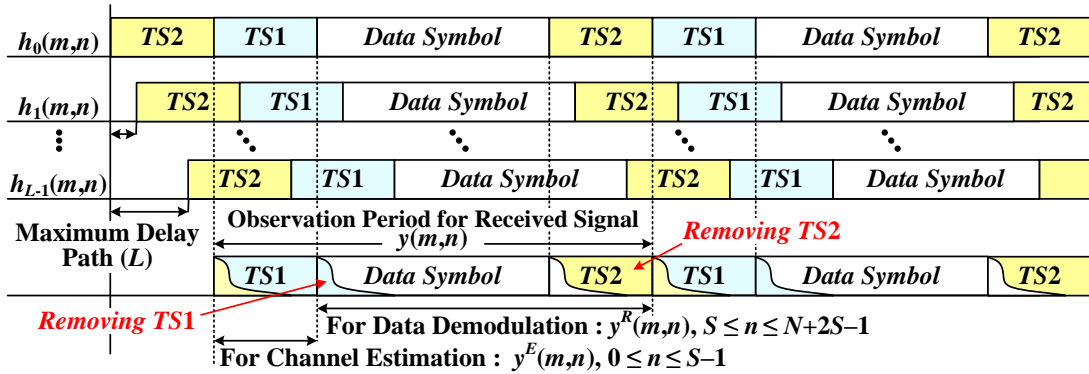
Figure 4.1(a) shows the frame format for TS-OFDM signal in the time domain which be used in the proposed MMSE-FDE method. In the frame format, the time domain TS is added at both ends of every data symbol in the time domain which be used in the estimation of CIR at every sampling time. The time domain TS with the estimated CIR is also used to remove the interferences from the TS signals occurred at both ends of data symbol. Figure 4.2 shows the structure of transceiver for the proposed MMSE-FDE method for TS-OFDM signal. At the transmitter, the input frequency domain data information is modulated by the quadrature-phase shift keying (QPSK) and then the modulated signal $X(m,k)$ at the k -th subcarrier of m -th symbol is converted to the time domain signal by N -point inverse fast Fourier transform (IFFT) which is given by,

$$x(m,n) = \frac{1}{\sqrt{N}} \sum_{k=0}^{N-1} X(m,k) \cdot e^{j\frac{2\pi kn}{N}}, \quad 0 \leq n \leq N-1 \quad (4.10)$$

where $x(m,n)$ is the transmitted time domain OFDM signal at the n -th time sample. Then, the same data pattern of TS1 and TS2 with the length of S samples are added at both ends of data symbol which is given by,



(a) Frame format for TS-OFDM signal at transmitter.



(b) TS-OFDM signal in time-varying multipath fading channels.

Figure 4.1: Basic Frame format of TS-OFDM signal at transmitter (a) and receiver (b).

4.3 Proposed MMSE-FDE Method for TS-OFDM Signal

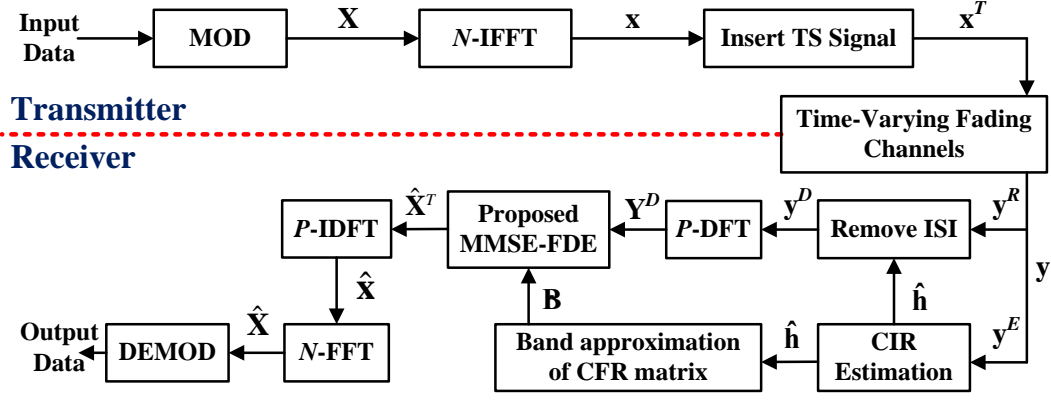


Figure 4.2: Structure of transceiver for proposed MMSE-FDE method.

$$x^T(m, n) = \begin{cases} TS1: b(n), & 0 \leq n \leq S-1 \\ \text{Data}: x(m, n-S), & S \leq n \leq N+S-1 \\ TS2: b(n-N-S), & N+S \leq n \leq N+2S-1 \end{cases} \quad (4.11)$$

where $b(n)$ is the time domain TS signals both for TS1 and TS2 and $x^T(m, n)$ is the transmitted time domain signal including both TS1 and TS2 signals.

Figure 4.1(b) shows the received TS-OFDM signal in the time-varying multipath fading channels. At the receiver, assuming that the synchronization of symbol timing is perfect, the received time domain OFDM signal $y(m, n)$ after passing through the time-varying fading channels can be expressed by,

$$y(m, n) = \sum_{l=0}^{L-1} h_l(m, n) \cdot x^T(m, n-l) + w(m, n), \quad 0 \leq n \leq N+2S-1 \quad (4.12)$$

where $h_l(m, n)$ is the channel impulse response (CIR) at the n -th time sample of m -th data symbol for the l -th delay path, $w(m, n)$ is the additive white Gaussian noise (AWGN) with variance of σ^2 , and L is the number of delay paths occurred in the actual time-varying fading channels. Here it should be noted that the length of S is taken by longer than the length of delay path L to remove the interferences of TS1 and TS2 occurred at both ends of data symbol. From (4.12), the received signal $y(m, n)$ can be divided into two parts which consist of the observation period for the CIR estimation $y^E(m, n)$ with length of S samples and for the data demodulation period $y^R(m, n)$ with the length of $P=N+S$ samples, respectively.

4.3.2 Construction of Enhanced CIR Matrix

In the proposed MMSE-FDE method, the CIR $h_l(m,n)$ at every sampling time must be estimated at the receiver to remove the ISI from the TS1 and TS2 occurred at both ends of data symbol. In [82], the authors proposed a maximum likelihood (ML) based CIR estimation method for TS-OFDM at every sampling time which can achieve higher CIR estimation accuracy in high time-varying fading channels. The received time domain signal for the data demodulation with the length of $P (=N+S)$ samples as shown in Figure 4.1(b) is given by,

$$y^R(m,n) = \sum_{l=0}^{L-1} h_l(m,n) \cdot x^T(m,n-l) + w(m,n), \quad S \leq n \leq N+2S-1 \quad (4.13)$$

The received signal in (4.13) includes the interferences of TS1 and TS2 incurred at both ends of data symbol. By using the estimated CIR $\hat{h}_l(m,n)$ at every sampling time and the known data pattern of TS1 and TS2 in (4.11), the interferences of TS1 and TS2 can be removed by,

$$y^D(m,n) = \begin{cases} y^R(m,n) - \sum_{l=n-S+1}^{S-1} \hat{h}_l(m,n) \cdot b(n-l), & S \leq n \leq 2S-2 \\ y^R(m,n), & 2S-1 \leq n \leq N+S-1 \\ y^R(m,n) - \sum_{l=0}^{n-N-S} \hat{h}_l(m,n) \cdot b(n-N-S-l), & N+S \leq n \leq N+2S-1 \end{cases} \quad (4.14)$$

In the derivation of (4.14), the following relationships are used.

$$n-l \leq S-1, \quad x^T(m,n-l) = b(n-l) \quad (4.15)$$

$$n-l \geq N+S, \quad x^T(m,n-l) = b(n-N-S-l) \quad (4.16)$$

where $y^D(m,n)$ is the received time domain signal after removing the interferences of TS1 and TS2 signals. From (4.14), the received time domain signal $y^D(m,n)$ can be given by the following matrix operation.

$$\mathbf{y}_{P \times 1}^D = \mathbf{h}_{P \times N} \mathbf{x}_{N \times 1} + \mathbf{w}_{P \times 1} \quad (4.17)$$

where \mathbf{x} is the time domain signal with the size of $N \times 1$ corresponds to the transmitted time domain signal $x(m,n)$ in (4.10) and \mathbf{h} is the enhanced CIR matrix with the size of $P \times N$ which can be expressed by,

$$\mathbf{h} = \begin{bmatrix} h_0(m,S) & 0 & \dots & \dots & \dots & 0 \\ h_1(m,S+1) & h_0(m,S+1) & \ddots & & & \vdots \\ \vdots & h_1(m,S+2) & \ddots & \ddots & & \vdots \\ h_{S-1}(m,2S-1) & \vdots & \vdots & \ddots & \ddots & \vdots \\ 0 & h_{S-1}(m,2S-1) & \vdots & \vdots & \ddots & 0 \\ \vdots & \ddots & \ddots & \vdots & \vdots & h_0(m,N+S-1) \\ \vdots & & \ddots & \ddots & \vdots & h_1(m,N+S) \\ \vdots & & & \ddots & \ddots & \vdots \\ \vdots & & & & \ddots & h_{S-1}(m,N+2S-2) \\ 0 & \dots & \dots & \dots & \dots & 0 \end{bmatrix} \quad (4.18)$$

In (4.18), the enhanced CIR matrix at every sampling time is constructed by using the

4.3 Proposed MMSE-FDE Method for TS-OFDM Signal

corresponding data and TS signals which can acquire the frequency diversity gain in the deep fading channels [86].

4.3.3 Low-Complexity Enhanced MMSE-FDE Method

The received time domain signal \mathbf{y}^D given in (4.17) is converted to the frequency domain signal by P -point discrete Fourier transform (DFT) which can be expressed by,

$$\begin{aligned}\mathbf{Y}_{P \times 1}^D &= \mathbf{F}_{P \times P} \mathbf{y}_{P \times 1}^D \\ &= \mathbf{F}_{P \times P} \mathbf{h}_{P \times N} \mathbf{F}_{N \times P}^H \mathbf{F}_{P \times N} \mathbf{x}_{N \times 1} + \mathbf{F}_{P \times P} \mathbf{w}_{P \times 1} \\ &= \mathbf{H}_{P \times P} \mathbf{X}_{P \times 1}^T + \mathbf{W}_{P \times 1}\end{aligned}\quad (4.19)$$

where $(\cdot)^H$ is the Hermitian transpose operation, \mathbf{F} and \mathbf{F}^H are the DFT and inverse DFT (IDFT) matrixes. \mathbf{H} is the CFR matrix with the size of $P \times P$, \mathbf{W} is the noise component and \mathbf{X}^T is the frequency domain signal with the size of $P \times 1$ which includes the data symbol and its delay component after removing the interferences of TS1 and TS2. By using the MMSE-FDE method, the frequency domain signal $\hat{\mathbf{X}}^T$ can be equalized by,

$$\hat{\mathbf{X}}_{P \times 1}^T = (\mathbf{H}_{P \times P}^H \mathbf{H}_{P \times P} + \sigma_k^2 \mathbf{I}_P)^{-1} \mathbf{H}_{P \times P}^H \mathbf{Y}_{P \times 1}^D \quad (4.20)$$

where \mathbf{I} is the Identity matrix and σ^2 is the variance of AWGN. The calculation of inverse matrix in (4.20) requires the order of complexity $O[P^3]$ which leads significantly higher computation complexity. To reduce the complexity in this chapter, the full elements of CFR matrix \mathbf{H} are approximated by a banded matrix \mathbf{B} with the lower and upper bandwidth of Q_1 so as to employ the fast algorithm for inverse matrix calculation [87]. By using the banded matrix \mathbf{B} , (4.20) can be approximated by,

$$\begin{aligned}\hat{\mathbf{X}}_{P \times 1}^T &\approx (\mathbf{B}_{P \times P}^H \mathbf{B}_{P \times P} + \sigma_k^2 \mathbf{I}_P)^{-1} \mathbf{B}_{P \times P}^H \mathbf{Y}_{P \times 1}^D \\ &\approx \mathbf{G}_{P \times P}^{-1} \mathbf{B}_{P \times P}^H \mathbf{Y}_{P \times 1}^D\end{aligned}\quad (4.21)$$

where $\mathbf{G} = (\mathbf{B}^H \mathbf{B} + \sigma^2 \mathbf{I})$ is the Hermitian banded matrix with the lower and upper bandwidth $2Q_1$ of which inverse matrix can be calculated by using the fast algorithm for inverse matrix calculation [87]. By applying the fast algorithm for inverse matrix calculation to the banded matrix \mathbf{G} , the order of complexity becomes $O[3(Q_1+1)^2 P]$ which is significantly lower than that for the direct inverse matrix calculation $O[P^3]$. In the demodulation of frequency domain data information, the equalized frequency domain signal $\hat{\mathbf{X}}^T$ is converted to the time domain signal $\hat{\mathbf{x}}^T$ by P -points IDFT. Here it should be noted that the estimated time domain signal $\hat{x}^T(m, n)$ from $n=0$ to $N-1$ is correspond to the time domain data information $\hat{x}(m, n)$ in (4.10). From this fact, the equalized frequency domain data information $\hat{X}(m, k)$ can be obtained from the estimated time domain signal $\hat{x}^T(m, n)$ by N -points FFT.

4.3.4 Evaluation of Computation Complexity

Table 4.1 shows the order of complexities for the proposed, conventional MMSE-FDE [85] and the FAST-MMSE-FDE [81] methods. The order of complexities are evaluated for the processing loads required in the removing of ISI, construction of CFR matrix, calculation of inverse matrix and equalizations. In the table, the orders of complexities for N -point FFT and P -points DFT are evaluated by $O[N\log_2 N]$ and $O[P^2]$, respectively. In the next section, the order of complexities for all methods shown in Table 4.1 is evaluated by assuming the actual parameters.

Table 4.1: Order of complexities for proposed and conventional methods.

Equalization methods	Processing loads		
	Removing of ISI	Construction of CFR matrix	Inverse matrix calculation and equalization
Conv. MMSE-FDE for CP-OFDM [85]	N/A	$O[(2Q_1+3)N\log_2 N + N(Q_1+1)^2 + N(Q_1+1)]$	$O[N^2 + 3N(Q_1+1)^2]$
Conv. FAST-MMSE-FDE for TS-OFDM [81]	$O[S^2 - S]$	$O[P^2 + 2PS + P]$	$O[(2Q_2+1)P^2 + (2Q_2+3)P + PN]$
Prop. MMSE-FDE for TS-OFDM	$O[S^2 - S]$	$O[P^2 + (2Q_1+2)PS + P(Q_1+1)^2 + P(Q_1+1)]$	$O[2P^2 + N\log_2 N + 3P(Q_1+1)^2]$

N is the number of FFT/IFFT points, S is the length of TS and CP, $P=N+S$, Q_1 is the lower and upper bandwidths of banded matrix, and Q_2 is the order of Maclaurin's expansion.

4.4 Performance Evaluation for Proposed MMSE-FDE Method

In this section, various computer simulation results are presented for the proposed MMSE-FDE method for TS-OFDM signal as comparing with the conventional MMSE-FDE method for CP-OFDM signal [85] and FAST-MMSE-FDE method for TS-OFDM signal [81]. The simulation parameters to be used in the following evaluations are listed in Table 4.2. The channel is the time-varying multipath fading channels with $L=14$ delay paths which are modeled by the exponential power delay profile with -1dB decay constant. In the conventional FAST-MMSE-FDE method for TS-OFDM signal, the order of Maclaurin's expansion in the calculation of inverse matrix is set to $Q_2=1$ as using in [81]. In the conventional MMSE-FDE method for CP-OFDM signal and proposed MMSE-FDE method for TS-OFDM signal, the lower and upper bandwidth of the banded matrix \mathbf{B} is set by $Q_1=3, 5$ and 7. As for the channel estimation method, the conventional MMSE-FDE method for CP-OFDM signal usually employed the scattered pilot subcarriers method in the estimation of CFR. The scattered pilot subcarriers are inserted at every data symbol frequency interval $FIP=8$. The proposed TS-OFDM and conventional TS-OFDM employed the time domain TS in the CFR estimation with length of $S=16$. In the following evaluations, the normalized Doppler frequency $R_D=f_{\text{dmax}}/\Delta f$ is employed as the measure of time-varying fading channels in which f_{dmax} is the maximum Doppler frequency and Δf is the OFDM subcarrier spacing.

Table 4.2: Simulation parameters.

Parameter	Value
Number of FFT points (N)	128
Number of subcarriers (K)	128
Number of data symbol (M)	65
Length of time domain TS for TS-OFDM (S)	16
Length of CP for CP-OFDM (N_g)	16
Lower and upper bandwidths of banded matrix (Q_1)	3, 5, 7
Order of power series expansion (Q_2) [81]	1
Modulation method for data subcarriers	QPSK
Allocated frequency bandwidth	5MHz
Radio carrier frequency	5GHz
Rayleigh multipath fading channel model	
Delay profile	Exponential
Decay constant	-1
Number of delay paths (L)	14
Number of Arriving Rays Angle	20

4.4 Performance Evaluation for Proposed MMSE-FDE Method

Figure 4.3 shows the BER performances of proposed MMSE-FDE method for the TS-OFDM signal when changing the normalized Doppler frequency R_D at the operation $C/N=35\text{dB}$. In the figure, the conventional MMSE-FDE method for the CP-OFDM signal [85] and FAST-MMSE-FDE method for TS-OFDM signal [81] are also shown as the purposes of comparison with the proposed MMSE-FDE method. In the conventional MMSE-FDE method for CP-OFDM and proposed MMSE-FDE method for TS-OFDM, the lower and upper bandwidth of the banded matrix \mathbf{B} is set by $Q_1=5$. From the figure, it can be observed that the proposed MMSE-FDE method shows better BER performance than the conventional one-tap FDE method for CP-OFDM, conventional MMSE-FDE method for CP-OFDM and FAST-MMSE-FDE method for TS-OFDM. Here it should be noted that the degradation of BER performances as compared with the proposed MMSE-FDE method are caused by no acquisition of frequency diversity gain in the conventional MMSE-FDE method for CP-OFDM, and the assumption of linear changing of CIR and the approximation of first order Maclaurin's expansion in the FAST-MMSE-FDE method for TS-OFDM, respectively.

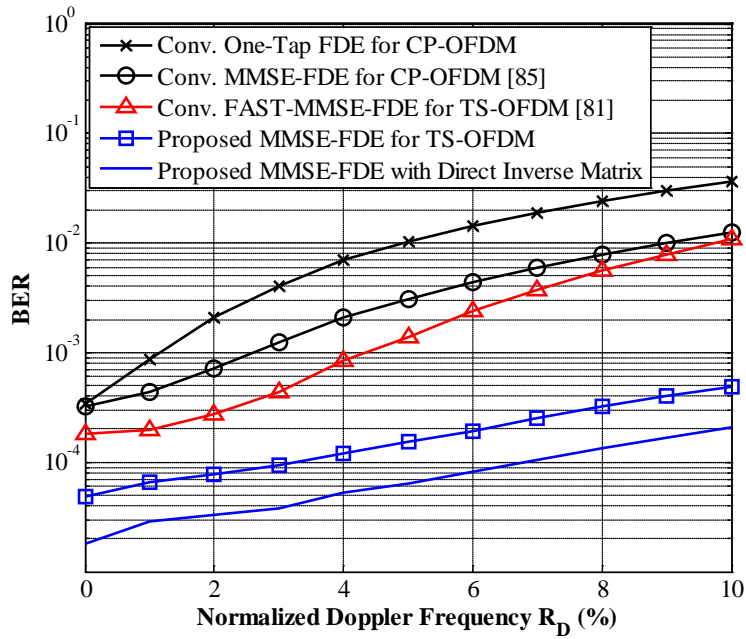


Figure 4.3: BER performance for proposed MMSE-FDE method when changing R_D at $C/N=35\text{dB}$.

4.4 Performance Evaluation for Proposed MMSE-FDE Method

Figure 4.4 shows the BER performances for the proposed MMSE-FDE and conventional MMSE-FDE methods when changing operation C/N at normalized Doppler frequency $R_D=5\%$. In the figure, the BER performance for the proposed MMSE-FDE method of using the direct inverse matrix calculation is also shown as the purpose of comparison with the proposed MMSE-FDE method with the fast algorithm for inverse matrix calculation. From the figure, it can be observed that the proposed method with $Q_1=5$ can achieve better BER performance than the conventional MMSE-FDE methods. Here it should be noted that the degradation of BER performances as compared with the proposed method are caused by the lower CIR estimation accuracy of using pilot subcarriers and no acquisition of frequency diversity gain in the conventional MMSE-FDE for CP-OFDM, and the assumption of linear changing of CIR and the approximation of first order Maclaurin's expansion in the FAST-MMSE-FDE for TS-OFDM, respectively.

From Table 4.1 and assuming the above actual parameters, the ratios of complexity for the proposed MMSE-FDE method for TS-OFDM method over the conventional MMSE-FDE for CP-OFDM and FAST-MMSE-FDE for TS-OFDM methods are 2.4 and 1.1 times, respectively. From these complexities and BER performances in Figure 4.2 and 4.3, it can be concluded that proposed MMSE-FDE method with the fast algorithm for inverse matrix calculation can achieve better BER performance with small increment of complexity under higher mobile environments.

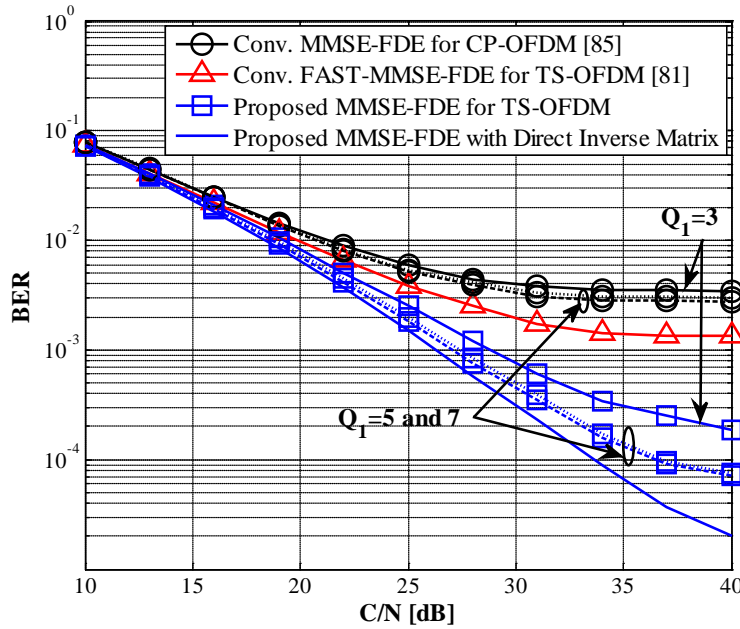


Figure 4.4: BER performance of proposed MMSE-FDE method when changing C/N at $R_D=5\%$.

4.5 Conclusions

This chapter proposed low-complexity MMSE-FDE method for the TS-OFDM signal under higher mobile environments. The salient features of proposed MMSE-FDE method are to enable the acquisition of the frequency diversity gain by using the enhanced CIR matrix, and to enable the reduction of complexity by using the fast algorithm for inverse matrix calculation. From the computer simulation results, this chapter confirmed that the proposed MMSE-FDE method for TS-OFDM signal can achieve better BER performance than the conventional MMSE-FDE methods with keeping lower complexity in higher time-varying fading channels.

CHAPTER 5

TIME DOMAIN EQUALIZATION METHOD FOR TS-OFDM SIGNAL UNDER HIGHER MOBILE ENVIRONMENTS

In higher time-varying fading channels, the signal quality of orthogonal frequency division multiplexing (OFDM) technique would be degraded relatively due to the occurrence of inter-carrier interference (ICI). To solve this problem, this chapter proposes a time domain equalization (TDE) method which can achieve better bit error rate (BER) performance with keeping lower computation complexity even in higher time-varying fading channels. The salient feature of proposed TDE method is to employ the partial differentiation for the time domain channel impulse response (CIR) matrix for solving the maximum likelihood (ML) equation in which the time domain CIR matrix becomes a symmetric banded matrix. From this feature, a low-complexity fast algorithm for inverse matrix calculation can be employed in the calculation of inverse matrix with keeping the same accuracy as that for the direct inverse matrix calculation. This chapter presents various computer simulation results to demonstrate the effectiveness of proposed TDE method for the TS-OFDM signal as comparing with conventional frequency domain equalization (FDE) methods under higher mobile environments.

5.1 Introduction

Orthogonal frequency division multiplexing (OFDM) has been employed as an efficient transmission technique in various wireless communications systems which require the reliable high data rate communications in the frequency-selective multipath fading channels [88]. Up to today, OFDM has been adopted as the standard transmission technique in the digital audio broadcasting (DAB), digital video broadcasting (DVB), wireless local area network (WLAN) and the fourth generation (4G) cellular systems [2]. The salient feature of OFDM technique is to employ the guard interval (GI) for avoiding the inter-symbol interference (ISI) with keeping the orthogonality among OFDM subcarriers even in multipath fading channels. To realize the property of this function, the cyclic prefix OFDM (CP-OFDM), zero padding OFDM (ZP-OFDM) and time domain training sequence inserted OFDM (TS-OFDM) techniques were proposed in the transmission of OFDM signal [59]. The CP-OFDM employs the CP as the GI, the ZP-OFDM employs the zero padding between OFDM data symbols as the role of GI which enables the reduction of transmission power and the TS-OFDM employs the pre-designed time domain training sequence such as a pseudo-noise (PN) sequence [89] or Chu sequence [74] as the role of GI besides for using in the channel estimation.

In the OFDM signal under the static or lower mobile environments, the channel impulse response (CIR) can be assumed to be the time-invariant within one OFDM symbol period. From this fact, the simple frequency domain equalization (FDE) method with one-tap filter can be used to compensate the distortion of multipath fading. However, the CIR is no more constant even within one OFDM symbol period in higher time-varying fading channels which are experienced by the users on the high speed trains or vehicles. In higher time-varying fading channels, the orthogonality among OFDM subcarriers is no more satisfied which leads the fatal degradation of bit error rate (BER) performance due to the occurrence of inevitable inter-carrier interference (ICI) caused by the higher Doppler frequency spread [66].

To solve the above problem, many frequency domain equalization methods were proposed to mitigate the ICI in higher time-varying channels [67,72,73,81,85,90,91,92]. These methods are designated as the frequency domain equalization (FDE) in which the equalization processing for the mitigation of ICI is conducted in the frequency domain. In [90] and [91], the ICI self-cancellation schemes were proposed to mitigate ICI at the cost of degradation in the transmission data rate. In [67], the FDE method with the minimum mean square error (MMSE-FDE) and successive interference cancellation (SIC) equalization methods were proposed for the CP-OFDM signal. These methods are required to employ the direct inverse matrix calculation for the channel frequency response (CFR) matrix in solving the simultaneous equations. However, the computation complexity for the inverse matrix calculation required at every symbol is relatively higher which leads serious problem in the implementation of practical receiver. To solve this problem, [85] proposed a low-complexity MMSE-FDE method for CP-OFDM signal with the fast algorithm for inverse matrix calculation [87]. In this method, the full elements of CFR matrix is approximated by a banded matrix so as to enable the employment of the fast algorithm for inverse matrix calculation. However the BER performance would be degraded in higher time-varying fading channels due to the approximation for the full elements of CFR matrix by the banded matrix. In [92], the fast sub-optimal FAST-MMSE-FDE method was proposed for the ZP-OFDM signal under the assumption of perfect channel knowledge. Although this method can achieve lower

5.1 Introduction

complexity by assuming the linear changing of CIR within one OFDM symbol period, it has a difficulty to estimate the CFR matrix precisely by using the pilot subcarriers in the frequency domain because the received pilot subcarriers are also affected by the ICI in higher time-varying fading channels [72].

To solve the above problem on the CFR estimation by using the pilot subcarriers for the CP-OFDM and ZP-OFDM signals in higher time-varying fading channels, a pseudo noise (PN) time domain sequence is employed as the training sequence (TS) in the estimation of CFR as well as the role of GI for the TS-OFDM signal [73]. In [73], since an overlap and add frequency domain equalization (OLA-FDE) method is employed, the property of circular convolution is no more satisfied in higher time-varying fading channels which leads the fatal degradation of BER performance. In [81], the low-complexity OLA-MMSE-FDE and the FAST-MMSE-FDE methods were proposed for the TS-OFDM signal. These methods enable the considerable reduction of computation complexity by using the Maclaurin's expansion approximation technique in the calculation of inverse matrix under the assumption that the CIR is changing linearly within one symbol period. However the approximation of linear changing of CIR is no more effective in higher time-varying fading channels which leads the degradation of BER performance.

From the above backgrounds, this chapter proposes an equalization method of using the CIR matrix in the time domain instead of using the CFR matrix for the conventional FDE method. Hereafter the proposed method is designated as the time domain equalization (TDE) in which the equalization processing for the mitigation of ICI is conducted in the time domain. The feature of proposed TDE method is to employ the partial differentiation for the time domain CIR matrix for solving the maximum likelihood (ML) equation in which the time domain CIR matrix becomes a symmetric banded matrix. This feature enables to employ the fast algorithm for inverse matrix calculation which can achieve the same BER performance with much lower computation complexity as compared with that for the direct inverse matrix calculation [87]. These are completely different features from the conventional FDE method of which CFR matrix is the full elements of matrix. The proposed TDE method can also obtain the frequency diversity gain at the fading deep dips [86] which enables to achieve better BER performance than the conventional FDE methods of using the CFR matrix as referred in the above [67,72,73,81,85,90,91,92].

The remainder of this chapter is organized as follows. Section 5.2 proposes the time domain equalization (TDE) method with the fast algorithm for inverse matrix calculation for the TS-OFDM signal. Section 5.3 evaluates the overall computation complexity for the proposed TDE method as comparing with the various conventional FDE methods. Section 5.4 presents various computer simulation results to verify the effectiveness of proposed TDE method for the TS-OFDM signal as comparing with various conventional FDE methods both for the CP-OFDM and TS-OFDM signals. Finally, Section 5.5 draws some conclusions.

5.2 Proposal of Time Domain Equalization Method for TS-OFDM

This section presents the system model for the proposed TDE method with a new design of TS signal by using a time domain triangular window function for the TS-OFDM. This section also proposes the TDE method of using a low-complexity fast algorithm for inverse matrix calculation which can achieve better BER performance than that for the conventional FDE methods with keeping lower complexity even in higher time-varying fading channels.

5.2.1 System Model for Proposed TDE Method

Figure 5.1 shows the structure of transceiver for the proposed TDE method for the TS-OFDM signal. At the transmitter, the input data information is modulated by the quadrature-phase shift keying (QPSK) or quadrature-amplitude modulation (QAM) method in the frequency domain. The modulated signal $X(m, k)$ at the k -th subcarrier of m -th symbol is converted to the time domain signal by N -point inverse fast Fourier transform (IFFT) which can be given by,

$$x(m, n) = \frac{1}{\sqrt{N}} \sum_{k=0}^{N-1} X(m, k) \cdot e^{j \frac{2\pi kn}{N}}, \quad 0 \leq n \leq N-1 \quad (5.1)$$

where $x(m, n)$ is the time domain OFDM signal at the n -th time sample of m -th symbol.

Figure 5.2(a) shows the frame format for the proposed TS-OFDM signal with the time domain triangular window function. In the proposed frame format, the time domain TS1 and TS2 with the length of S samples are inserted at the start of every data symbol in which the length of S should be taken longer than the number of delay paths (L) occurred in the multipath fading channel. The time domain TS would be used in the estimation of CIR at every sampling time and also used as the role of GI to avoid the inter-symbol interference (ISI). The data pattern for the proposed TS1 and TS2 signals at the m -th symbol employs the same data pattern which is represented by $c(m, s)$. Furthermore, the TS1 and TS2 signals at the m -th data symbol are multiplied by the time domain triangular window function of $\Gamma(s)$ to suppress the leakage of PSD as shown in Figure 5.1. The time domain triangular window function $\Gamma(s)$ with the length of $2S$ samples is given by,

$$\Gamma(s) = \begin{cases} (s+1)/S, & 0 \leq s \leq S-1 \\ 2-s/S, & S \leq s \leq 2S-1 \end{cases} \quad (5.2)$$

The proposed TS1 and TS2 signals at the m -th data symbol after multiplying $\Gamma(s)$ can be expressed by,

$$C(m, s) = \begin{cases} d_1(m, s) = c(m, s) \cdot \Gamma(s), & 0 \leq s \leq S-1 \\ d_2(m, s) = c(m, s-S) \cdot \Gamma(s), & S \leq s \leq 2S-1 \end{cases} \quad (5.3)$$

where $C(m, s)$ with the length of $2S$ samples is the sequential data pattern of TS1 and TS2 from 0 to $2S-1$ in the time domain. Then, $C(m, s)$ is inserted at the start of every OFDM data symbol which is represented by,

5.2 Proposal of Time Domain Equalization Method for TS-OFDM

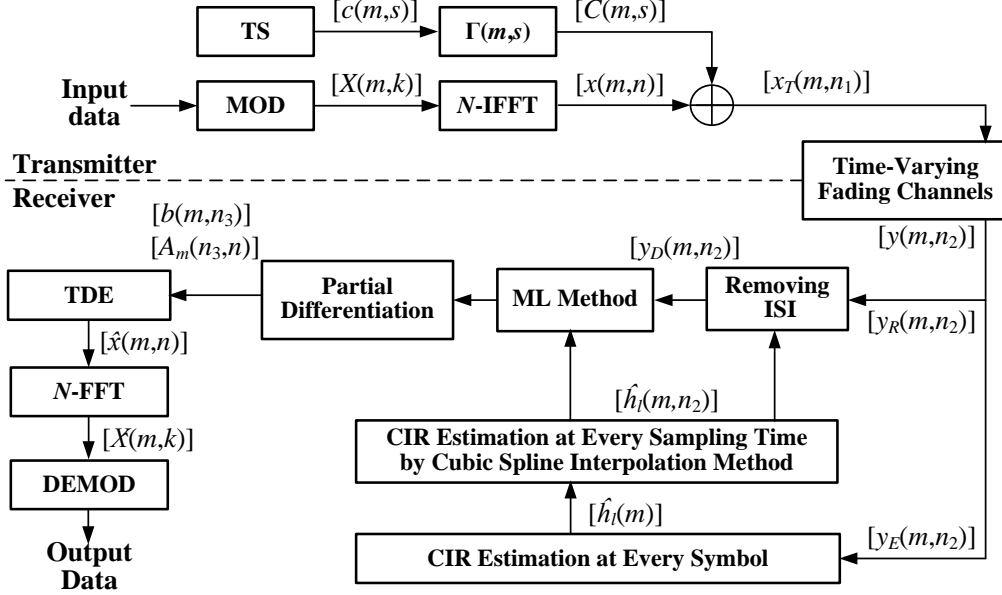


Figure 5.1: Structure of transceiver for proposed TDE method.

$$x_T(m, n_1) = \begin{cases} C(m, n_1), & 0 \leq n_1 \leq 2S - 1 \\ x(m, n_1 - 2S), & 2S \leq n_1 \leq N + 2S - 1 \end{cases} \quad (5.4)$$

where $x_T(m, n_1)$ is the transmission signal including the TS signal at the n_1 -th sample of m -th symbol with the length of $N+2S$ samples. Assuming that the synchronization of symbol timing at the receiver is perfect, the received time domain OFDM signal $y(m, n_2)$ at the n_2 -th sampling time of m -th symbol after passing through the multipath fading channels as shown in Figure 5.2(b) can be expressed by,

$$y(m, n_2) = \sum_{l=0}^{L-1} h_l(m, n_2) \cdot x_T(m, n_2 - l) + w(m, n_2), \quad 0 \leq n_2 \leq N + 2S - 1 \quad (5.5)$$

where $h_l(m, n_2)$ is the CIR at the n_2 -th time sample of m -th data symbol for the l -th delay path occurred in the actual time-varying fading channels, $w(m, n_2)$ is the additive white Gaussian noise (AWGN) with the variance of σ^2 , and L is the number of delay paths. As shown in Figure 5.1 and 2(b), the received signal $y(m, n_2)$ can be divided into two parts which consist of the observation period for the CIR estimation $y_E(m, n_2)$ with the length of S samples and for the data demodulation period $y_R(m, n_2)$ with the length of $P=N+S$ samples, respectively.

The received time domain TS2 signal $y_E(m, n_2)$ which be used in the estimation of CIR at every symbol can be expressed by,

$$y_E(m, n_2) = \sum_{l=0}^{L-1} h_l(m, n_2) \cdot d_2(m, n_2 - l) + w(m, n_2), \quad 0 \leq n_2 \leq S - 1 \quad (5.6)$$

where $d_2(m, n_2)$ is the TS2 signal with the triangular window function given in (5.3). Here it should be noted that the CIR is assumed to be constant during the short time period of TS1 and TS2 even in higher time-varying fading channels. Assuming $\hat{h}_l(m)$ is unknown parameters for the CIR at the m -th symbol, the expected received time domain TS2 signal $\hat{y}_E(m, n_2)$ can be given by,

$$\hat{y}_E(m, n_2) = \sum_{l=0}^{S-1} \hat{h}_l(m) \cdot d_2(m, n_2 - l), \quad 0 \leq n_2 \leq S-1 \quad (5.7)$$

The unknown parameters of complex amplitude of $\hat{h}_l(m)$ at the m -th symbol can be estimated by using the maximum likelihood (ML) estimation method under the constraint with minimizing the difference between the actual received TS signal in (5.6) and the expected received signal in (5.7). Here the estimated CIR $\hat{h}_l(m)$ corresponds to the CIR at the middle sampling time of TS1. The time domain CIR $\hat{h}_l(m, n_2)$ at every sampling time can be estimated by applying the cubic spline interpolation method for the CIR estimated at every symbol over one frame [78].

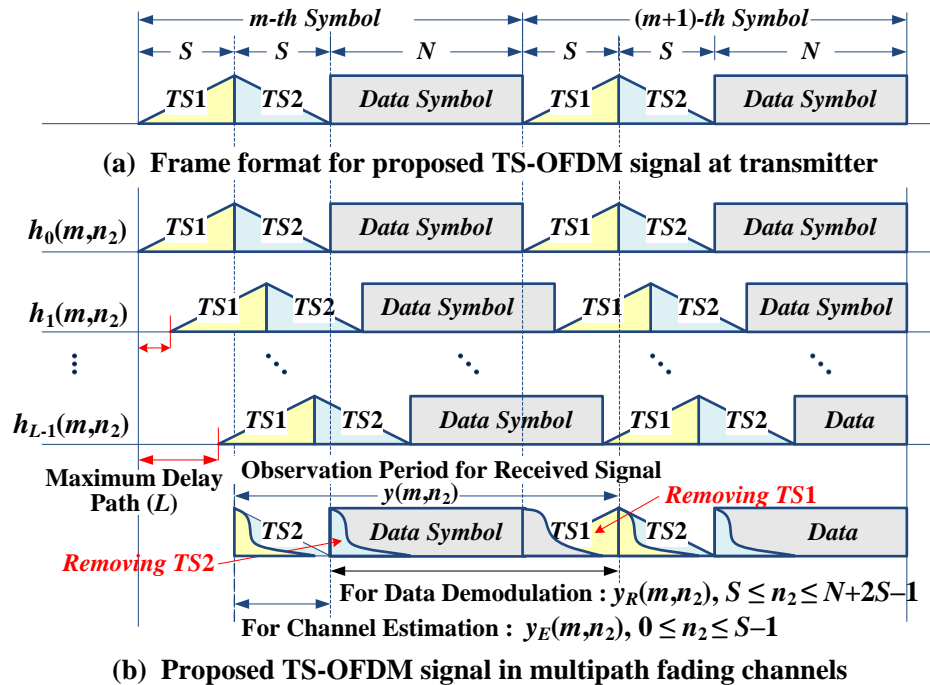


Figure 5.2: Structure of TS-OFDM signal in multipath fading channels.

5.2.2 Low-Complexity Time Domain Equalization Method

Considering the observation period for the data demodulation $y_R(m, n_2)$ as shown in Figure 5.2(b), the received time domain data signal can be given by,

$$y_R(m, n_2) = \sum_{l=0}^{L-1} h_l(m, n_2) \cdot x_T(m, n_2 - l) + w(m, n_2), \quad S \leq n_2 \leq N + 2S - 1 \quad (5.8)$$

where $x_T(m, n_2)$ is the transmitted time domain signal given in (5.4) and $h_l(m, n_2)$ is the time domain CIR at every sampling time in the actual time-varying fading channels. From Figure 5.2(b), it can be observed that the received signal in (5.8) includes the ISI from $d_2(m, s)$ (TS2 of current symbol) and $d_1(m+1, s)$ (TS1 of next symbol). By using the estimated CIR $\hat{h}_l(m, n_2)$ at every sampling time and the known data patterns of TS1 and TS2 with the time domain triangular window function given in (5.3), the ISI from the TS signal at the both ends of data symbol can be removed by using the following equation.

$$y_D(m, n_2) = \begin{cases} y_R(m, n_2) - \sum_{l=n_2-S+1}^{S-1} \hat{h}_l(m, n_2) \cdot d_2(m, n_2 - l), & (S \leq n_2 \leq 2S - 2) \\ y_R(m, n_2), & (2S - 1 \leq n_2 \leq N + S - 1) \\ y_R(m, n_2) - \sum_{l=0}^{n_2-N-S} \hat{h}_l(m, n_2) \cdot d_1(m+1, n_2 - N - S - l), & (N + S \leq n_2 \leq N + 2S - 2) \end{cases} \quad (5.9)$$

In the derivation of (5.9), the following relationships are used.

$$n_2 - l \leq S - 1, \quad x_T(m, n_2 - l) = d_2(m, n_2 - l) \quad (5.10)$$

$$n_2 - l \geq N + S, \quad x_T(m, n_2 - l) = d_1(m+1, n_2 - N - S - l) \quad (5.11)$$

where $y_D(m, n_2)$ in (5.9) is the received time domain signal after removing the ISI from the TS. The received time domain signal $y_D(m, n_2)$ over the observation period with P ($=N+S-1$) samples which includes the time domain data symbol and TS1 after removing the ISI can be used in the proposed TDE. By using the observation period of P samples including the TS signal, the proposed TDE method can achieve the frequency diversity gain at the fading deep dips which could achieve better BER performance than the conventional FDE methods with the observation period of N samples both under the quasi-static and higher mobile environments [86].

When the transmitted time domain data signal $\hat{x}(m, n)$ is assumed as the unknown parameters, the expected received signal $\hat{y}_D(m, n_2)$ without the ISI which corresponds to the actual received signal in (5.9) can be expressed by,

$$\hat{y}_D(m, n_2) = \begin{cases} \sum_{l=0}^{n_2-S} \hat{h}_l(m, n_2) \hat{x}(m, n_2 - S - l), & (S \leq n_2 \leq 2S - 2) \\ \sum_{l=0}^{S-1} \hat{h}_l(m, n_2) \hat{x}(m, n_2 - S - l), & (2S - 1 \leq n_2 \leq N + S - 1) \\ \sum_{l=n_2-N-S+1}^{S-1} \hat{h}_l(m, n_2) \hat{x}(m, n_2 - S - l), & (N + S \leq n_2 \leq N + 2S - 2) \end{cases} \quad (5.12)$$

The unknown parameter of time domain data signal $\hat{x}(m, n)$ which corresponds to the transmitted time domain data given in (5.1) can be estimated by solving the following ML

5.2 Proposal of Time Domain Equalization Method for TS-OFDM

equation under the constraint for minimizing the difference between the actual received signal $y_D(m, n_2)$ in (5.9) and the expected received signal $\hat{y}_D(m, n_2)$ in (5.12).

$$\Gamma = \arg \min_{\hat{x}(m, n)} \left[\sum_{n_2=S}^{N+2S-2} \|y_D(m, n_2) - \hat{y}_D(m, n_2)\|^2 \right] \quad (5.13)$$

The ML equation in (5.13) can be transformed to the simultaneous equations by taking the partial differentiation for the unknown parameters $\hat{x}^*(m, n_3)$, ($0 \leq n_3 \leq N-1$) which can be expressed by,

$$\frac{\partial \Gamma}{\partial \hat{x}^*(m, n_3)} = \frac{\partial \left(\sum_{n_2=S}^{N+2S-2} \|y_D(m, n_2) - \hat{y}_D(m, n_2)\|^2 \right)}{\partial \hat{x}^*(m, n_3)} = 0 \quad (5.14)$$

where $*$ represents the conjugate complex. By using (5.14), the ML equation in (5.13) can be expressed by the following simultaneous equations with N unknown time domain data information of $[\hat{x}(m, n)]$.

$$[b(m, n_3)]_{N \times 1} = [A_m(n_3, n)]_{N \times N} [\hat{x}(m, n)]_{N \times 1} \quad (5.15)$$

where $[b(m, n_3)]$ and $[A_m(n_3, n)]$ are the received time domain signal and the CIR matrix both after the partial differentiation, respectively which are given by,

$$\begin{aligned} [b(m, n_3)]_{N \times 1} &= \sum_{n_2=S}^{N+2S-2} y_D(m, n_2) \frac{\partial \hat{y}_D^*(m, n_2)}{\partial \hat{x}^*(m, n_3)} \\ &= [\hat{h}_l^H(m, n_3)]_{N \times P} [y_D(m, n_2)]_{P \times 1}, \quad 0 \leq n_3 \leq N-1 \end{aligned} \quad (5.16)$$

$$\begin{aligned} [A_m(n_3, n)]_{N \times N} &= \sum_{n_2=S}^{N+2S-2} \hat{y}_D(m, n_2) \frac{\partial \hat{y}_D^*(m, n_2)}{\partial \hat{x}^*(m, n_3)} \\ &= [\hat{h}_l^H(m, n_3)]_{N \times P} [\hat{h}_l(m, n_2)]_{P \times N}, \quad 0 \leq n_3 \leq N-1 \end{aligned} \quad (5.17)$$

where $(\cdot)^H$ is the Hermitian transposition. In the deviation of (5.16) and (5.17), the following relationships are used.

$$n_3 = n_2 - S - l \quad \text{in} \quad \frac{\partial \hat{y}_D^*(m, n_2)}{\partial \hat{x}^*(m, n_3)} \quad (5.18)$$

$$n = n_2 - S - l \quad \text{in} \quad \hat{y}_D(m, n_2) \quad (5.19)$$

From (5.15), the unknown parameters $[\hat{x}(m, n)]$ can be solved by using the inverse matrix of $[A_m(n_3, n)]$ which can be given by,

$$[\hat{x}(m, n)]_{N \times 1} = [A_m(n_3, n)]_{N \times N}^{-1} [b(m, n_3)]_{N \times 1} \quad (5.20)$$

From (5.20), the proposed TDE method is required for the inverse matrix calculation which leads relatively high computation complexity with the order of $O(N^3)$. To solve this problem, this chapter proposes a low-complexity TDE method by using the good property of time domain CIR matrix $[A_m(n_3, n)]$ given after the partial differentiation. From (5.17), the CIR matrix $[A_m(n_3, n)]$ can be represented by,

5.2 Proposal of Time Domain Equalization Method for TS-OFDM

$$A_{i,j} = \begin{bmatrix} A_{0,0} & A_{0,1} & \cdots & A_{0,S-1} & 0 & \cdots & 0 \\ A_{0,1}^H & A_{1,1} & & & \ddots & \ddots & \vdots \\ \vdots & & \ddots & & & \ddots & 0 \\ A_{0,S-1}^H & & & \ddots & & & A_{N-S,N-1} \\ 0 & \ddots & & & \ddots & & \vdots \\ \vdots & \ddots & \ddots & & & A_{N-2,N-2} & A_{N-2,N-1} \\ 0 & \cdots & 0 & A_{N-S,N-1}^H & \cdots & A_{N-2,N-1}^H & A_{N-1,N-1} \end{bmatrix}_{N \times N} \quad (5.21)$$

In (5.21), $A_m(i,j)$ in (5.17) is represented by $A_{i,j}$ and the index of m -th symbol is omitted for brevity. From (5.21), it can be seen that the matrix is the banded matrix with the upper and lower bandwidth (Q_1) of length ($S-1$) whose non-zero entries are confined to a diagonal bands. Also the lower band matrix with the index of (j,i) below the diagonal terms is the Hermitian transpose of upper band matrix with index of (i,j) . From these features, the CIR matrix $[A_m(n_3,n)]$ after the partial differentiation becomes the symmetric banded matrix with the block size of $(S \times S)$. From this fact, it is possible to employ the low-complexity fast algorithm for inverse matrix calculation [87] for solving (5.20). This feature of time domain CIR matrix for the proposed TDE method is completely different from the frequency domain CFR matrix for the conventional FDE methods of which CFR matrix is the full elements of matrix [67,72,73,81,85,90,91,92]. Here it should be noted that although the CFR matrix of the conventional MMSE-FDE method for the CP-OFDM signal is not the banded matrix, it is possible to employ the fast algorithm for inverse matrix calculation by assuming that the elements in the CFR matrix both at the lower and upper sides of diagonal bands are small enough [85]. However this assumption would be no more effective in higher time-varying fading channels because the elements both at the lower and upper sides of diagonal bands in the CFR matrix are unable to be approximated as the negligible quantity. This means that the conventional MMSE-FDE method with the fast algorithm for inverse matrix calculation in [85] can achieve the reduction of computation complexity at the cost of considerable BER degradation in higher time-varying fading channels.

In [87], the fast algorithm for inverse matrix calculation is proposed for the symmetric banded matrix which can calculate the inverse matrix as the same accuracy as that for the direct inverse matrix calculation with much lower computation complexity. The key idea of this algorithm is to construct the small hierarchy of Schur complement blocks and then extracting the inverse matrix of diagonal hierarchy of Schur complements blocks. In (5.21), the size of small hierarchy of Schur complement blocks is equal to the length of TS ($=S$). By using this algorithm, the inverse matrix of (5.21) can be calculated perfectly with the same accuracy as that for the direct inverse matrix calculation. The order of computation complexity required in the calculation of inverse matrix for the banded matrix $[A_m(n_3,n)]$ with the size of $(N \times N)$ when employing the fast algorithm for inverse matrix calculation can be reduced to $O[3NS^2]$. This complexity is much smaller than that for the direct inverse matrix calculation which requires the complexity $O[N^3]$. The overall computation complexities for the proposed TDE and conventional FDE methods are evaluated in Section 5.3.

By converting the estimated time domain data information $[\hat{x}(m,n)]$ in (5.20) to the frequency domain by using N -point FFT, the frequency domain data information $[\hat{X}(m,k)]$ can be obtained and demodulated as shown in Figure 5.1.

5.3 Evaluation of Computation Complexity

This section evaluates the computation complexity for the proposed TDE method. Table 5.1 shows the order of complexities for the proposed TDE method when using the direct inverse matrix calculation and the low-complexity fast algorithm for inverse matrix calculation. In the table, the conventional MMSE-FDE method for the CP-OFDM [67,85], the OLA-MMSE-FDE method for the TS-OFDM, and the FAST-MMSE-FDE method for the TS-OFDM [81] are also shown for the purpose of comparisons with the proposed TDE method.

In the proposed TDE method for the TS-OFDM with the fast algorithm for inverse matrix calculation, the removing of ISI incurred both ends of data symbol from the TS given in (5.9) requires the complexity $O[S^2-S]$. The construction of the time domain received signal $[b(m, n_3)]$ and the CIR matrix $[A_m(n_3, n)]$ with the partial differentiation given in (5.16) and (5.17) require the complexity $O[NS]$ and $O[NS^2]$, respectively. The fast algorithm for inverse matrix calculation for the symmetric banded matrix $[A_m(n_3, n)]$ given in (5.21) requires the complexity $O[3NS^2]$ [87]. The multiplication of $[A_m(n_3, n)]^{-1}$ and $[b(m, n_3)]$ matrixes which corresponds to the time domain equalization to obtain the time domain signal $[\hat{x}(m, n)]$ in (5.20) requires the complexity $O[N^2]$. Finally, N -point FFT to $[\hat{x}(m, n)]$ for obtaining the frequency domain data information $[\hat{X}(m, k)]$ requires the complexity $O[N \log_2 N]$.

In the conventional MMSE-FDE method for the CP-OFDM [85], the CFR matrix is approximated by the banded matrix with the block size $(Q_1+1) \times (Q_1+1)$, where Q_1 is the lower and upper bandwidth of approximated CFR banded matrix. The construction of the approximated banded CFR matrix with the upper and lower bandwidth of Q_1 and the received frequency domain signal matrix including one N -point FFT require the complexity $O[(2Q_1+2)N \log_2 N + N(Q_1+1)^2 + N(Q_1+1) + N \log_2 N]$. The fast algorithm for inverse matrix calculation for the approximated CFR banded matrix with the bandwidth of Q_1 requires the complexity $O[3N(Q_1+1)^2]$. Finally, the frequency domain equalization for obtaining the frequency domain data information requires the complexity $O[N^2]$.

In the conventional OLA-MMSE-FDE and FAST-MMSE-FDE methods for the TS-OFDM signals, the Maclaurin's expansion algorithm is employed for the approximation of inverse matrix calculation [81]. The construction of CFR matrix and the received frequency domain signal matrix for the conventional OLA-MMSE-FDE and FAST-MMSE-FDE methods require the complexity $O[N \log_2 N + 3N]$ and $O[P^2 + 3P]$, respectively. In [81], the order of total complexity both for the inverse matrix calculation with the order of Maclaurin's expansion of Q_2 and the equalization in the frequency domain are given by $O[2Q_2 N \log_2 N + (2Q_2 + 3)N]$ for the OLA-MMSE-FDE method and $O[N^2 + (2Q_2 + 1)P^2 + (2Q_2 + 3)P]$ for the FAST-MMSE-FDE method, respectively. Here it should be noted that the order of complexities for N -points FFT (where N is the power of 2) and P -points DFT (where P is not the power of 2) are given by $O[N]$ and $O[P]$, respectively in [81]. However, these complexities are given by $O[N \log_2 N]$ and $O[P^2]$, respectively in this chapter. By using Table 5.1, the comparisons of overall computation complexities between the conventional FDE and proposed TDE methods when assuming the actual parameters are evaluated in Section 5.4.

5.3 Evaluation of Computation Complexity

Table 5.1: Order of computation complexity for proposed TDE and conventional FDE methods.

Equalization methods with direct inverse matrix calculation			
Method	Removing ISI	Construction of channel matrix and received signal	Calculation of inverse matrix and equalization
MMSE-FDE [67]	N/A	$O[N^3+2N^2\log_2N+N^2+N\log_2N]$	$O[N^3+N^2]$
OLA-MMSE-FDE [81]	$O[S^2-S]$	$O[N^3+2N^2\log_2N+N^2+N\log_2N]$	$O[N^3+N^2]$
FAST-MMSE-FDE [81]	$O[S^2-S]$	$O[P^3+2SP^2+2P^2]$	$O[P^3+P^2+N^2]$
Proposed TDE	$O[S^2-S]$	$O[NS^2-NS]$	$O[N^3+N^2+N\log_2N]$
Equalization methods with complexity reduction algorithms			
Method	Removing ISI	Construction of channel matrix and received signal	Calculation of inverse matrix and equalization
MMSE-FDE [85]	N/A	$O[(2Q_1+2)N\log_2N+N(Q_1+1)^2+N(Q_1+1)+N\log_2N]$	$O[3N(Q_1+1)^3+N^2]$
OLA-MMSE-FDE [81]	$O[S^2-S]$	$O[N\log_2N+3N]$	$O[2Q_2N\log_2N+(2Q_2+3)N]$
FAST-MMSE-FDE [81]	$O[S^2-S]$	$O[P^2-3P]$	$O[(2Q_2+1)P^2+(2Q_2+3)P+N^2]$
Proposed TDE	$O[S^2-S]$	$O[NS^2-NS]$	$O[3NS^2+N^2+N\log_2N]$

N is the number of FFT/IFFT points, S is the length of TS, Q_1 is the bandwidth of CFR matrix, Q_2 is the order of Maclaurin's expansion, and $P=N+S-1$.

5.4 Performance Evaluation for Proposed TDE Method

In this section, various computer simulation results are presented for the proposed TDE method as comparing with various conventional FDE methods both for the CP-OFDM and TS-OFDM signals. The simulation parameters to be used in the following evaluations are listed in Table 5.2. In the conventional MMSE-FDE with the fast algorithm for inverse matrix calculation for the CP-OFDM signal, the CFR matrix is approximated by the banded matrix with the lower and upper bandwidth of $Q_1=2$ as using in [85] and $Q_1=15$ which is the same bandwidth for the proposed TDE method with the symmetric banded matrix. In the conventional FDE with the OLA-MMSE-FDE and FAST-MMSE-FDE methods for the TS-OFDM signals, the order of Maclaurin's expansion in the calculation of inverse matrix is set to $Q_2=1$ as using in [81]. The Rayleigh multipath fading channel is assumed by the Jake's Doppler spectrum model with an exponential power delay profile having the power decay constant -1 dB and the length of delay path $L=14$. The length of TS both for the proposed and conventional TS-OFDM signals is taken by $S=16$. In the following evaluations, the normalized Doppler frequency $R_D=f_{\text{dmax}}/\Delta f$ (%) is employed as the measure of mobile environments in which f_{dmax} is the maximum Doppler frequency and Δf is the OFDM subcarrier spacing.

Table 5.2: Simulation parameters.

Parameter	Value
Number of data subcarriers (N)	128
Number of FFT/IFFT points (N)	128
Length of time domain TS for TS-OFDM (S)	16
Length of GI for CP-OFDM (N_g)	16
Bandwidth of approximated banded matrix (Q_1)	2 and 15
Order of Maclaurin's expansion (Q_2)	1
Number of symbols per one frame (M)	64
Allocated OFDM frequency bandwidth	2MHz
OFDM subcarrier spacing (Δf)	78.125kHz
Modulation method for data subcarriers	QPSK
Modulation method for data subcarriers	QPSK and 16QAM
Radio carrier frequency	5GHz
Rayleigh multipath fading channel model	
Delay profile	Exponential
Decay constant	-1
Number of delay paths (L)	14
Number of scattered rays per one delay path	20
Normalized Doppler frequency (R_D)	0~10%

5.4 Performance Evaluation for Proposed TDE Method

Figure 5.3 shows the BER performances of the proposed TDE method for the TS-OFDM signal with the fast algorithm for inverse matrix calculation when changing the normalized Doppler frequency R_D . The modulation method is QPSK and the C/N is 35dB. In the figure, the conventional MMSE-FDE for CP-OFDM of using the approximated banded matrix with the lower and upper bandwidth of $Q_1=2$ and $Q_1=15$ [85], and the OLA-MMSE-FDE and FAST-MMSE-FDE methods for TS-OFDM with the Maclaurin's expansion order of $Q_2=1$ [81] are also shown as the purpose of comparisons with the proposed TDE method. In the conventional MMSE-FDE for the CP-OFDM signal, the scattered pilot subcarriers in the frequency domain are usually employed in the estimation of CFR matrix. However the estimation accuracy of CFR matrix by using the scattered pilot subcarriers would be degraded due to the occurrence of ICI for the received pilot subcarriers in higher time-varying fading channels [72]. From this fact, this chapter assumes that the CIR estimated by the proposed TS-OFDM signal is employed in the construction of CFR matrix even for the conventional MMSE-FDE method for the CP-OFDM signal so as to compare the BER performance with the proposed TDE method fairly under the assumption of same channel estimation accuracy.

From the figure, it can be observed that the proposed TDE method for the TS-OFDM signal with the fast algorithm for inverse matrix calculation shows much better BER performance than the conventional OLA-MMSE-FDE and FAST-MMSE-FDE methods with the Maclaurin's expansion method [81] and MMSE-FDE method [85] even when the banded matrix is approximated by $Q_1=15$. These are the reasons that the channel frequency matrix for the conventional MMSE-FDE method is generated by using the approximated banded matrix and the OLA-MMSE and FAST-MMSE methods are generated assuming the linear approximation of CIR in the time-varying fading channels. These approximation and assumption would lead the inevitable error in the calculation of inverse matrix especially in higher time-varying fading channels. Here it should be noted that the BER performance of proposed TDE method with the fast algorithm for inverse matrix calculation shows the same BER performance as that for using the direct inverse matrix calculation as explained in the sub-section 5.2.3 of Section 5.2.

Figure 5.4 and 5.5 show the BER performances versus C/N for the proposed TDE method with the fast algorithm for inverse matrix calculation when the modulation method is QPSK and the normalized Doppler frequencies are $R_D=3\%$ and 10% which correspond to lower and higher mobile environments, respectively. Here the normalized Doppler frequencies $R_D=3\%$ and 10% correspond to the vehicle speeds at 100km/hrs and 340km/hrs, respectively. In the figures, the BER performances of conventional low-complexity MMSE-FDE for CP-OFDM of using the approximated banded matrix with the bandwidth of $Q_1=2$ and $Q_1=15$ [85], and the OLA-MMSE-FDE and FAST-MMSE-FDE methods for TS-OFDM with the Maclaurin's expansion order of $Q_2=1$ [81] are also shown as the purpose of comparisons with the proposed TDE method. From Figure 5.4 and 5.5, it can be observed that the proposed method shows much better BER performance than the conventional methods under both lower and higher mobile environments. However the conventional methods show better BER performance only under lower mobile environments because of employing the approximation in the construction of CFR matrix so as to reduce the computation complexity. The proposed TDE method also shows better BER performance than the conventional MMSE-FDE method even when the banded matrix is approximated by $Q_1=15$ which corresponds to the same computation complexity as the proposed TDE method.

5.4 Performance Evaluation for Proposed TDE Method

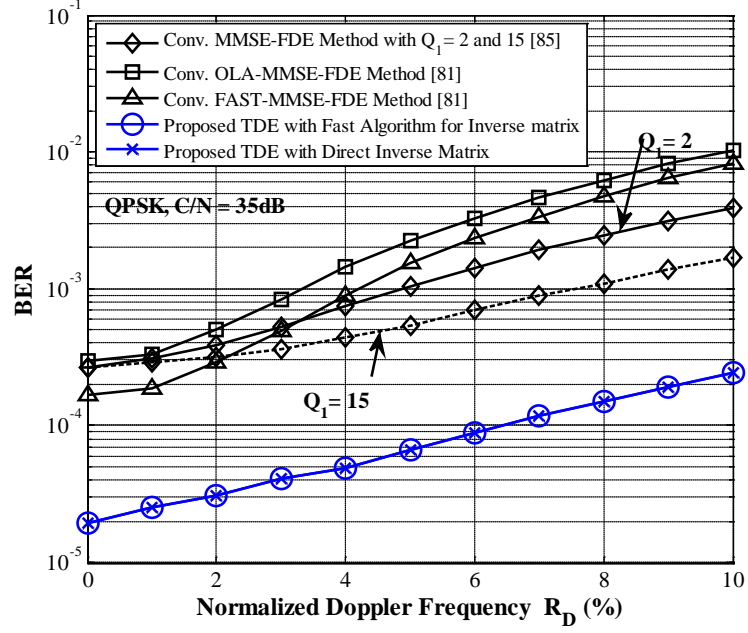


Figure 5.3: BER performances versus the normalized Doppler frequency R_D when the modulation method is QPSK and C/N is 35dB.

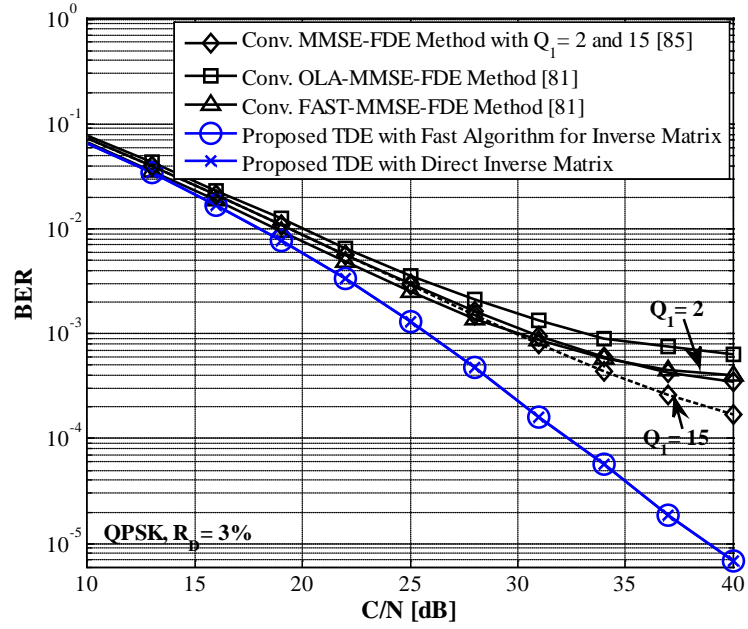


Figure 5.4: BER performances versus C/N when the modulation method is QPSK and normalized Doppler frequency R_D is 3%.

5.4 Performance Evaluation for Proposed TDE Method

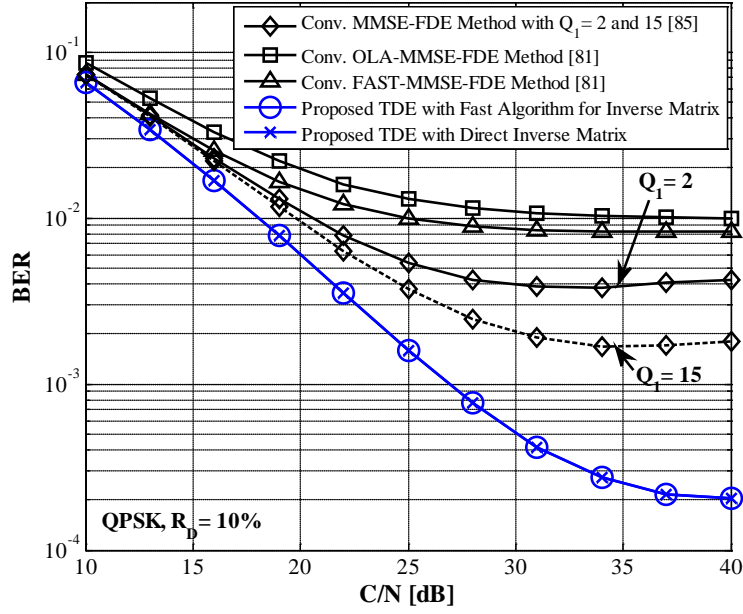


Figure 5.5: BER performances versus C/N when the modulation method is QPSK and normalized Doppler frequency R_D is 10%.

Figure 5.6 shows the BER performances versus C/N for the proposed TDE method when the modulation method is 16QAM and the normalized Doppler frequency R_D is 6% which correspond to the vehicle speed at 200 km/hrs. From the figure, it can be concluded that the proposed TDE method with the low-complexity fast algorithm for inverse matrix calculation can achieve much better BER performance than the conventional FDE methods of using the complexity reduction methods even when employing higher efficient 16QAM modulation.

Figure 5.7 shows the overall computation complexities for the conventional FDE methods and proposed TDE method when changing the number of FFT/IFFT points (N). The overall computation complexities include the processing loads for the removing of ISI from the TS, construction of channel matrix, calculation of inverse matrix and equalizations in the frequency and time domains as shown in Table 5.1. In the complexity evaluations, the lower and upper bandwidth employed in the approximation of banded CFR matrix for the conventional MMSE-FDE are evaluated by $Q_1=2$ as using in [85] and $Q_1=15$ which corresponds to the same bandwidth as that for the proposed TDE with the fast algorithm for inverse matrix calculation. From the figure, it can be observed that the overall complexities for all methods of using the direct inverse matrix calculation are much higher than that for using the complexity reduction methods especially as increasing N . When N is 128, the order of complexity for the conventional MMSE-FDE with the fast algorithm for inverse matrix calculation with $Q_1=15$ and the FAST-MMSE-FDE of using the Maclaurin's expansion method with $Q_2=1$ are almost the same complexity as that for the proposed TDE method. However, the order of complexity for the conventional MMSE-FDE with $Q_1=2$ and the OLA-MMSE-FDE with $Q_2=1$ are much lower than the proposed TDE with the fast algorithm for inverse matrix calculation. However these computation complexity reductions for the conventional MMSE-FDE methods can achieve at the cost of considerable degradation of BER performances as shown in Figure 5.3, 5.4, 5.5 and 5.6, respectively.

5.4 Performance Evaluation for Proposed TDE Method

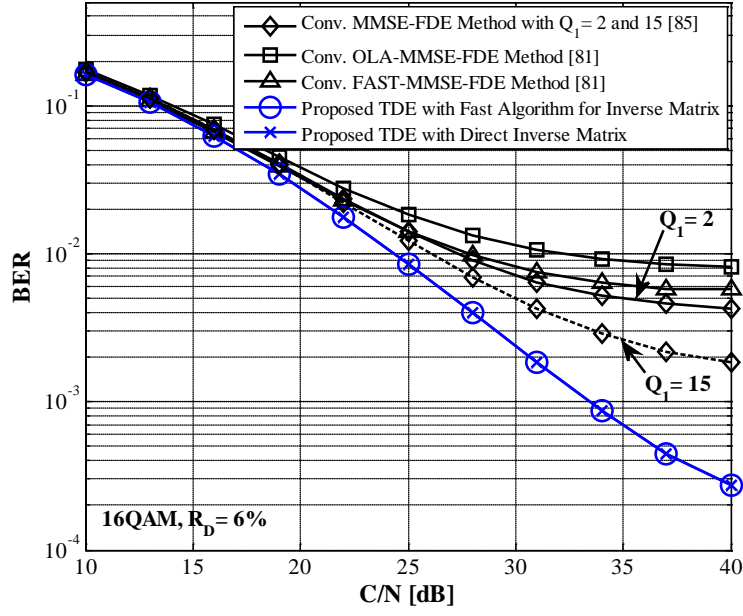


Figure 5.6: BER performances versus C/N when the modulation method is 16QAM and normalized Doppler frequency R_D is 6%.

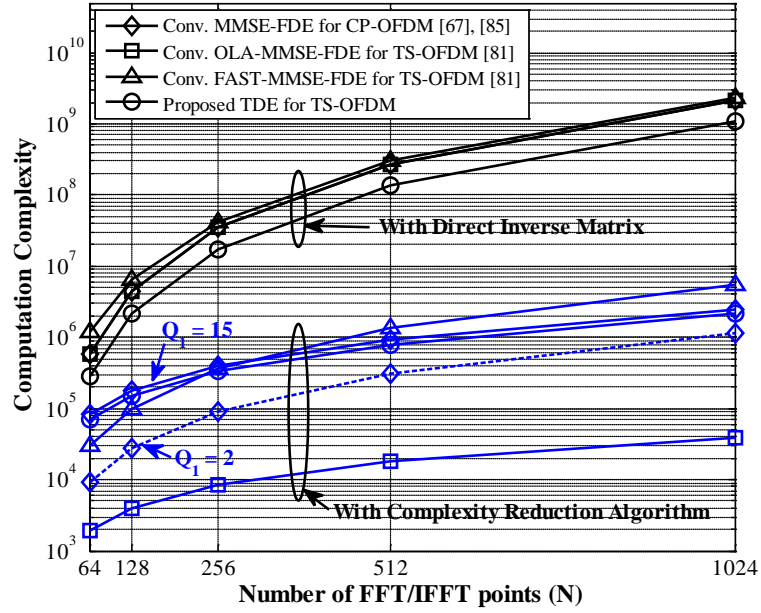


Figure 5.7: Comparisons of overall computation complexities for proposed TDE and conventional FDE methods when changing N .

5.5 Conclusions

This chapter proposed the time domain equalization (TDE) method for the TS-OFDM signal in higher time-varying fading channels. The salient features of proposed method are to employ the new design of TS signal in the estimation of CIR at every sampling time and the time domain equalization method of using the fast algorithm for inverse matrix calculation. To demonstrate the effectiveness of proposed TDE method, this chapter conducted various computer simulations. From the simulation results, this chapter confirmed that the proposed TDE method with the fast algorithm for inverse matrix calculation can achieve much better BER performance than the conventional FDE methods of using the complexity reduction methods with allowable increase of computation complexity in higher time-varying fading channels.

CHAPTER 6

ITERATIVE BASED TIME DOMAIN EQUALIZATION METHOD FOR DFTS-OFDM UNDER HIGHLY MOBILE ENVIRONMENTS

Under highly mobile environments, signal quality of discrete Fourier transform spreading-orthogonal frequency division multiplexing (DFTS-OFDM) with a frequency domain equalization method would be degraded relatively due to the occurrence of inter-channel interference (ICI). To solve this problem, this chapter proposes an iterative based time domain equalization (TDE) method with a time domain channel impulse response (CIR) estimation method for DFTS-OFDM signal. The salient features of proposed method are to employ a time domain training sequence (TS) in the estimation of CIR instead of using the conventional pilot subcarriers and to employ the TDE method with a maximum likelihood (ML) estimation method instead of using the conventional one-tap minimum mean square error frequency domain equalization (one-tap MMSE-FDE) method. This chapter also proposes a low-complexity iterative based TDE method by using a good property of symmetric banded CIR transfer matrix for solving the simultaneous equations instead of using a direct calculation of inverse matrix. This chapter presents various simulation results under highly mobile environments to demonstrate the effectiveness of proposed iterative based TDE with the CIR estimation method for the TS inserted DFTS-OFDM signal as comparing with the conventional one-tap MMSE-FDE and TDE methods.

6.1 Introduction

Discrete Fourier transform spreading-orthogonal frequency division multiplexing (DFTS-OFDM) has been received a lot of attentions as an alternative technique to OFDM from its lower peak to averaged power ratio (PAPR) and robustness to multipath fading by using a simple one-tap minimum mean square error frequency domain equalization (one-tap MMSE-FDE) method [63,93-95]. From these advantages, the DFTS-OFDM with one-tap MMSE-FDE method has been adopted as the standard transmission technique for the uplink from the user terminal to the base station in the 4th generation mobile communication system (LTE: Long Term Evolution) [96-97].

When assuming the quasi-static or slow time-varying fading channel, the time domain CIR can be considered as a constant during one DFTS-OFDM symbol period. Figure 6.1 shows a schematic diagram for the relationships between the CIR in the time domain and the CFR in the frequency domain where the CFR can be obtained by performing a DFT to the CIR at a certain sampling time during one symbol period. Figure 6.1(a) shows the CIR and its corresponding CFR in the quasi-static channel. From the Figure, it can be seen that the CIRs at the three sampling times are almost constant. Accordingly the CFRs converted from the CIRs at these three sampling times during one symbol period are also almost the same responses as shown in Figure 6.1(a). From this fact, the received DFTS-OFDM signal affected by the slow time-varying fading distortion can be equalized precisely by using the one-tap MMSE-FDE method with the fixed CFR converted from the CIR at any sampling time during one symbol period.

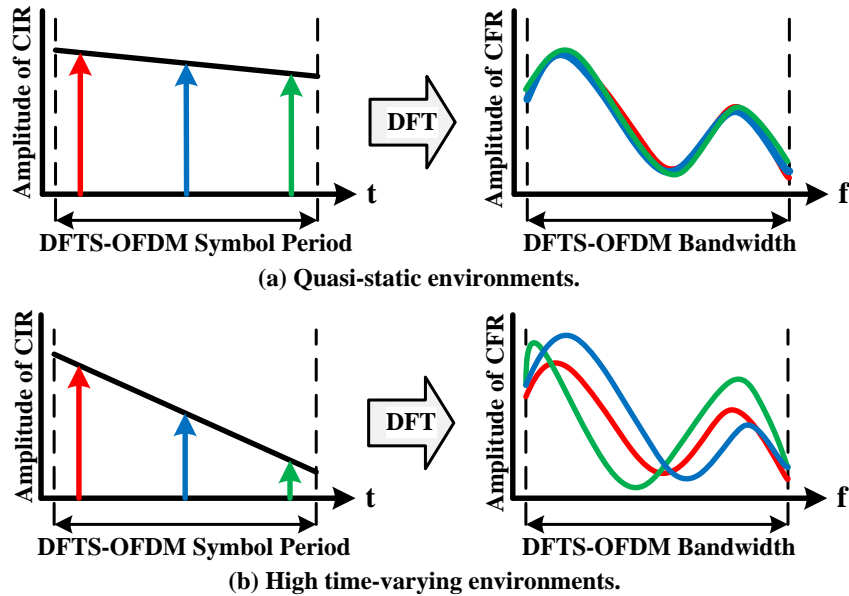


Figure 6.1: Relationships between CIR and CFR.

When assuming the highly time-varying fading channel occurred in the data communications such as high speed vehicle to vehicle (V2V) and high speed trains communications [98], the time domain CIR would be no more constant even during one DFTS-OFDM symbol period. Figure 6.2 shows an example of computer simulation results of time domain CIR for 1st to 3rd delay paths at every sampling time in the Rician multipath

fading channel. In the simulation, the normalized Doppler frequency $f_{\text{dmax}}/\Delta f$ is taken by 5% where f_{dmax} is the maximum Doppler frequency spread and Δf is the subcarrier spacing of DFTS-OFDM signal. From the Figure, it can be seen that the amplitude of time domain CIR is changing relatively even during one DFTS-OFDM symbol period. Figure 6.1(b) shows the relationships between the time domain CIR and its corresponding frequency domain CFR in higher time-varying fading channel. The time domain CIRs are changing during one symbol period and the frequency domain CFRs converted from the time domain CIRs at the different sampling times are much different as shown in Figure 6.1(b). From this fact, it is difficult to mitigate the time-varying fading distortion by the one-tap MMSE-FDE method of using one fixed CFR over one symbol period which leads the fatal degradation of BER performance.

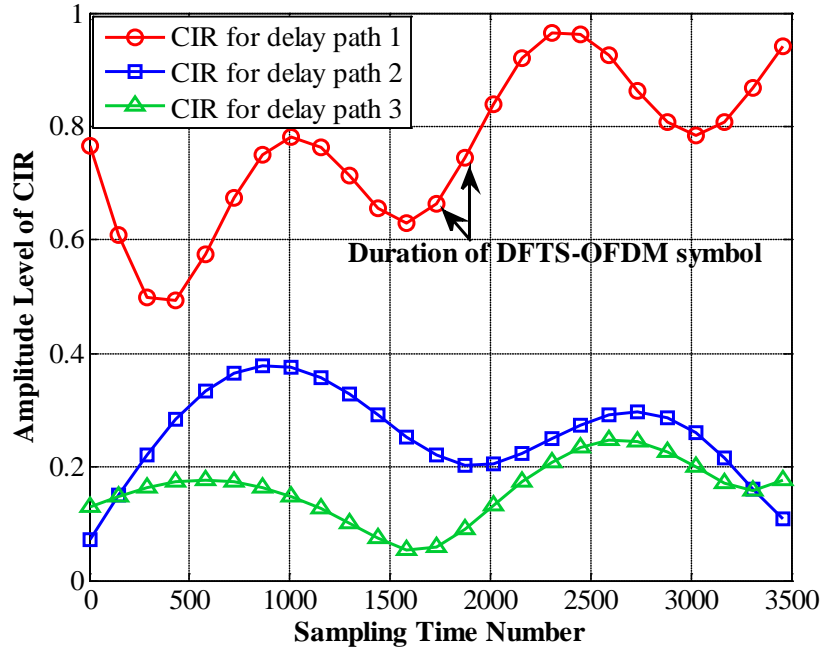


Figure 6.2: Amplitude of CIR at every sampling time in high time-varying channel.

Up to today, many FDE methods of using the CFR transfer matrix were proposed for the OFDM signal which can mitigate ICI under highly mobile environments [82,99,100]. The authors proposed an iterative based FDE method for the OFDM signal which can solve the inverse of CFR matrix iteratively with a smaller computation complexity than that of using the inverse matrix calculation [82]. By using the iterative based FDE method, the order of computation complexity $O(N^3)$ required in the inverse matrix calculation can be reduced to $O(N_{\text{Aver}} \cdot N^2)$. Where N is the number of FFT points and N_{Aver} is the average number of required iterations. However, the order of complexity for the iterative based FDE method is still higher and this method is conducted in the frequency domain which requires higher computation complexity with the order of $O(N^2 \cdot \log_2 N)$ in the construction of CFR transfer matrix. To solve the problem on the FDE method, [101-102] proposed a time domain equalization (TDE) methods for the DFTS-OFDM signal. Although these methods can mitigate the ICI precisely with lower complexity in the construction of time domain CIR transfer matrix, it is required to calculate the inverse matrix at every data symbol which leads extremely higher computation complexity and it is unsuitable in the practical implementation of DFTS-OFDM receiver especially when N is larger.

6.1 Introduction

To solve the above problems, this chapter proposes an iterative based TDE method for the time domain training sequence (TS) inserted DFTS-OFDM signal under highly mobile environments. The salient features of proposed TDE method are to employ the CIR transfer matrix in the mitigation of ICI and to employ the preconditioned conjugate gradient squared (PCGS) algorithm [103] in the calculation of inverse matrix instead of using the direct inverse matrix calculation. By using the proposed TDE method for the TS inserted DFTS-OFDM signal, the order of complexities required in the construction of time domain CIR transfer matrix and in the calculation of inverse matrix are $O(S^2 \cdot N)$ and $O(2S \cdot N \cdot N_{Aver})$, respectively which are much lower complexity than $O(N^2 \cdot N_{Aver})$ and $O(N^2 \cdot \log_2 N)$ for the conventional iterative based FDE method for the OFDM signal [82]. Where S is the length of time domain TS signal which corresponds to the guard interval (GI) of OFDM signal. The proposed iterative based TDE method can achieve much better BER performance than that for the conventional One-Tap MMSE-FDE method and almost the same BER performance as that for the TDE method of using the direct inverse matrix calculation [101-102] with much lower computation complexity under highly mobile environments.

The remainder of this chapter is organized as follows. Section 6.2 presents the structure of proposed transceiver for proposed DFTS-OFDM signal. Section 6.3 proposes a low-complexity iterative based TDE with a time domain CIR estimation method for the DFTS-OFDM signal. Section 6.4 presents various computer simulation results to verify the effectiveness of proposed iterative based TDE method as comparing with the conventional methods, and Section 6.5 draws some conclusions.

6.2 System Structure for DFTS-OFDM Signal

This section presents the system model for the proposed DFTS-OFDM signal by using the estimated CIR at every sampling time.

6.2.1 TS inserted DFTS-OFDM System

Figure 6.3 shows the frame format for the TS inserted DFTS-OFDM signal which be used in the CIR estimation at every sampling time. The authors proposed the CIR estimation method at every sampling time for the TS inserted OFDM signal by using the maximum likelihood (ML) estimation method [102]. This chapter employs this CIR estimation method for the TS inserted DFTS-OFDM signal. The time domain training sequences TS1 and TS2 with the length of S samples are added at the both ends of every data symbol which be used in the estimation of CIR at every sampling time and also used as the role of GI to remove the inter-symbol interference (ISI). Figure 6.4 shows a structure of transceiver for the TS inserted DFTS-OFDM system with the proposed iterative based TDE method. At the transmitter, the data information is encoded by a forward error correction (FEC) code [104] and the encoded data is modulated in the time domain. M modulated data is converted to M data subcarriers by M -points DFT which is given by,

$$X_D(m, k) = \sum_{n=0}^{M-1} x_D(m, n) \cdot e^{-j \frac{2\pi kn}{M}}, \quad 0 \leq k \leq M-1 \quad (6.1)$$

where $x_D(m, n)$ is the time domain data signal at the n -th sampling time of the m -th symbol and $X_D(m, k)$ is the frequency domain data signal at the k -th subcarriers. The M data subcarriers of $X_D(m, k)$ are mapped into within the allocated frequency bandwidth with N subcarriers which is called the subcarrier mapping. When the M data subcarriers are mapped into the certain frequency band continuously from the starting subcarrier number N_{Z1} to N_{Z2} ($N_{Z2} - N_{Z1} + 1 = M$) within N subcarriers, null subcarriers (zero padding) are added at the both ends of M data subcarriers. The frequency domain signal over N subcarriers after subcarrier mapping can be given by,

$$X(m, k_1) = \begin{cases} 0 \text{ (zero padding)}, & 0 \leq k_1 \leq N_{Z1} - 1 \\ X_D(m, k_1 - N_{Z1}), & N_{Z1} \leq k_1 \leq N_{Z2} \\ 0 \text{ (zero padding)}, & N_{Z2} + 1 \leq k_1 \leq N \end{cases} \quad (6.2)$$

where $(N-M)/2$ is the number of zero padding added at the both ends of M data subcarriers in the frequency domain. After subcarrier mapping, $X(m, k_1)$ including the zero padding is converted into the time domain signal as similar to the conventional OFDM signal by N -point IFFT which is given by,

$$x(m, n_1) = \frac{1}{\sqrt{N}} \sum_{k_1=N_{Z1}}^{N_{Z2}} X(m, k_1) \cdot e^{j \frac{2\pi n_1 k_1}{N}}, \quad 0 \leq n_1 \leq N-1 \quad (6.3)$$

After adding the TS1 and TS2 at the both ends of data symbol as shown in Figure 6.3, the transmitted time domain signal $x_T(m, n_2)$ can be expressed by,

6.2 System Structure for DFTS-OFDM Signal

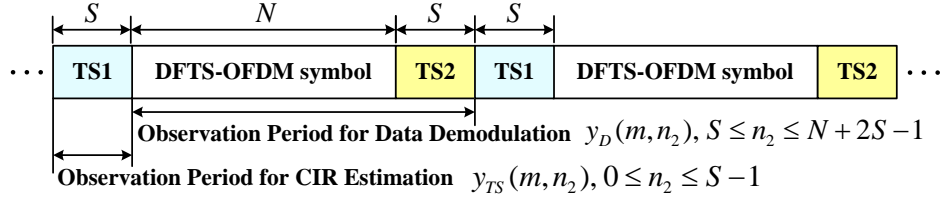


Figure 6.3: Proposed frame format in the time domain.

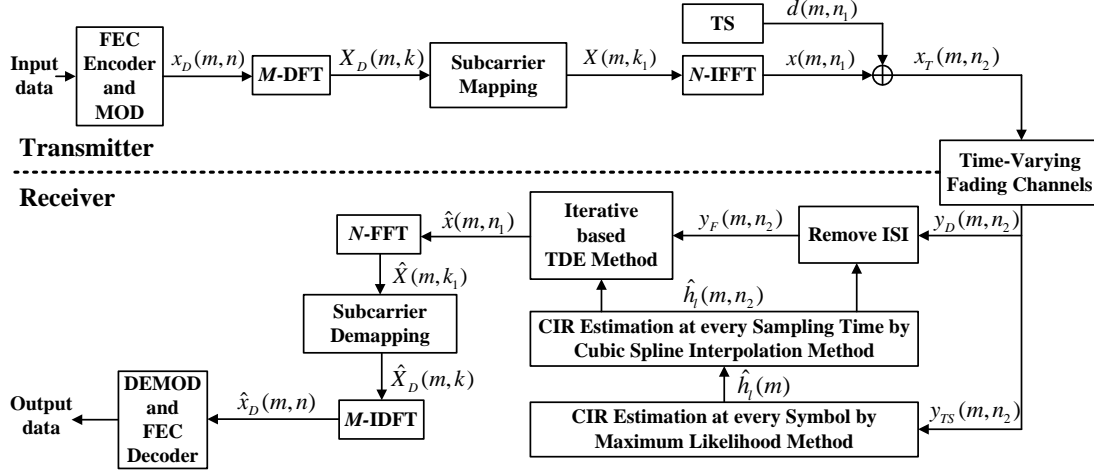


Figure 6.4: Structure of transceiver for DFTS-OFDM signal with proposed iterative based TDE method.

$$x_T(m, n_2) = \begin{cases} d_1(m, n_2), & 0 \leq n_2 \leq S-1 \\ x(m, n_2 - S), & S \leq n_2 \leq N + S - 1 \\ d_2(m, n_2 - N - S), & N + S \leq n_2 \leq N + 2S - 1 \end{cases} \quad (6.4)$$

where d_1 and d_2 are the time domain TS1 and TS2 with the length of S samples ($0 \leq n_2 \leq S-1$) of which data patterns are known at the receiver. For simplicity, this chapter assumes that the data patterns both for TS1 and TS2 are assumed to be the same as $d(m, n_2)$. The length of S should be taken longer than the length of delay paths (L) as the same as the role of GI to remove the ISI.

6.2.2 CIR Estimation method for TS inserted DFTS-OFDM Signal

The received time domain TS1 signal $y_{TS}(m, n_2)$ during the observation period for CIR estimation from 0 to $S-1$ as shown in Figure 6.3 can be expressed by,

$$y_{TS}(m, n_2) = \sum_{l=0}^{L-1} h_l(m, n_2) \cdot d_1(m, n_2 - l) + w(m, n_2), \quad 0 \leq n_2 \leq S-1 \quad (6.5)$$

where $d_1(m, n_2)$ is the TS1 signal given in (6.4), $h_l(m, n_2)$ is the complex amplitude of CIR for the l -th delay path at the n_2 -th sampling time of m -th symbol and $w(m, n_2)$ is the additive white Gaussian noise (AWGN). Here it is assumed that $h_l(m, n_2)$ is the constant during the short period of TS1 even under highly mobile environments. Under the above assumption, the expected received TS1 signal passed through the multipath fading channels can be expressed by,

$$\hat{y}_{TS}(m, n_2) = \sum_{l=0}^{S-1} \hat{h}_l(m) \cdot d(m, n_2 - l), \quad 0 \leq n_2 \leq S-1 \quad (6.6)$$

The unknown parameters of complex amplitude of $\hat{h}_l(m)$ at the m -th symbol can be estimated by using the maximum likelihood (ML) estimation method under the constraint with minimizing the difference between the actual received TS signal in (5) and the expected received signal in (6.6). Here the estimated CIR $\hat{h}_l(m)$ corresponds to the CIR at the middle sampling time of TS1. The time domain CIR $\hat{h}_l(m, n_2)$ at every sampling time can be estimated by applying the cubic spline interpolation method for the CIR estimated at every symbol over one frame [102]. Figure 6.5 shows a schematic diagram for the cubic spline interpolation method to estimate the time domain CIR at every sampling time. The estimation accuracy of time domain CIR at every sampling time will be evaluated in Section 6.4.

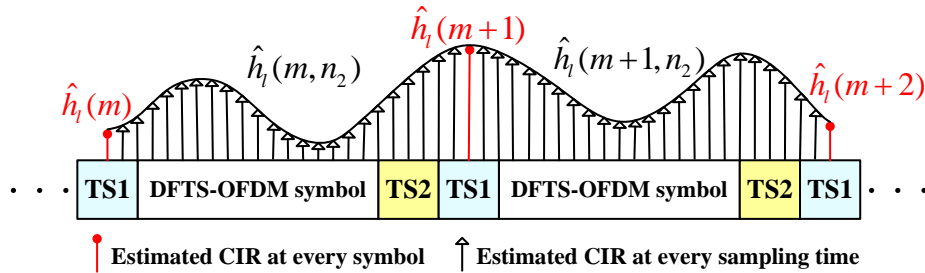


Figure 6.5: Estimation of CIR at every sampling time by using cubic spline interpolation method.

6.3 Proposal of Time Domain Equalization Method

To solve the ICI problem on the conventional one-tap MMSE-FDE method under highly mobile environments, this chapter proposes an iterative based TDE method for the TS inserted DFTS-OFDM signal by using the estimated CIR at every sampling time.

6.3.1 Proposed Time Domain Equalization Method

Figure 6.6 shows the received time domain signal in time-varying fading channel. By assuming the actual channel impulse response $h_l(m, n_2)$ at every sampling time, the received time domain data signal $y_D(m, n_2)$ during the observation period for the data demodulation from S to $N+2S-1$ as shown in Figure 6.3 can be expressed by,

$$y_D(m, n_2) = \sum_{l=0}^{L-1} h_l(m, n_2) \cdot x_T(m, n_2 - l) + w(m, n_2), \quad S \leq n_2 \leq N + 2S - 1 \quad (6.7)$$

where $x_T(m, n_2 - l)$ corresponds to the transmitted time domain signal given in (6.4) and the following relationships are employed in the derivation of (6.7).

$$n_2 - l \leq S - 1, \quad x_T(m, n_2 - l) = d(m, n_2 - l) \quad (6.8)$$

$$n_2 - l \geq N + S, \quad x_T(m, n_2 - l) = d(m, n_2 - N - S - l) \quad (6.9)$$

The actual received data signal in (6.7) includes the ISI which are added at the start and end of data symbol from the TS1 and TS2 signal, respectively as shown in Figure 6.6. By using the estimated CIR $\hat{h}_l(m, n_2)$ at every sampling time and the data pattern of $d(m, n_2)$ both for TS1 and TS2 which are known at the receiver, the ISI from the TS1 and TS2 signals can be removed by the following equation.

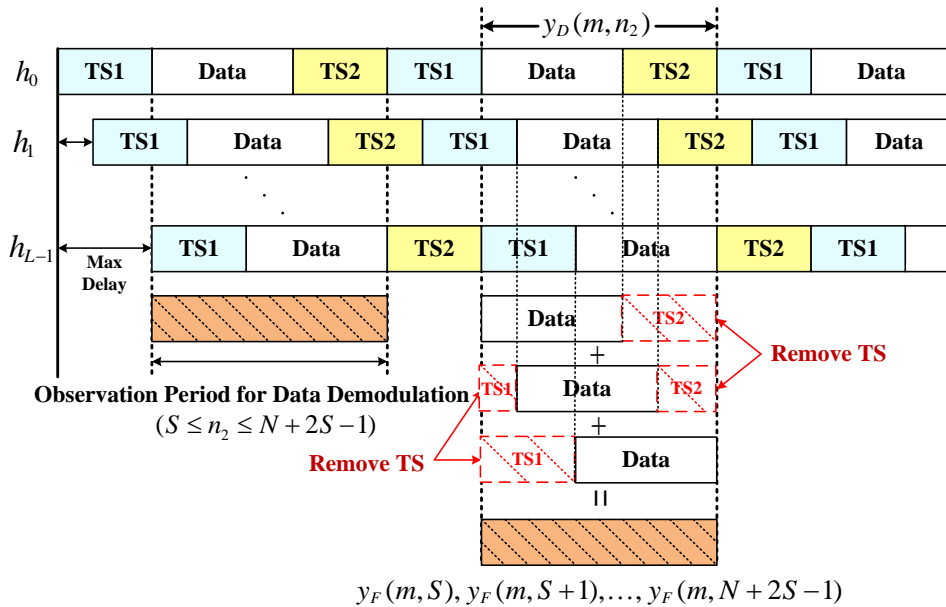


Figure 6.6: Received time domain signal in multipath fading channel.

6.3 Proposal of Time Domain Equalization Method

$$y_F(m, n_2) = \begin{cases} y_D(m, n_2) - \sum_{l=n_2-S+1}^{S-1} \hat{h}_l(m, n_2) \cdot d(m, n_2 - l), & (S \leq n_2 \leq 2S-2) \\ y_D(m, n_2), & (2S-1 \leq n_2 \leq N+S-1) \\ y_D(m, n_2) - \sum_{l=0}^{n_2-N-S} \hat{h}_l(m, n_2) \cdot d(m, n_2 - N - S - l), & (N+S \leq n_2 \leq N+2S-2) \end{cases} \quad (6.10)$$

where $y_F(m, n_2)$ is the received time domain signal after removing the ISI from the actual received DFTS-OFDM signal $y_D(m, n_2)$ in (6.7).

When the transmitted time domain data signal $x(m, n_1)$ given in (6.3) is assumed as the unknown parameters, the expected time domain received data $\hat{y}_E(m, n_2)$ without the ISI which corresponds to (6.10) can be given by,

$$\hat{y}_E(m, n_2) = \begin{cases} \sum_{l=0}^{n_2-S} \hat{h}_l(m, n_2) \cdot \hat{x}(m, n_2 - S - l), & (S \leq n_2 \leq 2S-2) \\ \sum_{l=0}^{S-1} \hat{h}_l(m, n_2) \cdot \hat{x}(m, n_2 - S - l), & (2S-1 \leq n_2 \leq N+S-1) \\ \sum_{l=n_2-N-S+1}^{S-1} \hat{h}_l(m, n_2) \cdot \hat{x}(m, n_2 - S - l), & (N+S \leq n_2 \leq N+2S-2) \end{cases} \quad (6.11)$$

The unknown parameter of time domain data $\hat{x}(m, n_1)$ can be estimated by solving the following maximum likelihood (ML) equation under the constraint with minimizing the difference between the actual received data signal $y_F(m, n_2)$ in (6.10) and the expected received data signal $\hat{y}_E(m, n_2)$ in (6.11).

$$\Upsilon = \arg \min_{\hat{x}(m, s)} \left[\sum_{n_2=S}^{N+2S-2} |y_F(m, n_2) - \hat{y}_E(m, n_2)|^2 \right] \quad (6.12)$$

The ML equation (6.12) can be solved by taking the partial differentiation for unknown parameters of $\hat{x}^*(m, n_3)$ which can be expressed by,

$$\frac{\partial \Upsilon}{\partial \hat{x}^*(m, n_3)} = \frac{\partial \left(\sum_{n_2=n_3}^{N+2S-2} |y_F(m, n_2) - \hat{y}_E(m, n_2)|^2 \right)}{\partial \hat{x}^*(m, n_3)} = 0, \quad (0 \leq n_3 \leq N-1) \quad (6.13)$$

where $*$ represents the conjugate complex. By using (6.13), the ML equation (6.12) can be expressed by the following simultaneous equations with N unknown parameters of $\hat{x}(m, n_1)$.

$$[b(m, n_3)]_{N \times 1} = [A_m(n_3, n_1)]_{N \times N} \cdot [\hat{x}(m, n_1)]_{N \times 1} \quad (6.14)$$

where $b(m, n_3)$ and $A_m(n_3, n_1)$ can be expressed by,

$$b(m, n_3) = \sum_{n_2=S}^{N+2S-2} y_F(m, n_2) \cdot \frac{\partial \hat{y}_E^*(m, n_2)}{\partial \hat{x}^*(m, n_3)} = \underbrace{\left[\hat{h}_l^H(m, n_3) \right]}_{N \times (N+S-1)} \cdot \underbrace{\left[y_F(m, n_2) \right]}_{(N+S-1) \times 1}, \quad 0 \leq n_3 \leq N-1 \quad (6.15)$$

$$A_m(n_3, n_1) = \sum_{n_2=S}^{N+2S-2} \hat{y}_E(m, n_2) \cdot \frac{\partial \hat{y}_E^*(m, n_2)}{\partial \hat{x}^*(m, n_3)} = \underbrace{\left[\hat{h}_l^H(m, n_3) \right]}_{N \times (N+S-1)} \cdot \underbrace{\left[\hat{h}_l(m, n_1) \right]}_{(N+S-1) \times N}, \quad 0 \leq n_1 \leq N-1 \quad (6.16)$$

where $(\cdot)^H$ represents the Hermitian transpose operation and the following relationships are used in the derivation of (6.15) and (6.16).

6.3 Proposal of Time Domain Equalization Method

$$n_3 = n_2 - S - l \quad \text{in} \quad \frac{\partial \hat{y}_E^*(m, n_2)}{\partial \hat{x}^*(m, n_3)} \quad (6.17)$$

$$n_1 = n_2 - S - l \quad \text{in} \quad \hat{y}_E(m, n_2) \quad (6.18)$$

Here the CIR matrix $[\hat{h}_l(m, n_1)]$ in (6.16) is given by,

$$[\hat{h}_l(m, n_1)] = \begin{bmatrix} \hat{h}_0(m, S) & 0 & \cdots & 0 \\ \hat{h}_1(m, S+1) & \hat{h}_0(m, S+1) & \ddots & \vdots \\ \vdots & \hat{h}_1(m, S+2) & \ddots & 0 \\ \hat{h}_{S-1}(m, 2S-1) & \vdots & \ddots & \hat{h}_0(m, N+S-1) \\ 0 & \hat{h}_{S-1}(m, 2S-1) & \vdots & \hat{h}_1(m, N+S) \\ \vdots & \ddots & \ddots & \vdots \\ 0 & \cdots & 0 & \hat{h}_{S-1}(m, N+2S-2) \end{bmatrix} \quad (6.19)$$

From (6.19), the order of complexity required in the construction of CIR transfer matrix $A_m(n_3, n_1)$ in (6.16) which is obtained by the multiplication of $\hat{h}_l(m, n_1)$ and $\hat{h}_l^H(m, n_1)$, can be given by $O(S^2 \cdot N)$. The proposed TDE method of using the CIR transfer matrix can achieve lower complexity than that for the conventional FDE method [82] which employs the full elements of CFR transfer matrix with the complexity of $O(N^2 \cdot \log_2 N)$. The CIR transfer matrix $[A_m(n_3, n_1)]$ in (6.16) which is obtained after the partial differentiation can be represented by,

$$A_{i,j} = \begin{bmatrix} A_{0,0} & A_{0,1} & \cdots & A_{0,S-1} & 0 & \cdots & 0 \\ A_{0,1}^H & A_{1,1} & & & \ddots & \ddots & \vdots \\ \vdots & & \ddots & & & \ddots & 0 \\ A_{0,S-1}^H & & & \ddots & & & A_{N-S,N-1} \\ 0 & \ddots & & & \ddots & & \vdots \\ \vdots & \ddots & \ddots & & & A_{N-2,N-2} & A_{N-2,N-1} \\ 0 & \cdots & 0 & A_{N-S,N-1}^H & \cdots & A_{N-2,N-1}^H & A_{N-1,N-1} \end{bmatrix}_{N \times N} \quad (6.20)$$

In (20), $A_m(i, j)$ in (6.16) is represented by $A_{i,j}$ and the index of m -th symbol is omitted for brevity. From (20), it can be seen that the matrix is the banded matrix with the upper and lower bandwidth $(S-1)$ whose non-zero entries are confined to a diagonal bands. Also the lower band matrix with the index of (j, i) below the diagonal terms is the Hermitian transpose of upper band matrix with the index of (i, j) . From these facts, the CIR transfer matrix $[A_m(n_3, n_1)]$ in (6.16) is the symmetric banded matrix with the block size of $(N \times N)$. This chapter employs the good property of symmetric banded matrix in the proposed iterative based TDE method for further reduction of computation complexity. From (6.14), the unknown parameters $\hat{x}(m, n_1)$ can be simply solved by using the inverse matrix of $[A_m(n_3, n_1)]$ which is given by,

$$[\hat{x}(m, n_1)]_{N \times 1} = [A_m(n_3, n_1)]_{N \times N}^{-1} \cdot [b(m, n_3)]_{N \times 1} \quad (6.21)$$

where $[\cdot]^{-1}$ represents the inverse matrix. In (6.21), the order of complexity for the calculation of inverse matrix with size of $N \times N$ is $O(N^3)$ which is required at every data symbol demodulation. To reduce the computation complexity for the proposed TDE method, the next section proposes an iterative based TDE method which employs the precondition conjugate gradient squared (PCGS) algorithm for the symmetric banded CIR matrix as given in (6.20).

6.3.2 Proposed Iterative based TDE Method

The conjugate gradient squared (CGS) algorithm [103] is well known as one of the iterative methods which can solve the linear simultaneous equations for N unknown parameters with much smaller computation complexity as compared with that of using the inverse matrix calculation. Let consider the simultaneous equations $\mathbf{A}\hat{\mathbf{x}}=\mathbf{b}$, where \mathbf{A} corresponds to $A_m(n_3, n_1)$ in (6.14) and its matrix is the symmetric banded matrix with the size of $N \times N$. The exact CGS solution can be obtained after at most N steps. Hence, stopping the iteration after $N_{\text{iter}} (< N)$ steps would yield an approximate solution for the problem. In the equalization of every data symbol, the CGS algorithm minimizes iteratively the cost function in a reduced-rank Krylov subspace. When the spectral condition number of the matrix \mathbf{A} is too high, a preconditioned matrix \mathbf{D} is employed which is called the precondition CGS (PCGS) algorithm. The PCGS algorithm solves the simultaneous equations by,

$$\mathbf{D}^{-1}\mathbf{A}\hat{\mathbf{x}} = \mathbf{D}^{-1}\mathbf{b} \quad (6.22)$$

where the inversion of matrix \mathbf{D} should be a computationally efficient operation. In the rest of our analysis, assuming the simplicity that the matrix $D(m)$ is constructed by the diagonal of matrix $A_m(n_3, n_1)$ and the initial solution of $\hat{x}(m, n_1)$ can be given by,

$$[\hat{x}(m, n_1)]_{N \times 1}^{(0)} = [D(m)]_{N \times N}^{-1} \cdot [b(m, n_3)]_{N \times 1} \quad (6.23)$$

In PCGS algorithm [103], the residual vector $\mathbf{r}^{(i)}$ can be regarded as the product of $\mathbf{r}^{(0)}$ and the i -th degree polynomial in matrix \mathbf{A} which is expressed by,

$$\mathbf{r}^{(i)} = \mathbf{P}_i(\mathbf{A})\mathbf{r}^{(0)} \quad (6.24)$$

where $\mathbf{P}_i(\mathbf{A})$ is the polynomial of \mathbf{A} at the i -th degree and $\mathbf{r}^{(0)}$ is obtained from the initial solution given in (23) as $\mathbf{r}^{(0)} = \mathbf{b} - \mathbf{A}\hat{\mathbf{x}}^{(0)}$. The iteration coefficients can be recovered from the i -th vectors $\mathbf{r}^{(i)}$ and it turns out to be easy to find the corresponding approximations for $[\hat{x}(m, n_1)]$. From (6.24), the multiplication of $\mathbf{P}_i(\mathbf{A})\mathbf{r}^{(0)}$ is required at every symbol. Since the CIR transfer matrix \mathbf{A} given in (6.20) is the symmetric banded matrix, the order of complexity for this multiplication requires only $O(2S \cdot N)$ which is lower than the conventional iterative based FDE method of using the full elements of CFR transfer matrix [82] which requires the order of complexity $O(N^2 \cdot \log_2 N)$.

The repetition of PCGS algorithm is stopped when the following normalized mean square error ($NMSE$) between the $(i-1)$ -th and i -th solutions of $[\hat{x}(m, n_1)]$ is smaller than the predetermined threshold level (TOL) [82].

$$NMSE = \frac{\sum_{n_1=0}^{N-1} \left| [\hat{x}(m, n_1)]^{(i)} - [\hat{x}(m, n_1)]^{(i+1)} \right|^2}{\sum_{n_1=0}^{N-1} \left| [\hat{x}(m, n_1)]^{(i)} \right|^2} \quad (6.25)$$

In the proposed iterative based TDE with the PCGS algorithm, the following procedures are repeated up to either the value of $NMSE$ in (6.25) becomes less than the predetermined threshold level (TOL) or the number of iterations reaches to the predetermined maximum number (N_{max}).

6.3 Proposal of Time Domain Equalization Method

Step1: The maximum iteration number is set to N_{\max} ($N_{\max}=5$), the threshold level is set to TOL and the initial solution of $[\hat{x}(m, n_1)]^{(0)}$ is given by (6.23).

Step2: Calculate the i -th solution of $[\hat{x}(m, n_1)]^{(i)}$ by the PCGS algorithm and calculate the $NMSE$ by (6.25).

Step3: Compare the $NMSE$ obtained at the i -th iteration with the predetermined threshold level of TOL . If the $NMSE$ is less than TOL , the $[\hat{x}(m, n_1)]^{(i)}$ is output as the estimated data information. If not, repeat the same procedures. If the number of iterations reaches to predetermined N_{\max} , $[\hat{x}(m, n_1)]^{(N_{\max})}$ is output as the estimated data information.

The order of computation complexity for the proposed PCGS algorithm can be evaluated by $O(2S \cdot N \cdot N_{Aver})$ which is lower complexity than that for $O(N^2 \cdot N_{Aver})$ when the PCGS algorithm is applied to the conventional FDE method [82] with the full elements of transfer CFR matrix. The order of complexity ratio between TDE with the inverse matrix calculation $O(N^3)$ and proposed TDE with the iterative method is evaluated by the following equation.

$$R_C = \frac{2S \cdot N \cdot N_{Aver}}{N^3} = \frac{2S \cdot (N_{Aver})}{N^2} \quad (6.26)$$

where N_{Aver} is the average number of required iterations which satisfies the predetermined threshold level of TOL . The average number of required iterations which may depend on the predetermined threshold level TOL , mobile environments and operating carrier to noise power ratio (C/N), which are evaluated by computer simulations in the next Section.

In the demodulation of time domain data information for the DFTS-OFDM signal, the estimated $\hat{x}(m, n_1)$ in (6.21) is converted to the frequency domain signal $\hat{X}(m, k)$ as given in (6.2) by N -points FFT. After subcarrier demapping to $\hat{X}(m, k)$, M data subcarriers $\hat{X}_D(m, k)$ as given in (6.2) can be obtained in the frequency domain. Then $\hat{X}_D(m, k)$ is converted to the time domain data $\hat{x}_D(m, n)$ by M -points IDFT as given in (6.1). The time domain information data can be obtained after demodulation and FEC decoding for $\hat{x}_D(m, n)$ which are all the opposite processing at the transmitter side as shown in Figure 6.4.

6.4 Performance Evaluations

In this section, various computer simulations are conducted to evaluate the performance of proposed iterative based TDE method as comparing with the conventional one-tap MMSE-FDE and TDE methods in highly time-varying fading channels. The simulation parameters to be used in the following evaluations are listed in Table 6.1. The total numbers of subcarriers (FFT points) is $N=128$, the numbers of data subcarriers (DFT points) is $M=96$, and the numbers of null subcarriers (zero padding) is $N-M=32$. The communications channel is modelled by the Rician fading channels which is usually experienced by the user on the higher speed vehicles or trains [98]. In the following evaluations, the normalized Doppler frequency $R_D=f_{d\max}/\Delta f$ (%) is employed as the measure of mobile conditions where $f_{d\max}$ is the maximum Doppler frequency and Δf is the subcarrier spacing of DFTS-OFDM signal.

Table 6.1: Simulation parameters.

Parameter	Value
Number of FFT/IFFT points (N)	128
Number of DFT/IDFT points (M)	96
Number of data subcarriers (M)	96
Number of zero padding ($N-M$)	32
Length of time domain TS for TS-OFDM (S)	16
Length of GI for CP-OFDM (N_g)	16
Number of symbols per one frame (N_S)	65
Modulation for training sequence (TS)	16QAM
Modulation method for data subcarriers	16QAM
Allocated OFDM frequency bandwidth	1MHz
Radio carrier frequency	5.9GHz
Forward Error Correction (FEC) Codec [104]	
Encoding	Convolution
FEC rate	1/2
Constraint length	7
Decoding	Viterbi with hard decision
Interleaver	Matrix size with one frame
Rician multipath fading channel model	
Rice factor (K)	6dB
Delay profile	Exponential
Decay constant	-1
Number of delay paths (L)	14
Number of scattered rays per one delay path	20

6.4 Performance Evaluations

The estimation accuracy for the time domain CIR at every sampling time is evaluated by the normalized mean square error (NMSE) which is given by,

$$\Psi_{NMSE} = \frac{\sum_{l=0}^{L-1} \sum_{m=0}^{N_S-1} \sum_{n_2=0}^{N+2S-1} |\hat{h}_l(m, n_2) - h_l(m, n_2)|^2}{\sum_{l=0}^{L-1} \sum_{m=0}^{N_S-1} \sum_{n_2=0}^{N+2S-1} |h_l(m, n_2)|^2} \quad (6.27)$$

where N_S is the number of DFTS-OFDM symbols per one frame.

Figure 6.7 shows the time domain CIR estimation accuracy at every sampling time which is evaluated by the normalized mean square error (NMSE) given in (6.27) for the proposed CIR estimation method of using the time domain TS when changing the normalized Doppler frequency R_D and operation C/N. From the figure, it can be observed that the proposed method can keep higher estimation accuracy even at lower operation C/N when R_D is up to 20% which corresponds to the vehicle speed at 381km/hr.

Figure 6.8 shows the BER performances for the proposed TDE method of using the direct inverse matrix calculation and the proposed iterative method with the PCGS algorithm when changing the threshold level (TOL) of $NMSE$ at the normalized Doppler frequency $R_D=15\%$ which correspond to the vehicle speed at 286 km/h. From the figure, it can be observed that the BER performance for proposed TDE with the iterative method is very close to that for the TDE with inverse matrix calculation regardless of the operation C/N when threshold level (TOL) is taken by less than 0.02. From these results in Figure 6.8, the threshold level $TOL=0.02$ is used in the following evaluations.

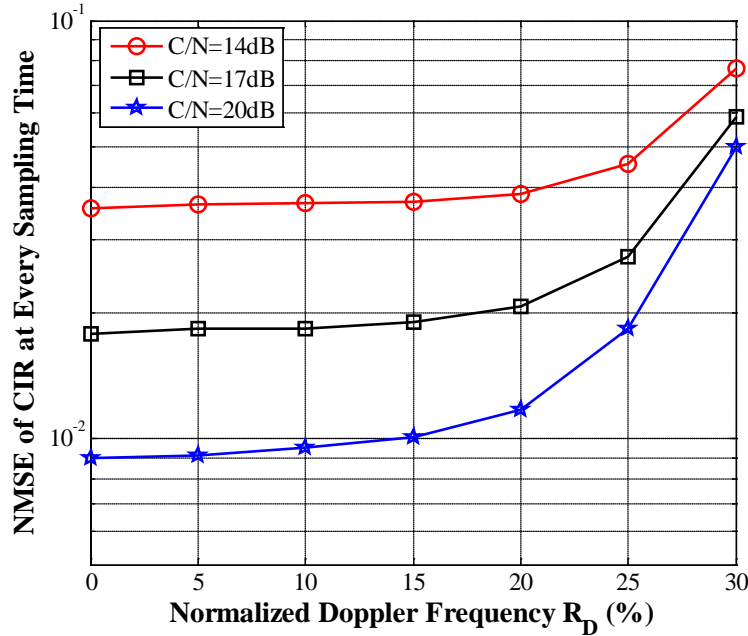


Figure 6.7: CIR estimation accuracy when changing R_D and operation C/N.

6.4 Performance Evaluations

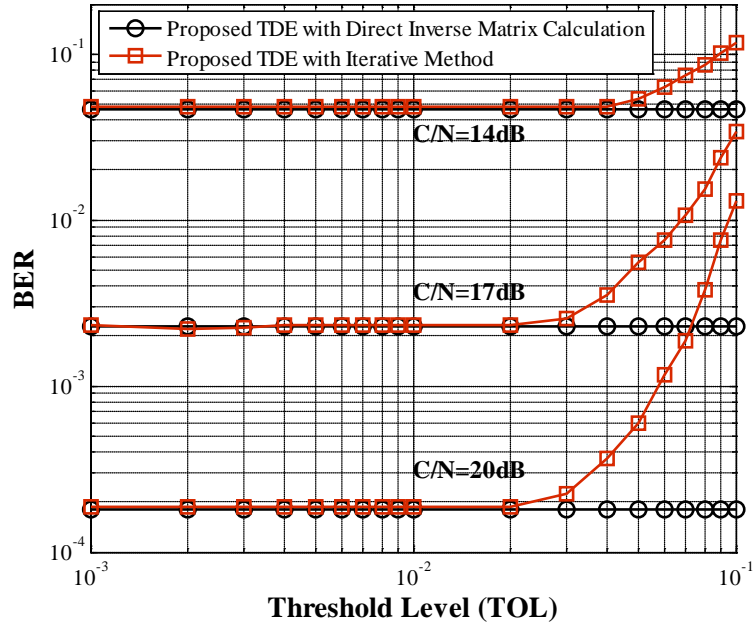


Figure 6.8: BER performance for proposed iterative based TDE method when changing TOL and C/N at $R_D=15\%$.

Figure 6.9 shows the average number of required iterations N_{Aver} which is satisfied with the predetermined $TOL=0.02$ when changing the normalized Doppler frequency R_D and the operating C/N. From the figure, it can be observed that the average number of iterations N_{Aver} becomes larger as increasing the normalized Doppler frequency R_D and as decreasing the operation C/N. The average number of required iterations N_{Aver} in Figure 6.9 is used in the evaluation of computation complexity.

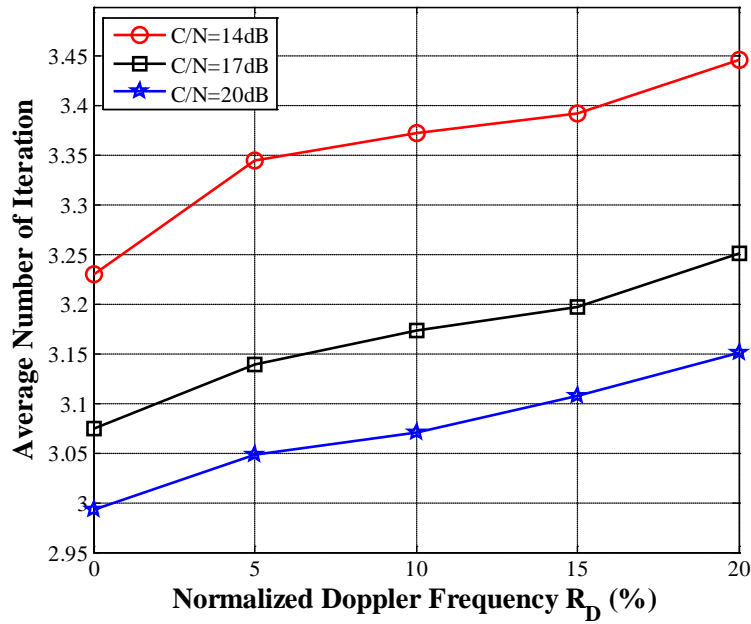


Figure 6.9: Average number of required iterations for proposed iterative based TDE method when changing R_D and C/N at $TOL= 0.02$.

6.4 Performance Evaluations

Table 6.2 shows the order of complexity ratio R_C between the proposed TDE with the iterative method and the inverse matrix calculation method which is evaluated by (6.26). From the table, it can be observed that the average number of iterations for the proposed iterative based TDE method is decreasing as increasing the operation C/N. This is the reason that the larger number of iterations is required to satisfy the predetermined small TOL at lower C/N. However, the average number of iterations N_{Aver} is keeping with less than 4 over all operation C/Ns even under higher mobile environments. From the results of complexity ratio R_C in Table 6.2, it can be concluded that the proposed iterative based TDE method can reduce the complexity by about 150 times as compared with the inverse matrix calculation method.

Table 6.2: Ratio of computation complexity for proposed iterative based TDE method.

C/N	Proposed iterative based TDE method ($N=128, S=16, TOL=0.02$)			
	$R_D (=f_{dmax}/\Delta f) = 5\%$		$R_D (=f_{dmax}/\Delta f) = 15\%$	
	N_{Aver}	Complexity ratio R_C in (6.26)	N_{Aver}	Complexity ratio R_C in (6.26)
14dB	3.34	0.0065	3.39	0.0066
17dB	3.13	0.0061	3.19	0.0062
20dB	3.04	0.0059	3.11	0.0061

Figure 6.10 shows the BER performances for the proposed TDE method as comparing with conventional one-tap MMSE-FDE and TDE methods of using GI when changing the normalized Doppler frequency R_D at the operation C/N=20dB. From the figure, it can be observed that the proposed TDE method shows better BER performance than the conventional TDE method. The proposed method can keep better performance until the normalized Doppler frequency $R_D=20\%$ with a little degradation of BER performance as compared with that in the static condition ($R_D=0\%$). On the contrary the BER performance of conventional one-tap MMSE-FDE method is degraded drastically when the normalized Doppler frequency R_D is larger than 5% (vehicle speed $\approx 95\text{km/hr.}$). The conventional TDE method shows better BER performance than the conventional one-tap MMSE-FDE method when the normalized Doppler frequency R_D is larger than 6%. However, the conventional TDE method shows worse BER performance than the one-tap MMSE-FDE method in the slow time-varying fading channel ($R_D<5\%$). This is the reason that the conventional TDE method of using GI cannot obtain the frequency diversity gain. On the contrary the proposed TDE method with TS signal which can compensate the ISI by using the estimated CIR and the known TS at the receiver shows the better BER performance than the MMSE-FDE method even in the slow time-varying fading channel. From these results, it can be concluded that the proposed TDE method with TS signal can achieve better BER performance than the conventional methods especially under highly mobile environments.

Figure 6.11 shows the BER performances for the proposed TDE method as comparing with conventional MMSE-FDE and TDE methods when changing C/N at the normalized Doppler frequency $R_D=15\%$ (vehicle speed $\approx 286\text{km/hr.}$), respectively. From the figures, it can be observed that the BER performance for the proposed TDE method shows much better BER performance than the conventional one-tap MMSE-FDE and TDE methods.

6.4 Performance Evaluations

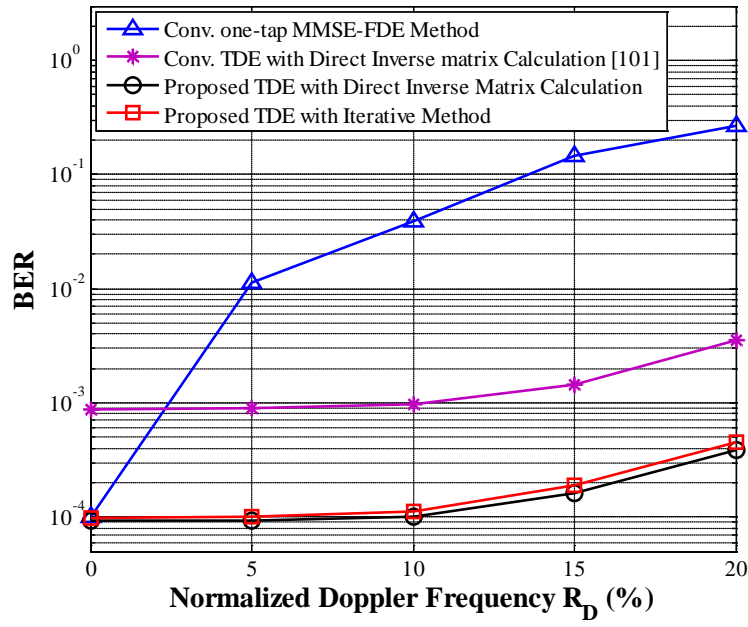


Figure 6.10: BER performance for proposed iterative based TDE method when changing R_D at $C/N=20$ dB.

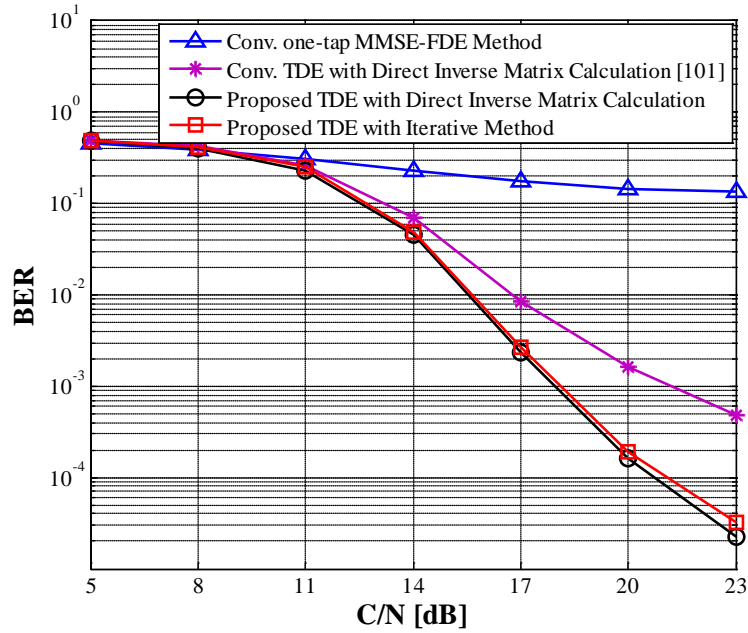


Figure 6.11: BER performance for proposed iterative based TDE method when changing C/N at $R_D=15\%$.

6.5 Conclusions

This chapter proposed the low-complexity iterative based TDE method with the time domain CIR estimation method for the TS inserted DFTS-OFDM signal under highly mobile environments. The proposed method employs the partial differentiation in solving the ML equation so as to be the symmetric banded CIR transfer matrix which allows the employment of iterative method for solving the simultaneous equations iteratively with much lower computation complexity than that for the direct inverse matrix calculation. From the computer simulation results, it can be concluded that the proposed iterative based TDE method can achieve much better BER performance than the conventional one-tap MMSE-FDE and TDE methods under highly mobile environments. It can be also concluded that the proposed TDE with the iterative method can achieve much lower computation complexity than that for the direct inverse matrix calculation method with keeping almost the same BER performance.

CHAPTER 7

CONCLUSIONS

Wireless OFDM technique offers many advantages such as the efficient usage of frequency bandwidth, robustness against multipath fading channel, and also simplicity system structure. From these advantages, OFDM is become the main research topic for the next generation of wireless communication systems in which it's already employed in several wireless communication standards. Unfortunately, the degradation of OFDM system performance caused by Doppler frequency spread under mobile environments is inevitable due to the user movement. Especially, when considers in higher time-varying fading channels with mobile transmitter or receiver. The effect of the channel impulse response (CIR) on the transmitted signal may vary considerably and this variation is depended on the relative of vehicle velocities and reflectivity properties which it can affect the time-frequency signature of the transmitted signal. As the results, the inter-carrier interference (ICI) would be occurred and leads the degradation of OFDM system performance.

From above discussions, the high quality of channel estimation and equalization algorithm at the OFDM receiver should be considered strictly throughout the wireless mobile communication systems, so as to guarantee an acceptable OFDM system performance with the ultimate goal of coherent data detection. In this thesis, the ICI mitigation method has been studied and evaluated both for channel estimation and also equalization methods. In addition, the channel estimation and equalization methods should be established according to the reasonable balance between the system performance and the receiver's complexity. In other words, a compromise of transceiver should be considered so as to maximize the spectral efficiency and reduce the complexity while maintaining an acceptable channel estimation and equalization performances, especially under higher mobile environments.

To achieve high channel estimation accuracy, this thesis firstly proposed a new design of TS signal in the estimation of CIR at every sampling time instead of using the pilot subcarriers. The feature of proposed channel estimation method are to employ a different data pattern of TS signal added to each OFDM data symbol over one frame and to employ the triangular window function for the TS signal as the waveform shaping both for reducing the leakage of power spectrum density (PSD) at the outside of OFDM allocated frequency bandwidth with keeping higher CIR estimation accuracy. From the simulation results, this thesis confirmed that the proposed TS signal can achieve lower leakage of power spectrum density at the outside of allocated OFDM frequency bandwidth with keeping higher CIR estimation accuracy even in higher time-varying fading channels.

In addition, this thesis also conducts the theoretical examinations for the effect of CIR estimation method of using the TS signal when the detected symbol timing has an offset from the ideal symbol timing. From the theoretical analysis and computer simulation results, this thesis confirmed that the symbol timing offset causes the same phase rotation both to the estimated channel frequency response (CFR) and the received data signal in frequency domain and this phase rotation can be canceled completely by the frequency domain equalization (FDE) at the receiver.

Channel estimation provides information about distortion of the transmission signal when it propagates through the channel environments. This information is then used by equalization processing so that the fading effect and/or co-channel interference can be removed and the original transmitted signal can be recovery. The equalization processing can be viewed as the operation in frequency domain equalization (FDE) or time domain equalization (TDE) in which these two separated domains have completely different feature in the construction of channel matrix.

As for the FDE method, this thesis proposed a new FDE method for the time domain TS inserted OFDM (TS-OFDM) signal under higher mobile environments. The salient features of proposed method are to enable the acquisition of frequency diversity gain by using an enhanced CIR matrix and to enable the reduction of complexity by using a fast algorithm for inverse matrix calculation. The proposed new FDE method can achieve better BER performance than the conventional FDE methods with keeping lower complexity under higher mobile environments. However, the full elements of CFR matrix in proposed FDE method are approximated by a banded matrix so as to enable the employment of the fast algorithm in the calculation of inverse matrix. The BER performance would be degraded in higher time-varying fading channels due to the approximation for the full elements of CFR matrix by the banded matrix. To solve this problem, this thesis also proposes an equalization method of using the CIR matrix in the time domain instead of using the CFR matrix for the FDE method. Hereafter the proposed method is conducted the equalization processing for the mitigation of ICI in the time domain. The feature of proposed TDE method is to employ the partial differentiation for the time domain CIR matrix for solving the maximum likelihood (ML) equation in which the time domain CIR matrix becomes a symmetric banded matrix. This feature enables to employ the fast algorithm for inverse matrix calculation which can achieve the same BER performance with much lower computation complexity as compared with that for the direct inverse matrix calculation. These are completely different features from the FDE methods of which CFR matrix is the full elements of matrix. Furthermore, the proposed TDE method can also obtain the frequency diversity gain at the deep fading which enables to achieve better BER performance both for lower and higher mobile environments.

This thesis extended the proposed channel estimation by using TS signal and TDE method to the Discrete Fourier transform spreading-OFDM (DFTS-OFDM). To solve the ICI problem with keeping low-complexity, this thesis proposed an iterative based TDE method for the time domain TS inserted DFTS-OFDM signal. The salient features of proposed TDE method are to employ the CIR transfer matrix in the mitigation of ICI and to employ the preconditioned conjugate gradient squared (PCGS) algorithm in the calculation of inverse matrix instead of using the direct inverse matrix calculation. The proposed iterative based TDE method can achieve much better BER performance than that for the conventional one-tap MMSE-FDE method and almost the same BER performance as that for the TDE method of using the direct inverse matrix calculation with much lower computation complexity under higher mobile environments.

The various computer simulation results were demonstrated in this thesis in the order to confirm and verify the effectiveness of above proposed methods. From the various simulation results, it can be concluded that the channel estimation accuracy, signal quality and computation complexity can be improved and enhanced by the proposed methods. The proposed methods are the great challenges and solutions for the next generation of wireless mobile communication systems.

APPENDIX A

LIST OF PUBLICATIONS

Journal Papers

- [1] Pornpawit Boonsrimuang, Pongsathorn Reangsuntea, Pisit Boonsrimuang, Kazuo Mori, and Hideo Kobayashi, "Proposal of Improved PTS Method Based on Split-Radix IFFT for OFDM Signal," *David Publishing Journal on Computer and Technology and Application*, Vol. 3, No. 6, pp. 425-430, June 2012.
- [2] Pongsathorn Reangsuntea, Pisit Boonsrimuang, Kazuo Mori, and Hideo Kobayashi, "Time Domain Equalization Method for DFTS-OFDM Signal without GI under Highly Mobile Environments," *ECTI Transactions on Computer and Information Technology*, Vol. 9, No. 2, pp. 150-159, November 2015.
- [3] Pongsathorn Reangsuntea, Pisit Boonsrimuang, Kousuke Sanada, Kazuo Mori, and Hideo Kobayashi, "Theoretical Examination of Channel Estimation Method for TS-OFDM Signal under Symbol Timing Offset," *IEICE Communications Express*, Vol. 5, No. 9, pp. 329-334, July 2016.
- [4] Pongsathorn Reangsuntea, Pisit Boonsrimuang, Kousuke Sanada, Kazuo Mori, and Hideo Kobayashi, "Enhanced MMSE-FDE Method for TS-OFDM under Higher Mobile Environments," *IEICE Communications Express*, Vol. 6, No. 1, pp. 53-58, January 2017.
- [5] Pongsathorn Reangsuntea, Pisit Boonsrimuang, Kazuo Mori, and Hideo Kobayashi, "Time Domain Equalization Method for TS-OFDM Signal under Higher Mobile Environments," *EURASIP Journal on Wireless Communications and Networking (Springer Open)*, Vol. 2017, No. 5, pp. 1-12, January 2017.
- [6] Pongsathorn Reangsuntea, Arttapol Reangsuntea, Pisit Boonsrimuang, Kazuo Mori, and Hideo Kobayashi, "Iterative Based Time Domain Equalization Method for DFTS-OFDM under Highly Mobile Environments," *ECTI Transactions on Computer and Information Technology*. (Under reviewing).

International Conference Articles

- [1] Pongsathorn Reangsuntea, Pornpawit Boonsrimuang, Pisit Boonsrimuang, and Hideo Kobayashi, "A New Weighting Factor of PTS OFDM with Low Complexity Base on Radix-4 IFFT for PAPR Reduction," in *Proc. of 1st International Symposium on Technology for Sustainability (ISTS2011)*, pp. 333-336, Thailand, January 2011.
- [2] Pornpawit Boonsrimuang, Pongsathorn Reangsuntea, Pisit Boonsrimuang, and Hideo Kobayashi, "A New Weighting Factor of PTS OFDM with Low Complexity Based on Split-Radix IFFT for PAPR Reduction," in *Proc. of 4th International Conference on Advanced Communication Technology (ICACT2012)*, pp. 2-6, Korea, February 2012.
- [3] Pornpawit Boonsrimuang, Panya Jirajaracheep, Pongsathorn Reangsuntea, Pisit Boonsrimuang, and Hideo Kobayashi, "A Low Complexity IPTS-Based Extended

- Split-Radix IFFT for PAPR Reduction in OFDM Systems,” in *Proc. of 9th International Conference on Electrical Engineering/Electronics, Computer, Telecommunications and Information Technology (ECTI-CON2012)*, pp. 1-4, Thailand, May 2012.
- [4] Pongsathorn Reangsuntea, Pisit Boonsrimuang, Pornpawit Boonsrimuang, and Hideo Kobayashi, “PAPR Reduction Performance Analysis Based on Partial Transmit Sequence,” in *Proc. of 1st International Conference on Engineering, Applied Sciences, and Technology (ICEAST2012)*, pp. 368-372, Thailand, November 2012.
- [5] Phethai Romrerng, Pongsathorn Reangsuntea, Pisit Boonsrimuang, and Hideo Kobayashi, “A New Weighting Factor of Reduced Computational Complexity PTS Scheme for PAPR Reduction,” in *Proc. of 10th IEEE Vehicular Technology Society Asia Pacific Wireless Communications Symposium (APWCS2013)*, pp. 168-172, Korea, August 2013.
- [6] Phethai Romrerng, Arjin Numsomran, Pongsathorn Reangsuntea, Pisit Boonsrimuang, and Hideo Kobayashi, “A Low Computation Complexity Algorithm for Improve PTS-Based PAPR Reduction Scheme,” in *Proc. of 2nd International Conference on Engineering, Applied Sciences, and Technology (ICEAST2013)*, pp. 209-213, Thailand, August 2013.
- [7] Thiti Jumnongarsa, Pongsathorn Reangsuntea, Tawil Paungma, Pisit Boonsrimuang, and Hideo Kobayashi, “PAPR Reduction by Permutation Sequences Scheme for OFDM-WLAN in 802.11 Systems,” in *Proc. 2nd of International Conference on Engineering, Applied Sciences, and Technology (ICEAST2013)*, pp. 215-219, Thailand, August 2013.
- [8] Arttapol Reangsuntea, Pornpawit Boonsrimuang, Pongsathorn Reangsuntea, Pisit Boonsrimuang, and Hideo Kobayashi, “A Low-Complexity PS based Radix IFFT method for PAPR Reduction in OFDM systems,” in *Proc. of 16th International Conference on Advanced Communication Technology (ICACT2014)*, pp. 273-278 Korea, February 2014.
- [9] Pongsathorn Reangsuntea, Pisit Boonsrimuang, Katsuhiro Naito, Kazuo Mori, and Hideo Kobayashi, “Proposal of Channel Estimation Method for OFDM Systems under High Mobile Environments,” in *Proc. of 11st International Conference on Electrical Engineering/Electronics, Computer, Telecommunications and Information Technology (ECTI-CON2014)*, pp. 1-6, Thailand, May 2014.
- [10] Pongsathorn Reangsuntea, Pisit Boonsrimuang, Kazuo Mori, and Hideo Kobayashi, “Iterative Based Time Domain Equalization Method for OFDM Signal under High Mobile Environments,” in *Proc. of 8th International Conference on Signal Processing and Communication Systems (ICSPCS2014)*, pp. 1-6, Australia, December 2014.
- [11] Pongsathorn Reangsuntea, Mio Hourai, Pisit Boonsrimuang, Kazuo Mori, and Hideo Kobayashi, “Iterative based ML Demodulation Method for OFDM Signal under Higher Mobile Environments,” in *Proc. of 81st IEEE Vehicular Technology Conference (VTC2015-Spring)*, pp.1-6, Glasgow, UK, May 2015.
- [12] Pongsathorn Reangsuntea, Pisit Boonsrimuang, Kazuo Mori, and Hideo Kobayashi, “Time Domain Equalization Method for DFTS-OFDM Signal without GI under High Mobile Environments,” in *Proc. of 12nd International Conference on Electrical Engineering/Electronics, Computer, Telecommunications and Information Technology (ECTI-CON2015)*, pp. 1-6, Thailand, June 2015.

Appendix A

- [13] Pongsathorn Reangsuntea, Arttapol Reangsuntea, Pisit Boonsrimuang, Kazuo Mori, and Hideo Kobayashi, “Low-Complexity FDE Method for TS-OFDM Signal under Higher Time-Varying Channels,” in *Proc. of 13rd International Conference on Electrical Engineering/Electronics, Computer, Telecommunications and Information Technology (ECTI-CON2016)*, pp. 1-6, Thailand, June 2016.
- [14] Arttapol Reangsuntea, Pongsathorn Reangsuntea, Pisit Boonsrimuang, Kazuo Mori, and Hideo Kobayashi, “Iterative based Time Domain Equalization Method for DFTS-OFDM under Highly Mobile Environments,” in *Proc. of 13rd International Conference on Electrical Engineering/Electronics, Computer, Telecommunications and Information Technology (ECTI-CON2016)*, pp. 1-6, Thailand, June 2016.
- [15] Pongsathorn Reangsuntea, Pisit Boonsrimuang, Kousuke Sanada, Kazuo Mori, and Hideo Kobayashi, “Low-Complexity MMSE-FDE Method for TS-OFDM Signal Under High Mobile Environments,” in *Proc. of International Conference on Communication and Information Systems (ICCIS2016)*, pp. 78-82, Thailand, December 2016.

Local Conference Articles

- [1] Pongsathorn Reangsuntea, Pisit Boonsrimuang, Kazuo Mori, and Hideo Kobayashi “Proposal of Iterative Based Time Domain Equalization Method under Higher Mobile Environments,” in *Proc. of Tokai Conference (English Session)*, No. K2-4, September 2014.

APPENDIX B

AWARD

2015 Young Researcher's Encouragement Award from IEEE Vehicular Technology Conference (VTC2015-Spring), IEEE VTS Japan Chapter.

BIBLIOGRAPHY

- [1] S. Haykin, “*Communication Systems*,” 4th Edition, John Wiley and Sons, 2000.
- [2] R. Prasad, “*OFDM for Wireless Communications Systems*,” Artech House, Universal Personal Comm. series, 2004.
- [3] A. F. Molisch, “*Wireless Communications*,” 2nd Edition, Wiley, Dec. 2010.
- [4] Y. Akaiwa, “*Introduction to Digital Mobile Communications*,” Wiley, 1997.
- [5] X. Wang, and H. V. Poor, “Wireless Communication Systems: Advanced Techniques for Signal Reception,” *Prentice Hall Commun. Eng. and Emerging Tech. Series Theodore S. Rapp.*, Jun. 2002.
- [6] A. Goldsmith, “*Wireless Communications*,” Stanford University, 2004.
- [7] E. Baccarelli, R. Cusani, and S. Galli, “A novel adaptive receiver with enhanced channel tracking capability for TDMA-based mobile radio communications,” *IEEE Trans. Commun.*, vol. 16, no. 9, pp.1630-1639, Dec. 1998.
- [8] O. Simeone, O. Somekh, and Y. Bar-Ness, “Uplink Throughput of TDMA Cellular Systems with Multicell Processing and Amplify-and-Forward Cooperation Between Mobiles,” *IEEE Trans. Wireless Commun.*, vol. 6, no. 8, pp.1536-1276, Aug. 2007.
- [9] S. Buzzi, M. Lops, and A. M. Tulino, “A new family of MMSE multiuser receivers for interference suppression in DS/CDMA systems employing BPSK modulation,” *IEEE Trans. Commun.*, vol. 49, no. 1, pp.154-167, Jan. 2001.
- [10] W. Hamouda, and P. J. McLane, “Error control coding and space-time MMSE multiuser detection in DS-CDMA systems,” *Journal of Communications and Networks*, vol. 5, no. 3, pp.187-196, Sept. 2003.
- [11] Q. Yu, G. Bi, and G. Zhang, “Improved blind multipath estimation for long code DS-CDMA,” *Journal of Communications and Networks*, vol. 7, no. 3, pp.278-283, Sept. 2005.
- [12] K. Ryu, J. Jin, and Y. Park, “Performance analysis of multicarrier code select CDMA system for PAPR reduction in multipath channels,” *Journal of Communications and Networks*, vol. 11, no. 1, pp.11-19, Feb. 2009.
- [13] H. Cheon, and D. Hong, “Effect of channel estimation error in OFDM-based WLAN,” *IEEE Commun. Lett.*, vol. 6, no. 5, pp.190-192, Aug. 2002.
- [14] Y. S.Cho, J. Kim, W. Y. Yang, and C. G. Kang, “*Introduction to OFDM*,” 1st Edition, Wiley-IEEE Press, 2010.
- [15] L. L. Hanzo, Y. Akhtman, L. Wang, and M. Jiang, “*Channel Estimation for OFDM and MCCDMA*,” 1st Edition, Wiley-IEEE Press, 2011.
- [16] ETSI TR 101 190, v1.3.1, Digital Video Broadcasting (DVB); Implementation guidelines for DVB terrestrial television services; *Transmission aspects*, 2008-10.
- [17] ETSI TR 102 831, v1.2.1, Digital Video Broadcasting (DVB); Implementation guidelines for the second generation digital terrestrial television broadcasting systems (DVB-T2); *Transmission aspects*, 2012.
- [18] IEEE 802.11 Standard for Information technology, Telecommunications and information exchange between systems Local and metropolitan area networks: Wireless LAN Medium Access Control (MAC) and Physical Layer (PHY) Specifications, 2012.

Bibliography

- [19] ETSI TR 101 683, v1.1.1, Broadband Radio Access Network (BRAN); HIPERLAN Type 2; *System Overview*, 2000-02.
- [20] ARIB Std-T97, Mobile Broadband Wireless Access Systems (IEEE 802.20 TDD Wideband and 625k-MC Modes Application in Japan), 2008-11.
- [21] ITU Radio Regulations, CHAPTER II-Frequencies, ARTICLE 5 Frequency allocations, Section IV–Table of Frequency Allocations, 2012.
- [22] FCC, Amendment of the Commission’s Rules to Provide for Operation of Unlicensed NII Devices in the 5-GHz Frequency Range, Memorandum Opinion and Order, ET Docket No. 96-102, Jun. 1998.
- [23] https://en.wikipedia.org/wiki/IEEE_802.11.
- [24] R. Prasad, “*WLAN Systems and Wireless IP for Next Generation Communications*,” Artech House, 2002.
- [25] K. S. Gilhousen, I. M. Jacobs, R. Padovani, A. J. Viterbi, L. A. Weaver, Jr., and C. E. Wheatley III, “On the capacity of a cellular CDMA system,” *IEEE Trans. Veh. Tech.*, pp. 303–312, May 1991.
- [26] K. Rath and J. Uddenfeldt, “Capacity of digital cellular TDMA systems,” *IEEE Trans. Veh. Tech.*, pp. 323-332, May 1991.
- [27] Q. Hardy, “Are claims hope or hype?,” *Wall Street Journal*, pp. A1, Sep. 1996.
- [28] A. Mehrotra, “*Cellular Radio: Analog and Digital Systems*,” Artech House, 1994.
- [29] J. E. Padgett, C. G. Gunther, and T. Hattori, “Overview of wireless personal communications,” *Special Issue on Wireless Personal Commun., IEEE Commun. Mag.*, pp. 28-41, Jan. 1995.
- [30] J. D. Vriendt, P. Laine, C. Lerouge, X. Xu, “Mobile network evolution: a revolution on the move,” *IEEE Commun. Mag.*, pp. 104-111, April 2002.
- [31] P. Bender, P. Black, M. Grob, R. Padovani, N. Sundhushayana, A. Viterbi, “CDMA/HDR: A bandwidth efficient high speed wireless data service for nomadic users,” *IEEE Commun. Mag.*, July 2000.
- [32] 3GPP TR 36.913 V9.0.0, “Requirements for Further Advancements of E-UTRA (LTE-Advanced),” 2009-12.
- [33] ITU-R M. [IMT-TECH], “Requirements related to technical performance for IMT-Advanced radio interface(s),” Aug. 2008.
- [34] ITU-R, Acknowledgment of candidate submission from IEEE under step 3 of the IMT-Advanced process (IEEE technology), *Tech. Rep.*, Oct. 2009.
- [35] 3GPP TS 36.300, Evolved Universal Terrestrial Radio Access (E-UTRA) and Evolved Universal Terrestrial Radio Access Network (E-UTRAN); *Overall description*; Stage 2, 2009.
- [36] 3GPP TS 23.402 V8.0.0, Release 8, Architecture enhancements for non-3GPP accesses, 2007-12.
- [37] 3GPP TS 36.300 V9.7.0 Release 9, LTE; Evolved Universal Terrestrial Radio Access (E-UTRA) and Evolved Universal Terrestrial Radio Access Network (E-UTRAN); *Overall description*; Stage 2, 2004-11.
- [38] ITU-R, Circular letter 5/LCCE/2, *Tech. Rep.*, March 2008.
- [39] ITU-R, Acknowledgment of candidate submission from 3GPP proponent under step 3 of the IMT-Advanced process (3GPP technology), *Tech. Rep.*, 2009.
- [40] ITU-R, Acknowledgment of candidate submission from IEEE under step 3 of the IMT-Advanced process (IEEE technology), *Tech. Rep.*, October.

Bibliography

- [41] ITU-R, Acknowledgment of candidate submission from China (People's Republic of) under step 3 of the IMT-Advanced process (3GPP technology), *Tech. Rep.*, October.
- [42] ITU-R, Requirements related to technical performance for IMT-Advanced radio interface(s), *Report M.2134*, 2008.
- [43] J. Rombaut, "Optimization of Packetization Masks for Image Coding Based on an Objective Cost Function for Desired Packet Spreading," *IEEE Trans. Image Process.*, vol. 17, no. 10, pp. 1849-1863, Oct. 2008.
- [44] R. Zhang, "Cooperative Multi-Cell Block Diagonalization with Per-Base-Station Power Constraints," *IEEE Journal on Selected Areas in Commun.*, vol. 28, no. 9, pp. 1435-1445, Dec. 2010.
- [45] A. Spyropoulos, and C.S. Raghavendra, "Asymptotic capacity bounds for ad-hoc networks revisited: the directional and smart antenna cases," in *Proc. of IEEE Global Telecom.*, pp. 1-6, Dec. 2003.
- [46] Kun Zhao, S. Zhang, Z. Ying, T. Bolin, and S. He, "SAR Study of Different MIMO Antenna Designs for LTE Application in Smart Mobile Handsets," *IEEE Trans. Ant. and Prop.*, vol. 61, no. 6, pp. 3270-3279, Jun. 2013.
- [47] S. Chen, S. Sun, Y. Wang, G. Xiao, and R. Tamrakar, "A comprehensive survey of TDD-based mobile communication systems from TD-SCDMA 3G to TD-LTE(A) 4G and 5G directions," *China Communications*, vol. 12, no. 2, pp. 40-60, Feb. 2015.
- [48] V. Jungnickel, M. Schellmann, L. Thiele, T. Wirth, T. Haustein, O. Koch, W. Zirwas, and E. Schulz, "Interference-aware scheduling in the multiuser MIMO-OFDM downlink," *IEEE Commun. Mag.*, vol. 47, no. 6, Jun. 2009.
- [49] A. K. Dutta, K. V. S. Hari, and L. Hanzo, "Minimum-Error-Probability CFO Estimation for Multiuser MIMO-OFDM Systems," *IEEE Trans. Veh. Tech.*, vol. 64, no. 7, pp. 2804-2818, Jul. 2015.
- [50] Q. Wang, G. Ren, and J. Wu, "A Multiuser Detection Algorithm for Random Access Procedure With the Presence of Carrier Frequency Offsets in LTE Systems," *IEEE Trans. Commun.*, vol. 63, no. 9, pp. 3299-3312, Sept. 2015.
- [51] R. Xie, F. R. Yu, and H. Ji, "Dynamic Resource Allocation for Heterogeneous Services in Cognitive Radio Networks with Imperfect Channel Sensing," *IEEE Trans. Veh. Tech.*, vol. 61, no. 2, pp. 770-780, Feb. 2012.
- [52] D. Zhai, M. Sheng, X. Wang, and Y. Li, "Leakage-Aware Dynamic Resource Allocation in Hybrid Energy Powered Cellular Networks," *IEEE Trans. Commun.*, vol. 63, no. 11, pp. 4591-4603, Nov. 2015.
- [53] B. Sklar, *"Digital Communications: Fundamentals and Applications,"* Prentice Hall, 2000.
- [54] C. Haslett, *"Essentials of radio wave propagation,"* Cambridge University Press, 2008.
- [55] W. Lindsey, "Error probabilities for Rician fading multichannel reception of binary and N -ary signals," *IEEE Trans. Information Theory*, vol. 10, no. 4, pp. 339-350. Oct. 1964.
- [56] M. Nakagami, "The m -distribution; A general formula of intensity distribution of rapid fading," in *Proc. of Statistical Methods in Radio Wave Propagation*, pp 3-36, Jun. 1958.
- [57] R. H. Clarke, "A Statistical Theory of Mobile-Radio Reception," *Bell System Technical Journal*, vol. 47, no. 6, pp. 957-1000, Jul.-Aug. 1968.

- [58] G. Mkrtchyan, “*Estimation Parameter learning and Prediction of Time-Varying communication Channels*,” Ph.D dissertation, Mie university, Sept. 2006.
- [59] F. Hlawatsch, and G. Matz, “*Wireless Communications Over Rapidly Time-Varying Channels*,” Academic press, 2011.
- [60] D. Park, and H. Song, “A New PAPR Reduction Technique of OFDM System with Nonlinear High Power Amplifier,” *IEEE Trans. Cons. Elec.*, vol. 53, no. 2, pp. 327-332, May 2007.
- [61] P. Boonsrimuang, K. Mori, T. Paungma, and H. Kobayashi, “Proposal of Simple PAPR Reduction Method for OFDM Signal by Using Dummy Sub-Carriers,” *IEICE Trans. Commun.*, vol. E91-B, pp. 784-794, Mar. 2008.
- [62] Y. Wang, L.-H. Wang, J.-H. Ge, and B. Ai, “An Efficient Nonlinear Comanding Transform for Reducing PAPR of OFDM Signals,” *IEEE Trans. Broadcasting*, vol. 58, no. 4, pp. 677-684, Dec. 2012.
- [63] D. Falconer, S. L. Ariyavisitakul, A. Benyamin-Seeyar, and B. Eidson, “Frequency Domain Equalization for Single-Carrier Broadband Wireless Systems,” *IEEE Commun. Mag.*, Apr. 2002.
- [64] M. D. Nisar, H. Nottensteiner, and T. Hindelang, “On Performance Limits of DFT-Spread OFDM Systems”, in *Proc. of 16th International Conference on Mobile and Wireless Commun.*, Jul. 2007.
- [65] B. E. Priyanto, H. Codina, S. Rene, T. B. Sorensen, and P. Mogensen, “Initial Performance Evaluation of DFT-Spread OFDM Based SC-FDMA for UTRA LTE Uplink”, in *Proc. of 65th IEEE Vehi. Tech. Conf. (VTC)*, pp. 3175-3179, Apr. 2007.
- [66] H. C. Wu, “Analysis and characterization of intercarrier and interblock interferences for wireless mobile OFDM systems,” *IEEE Trans. Broadcasting*, vol. 52, no. 2, pp. 203–210, Jun. 2006.
- [67] Y. S. Choi, P. J. Volts, and F. A. Cassara, “On channel estimation and detection for multicarrier signals in fast and selective Rayleigh fading channels,” *IEEE Trans. Commun.*, vol. 49, no. 8, pp. 1375-1387, Aug. 2001.
- [68] P. Schniter, “Low-complexity equalization of OFDM in doubly selective channels,” *IEEE Trans. Signal Processing*, vol. 52, no. 4, pp. 1002-1011, Apr 2004.
- [69] T. Hrycak, S. Das, G. Matz, and H. G. Feichtinger, “Low complexity equalization for doubly selective channels modeled by a basis expansion,” *IEEE Trans. Signal Processing*, vol. 58, no. 11, pp. 5706-5719, Nov. 2010.
- [70] S. Takeuchi, K. Naito, K. Mori, and H. Kobayashi, “Proposal of Doppler Frequency Spread Compensation Method for OFDM Systems,” in *Proc. of 9th IEEE VTS Asia Pacific Wireless Communications Symposium (APWCS2012)*, CO-5, Aug. 2012.
- [71] T. Miyamoto, K. Naito, K. Mori, and H. Kobayashi, “Proposal of Doppler Estimation Method of Using Frequency Channel Response for OFDM Systems,” in *Proc. of 7th International Conference on Signal Processing and Communication Systems (ICSPCS2013)*, pp.1-6, Dec. 2013.
- [72] B. K. Engiz, C. Kurnaz, and H. Sezgin, “Performance analysis of pilot arrangement for OFDM systems over time varying frequency selective channels,” in *Proc. of 8th IEEE Wireless and Mobile Computing, Networking and Communications*, pp. 113-117, Oct. 2012.
- [73] J. Fu, C.-Y. Pan, Z. X. Yang, and L. Yang, “Low-complexity equalization for TDS-OFDM systems over doubly selective channels,” *IEEE Trans. Broadcasting*, vol. 51, no. 3, pp. 401–407, Sep. 2005.

- [74] T. Yamamoto and F. Adachi, "Training Sequence Inserted OFDM Transmission with MMSE-FDE," *IEICE Trans. Commun.*, vol. E97-B, no. 2, pp. 476-483, Feb. 2014.
- [75] J. Song, Z. Yang, L. Yang, K. Gong, C. Pan, J. Wang, and Y. Wu, "Technical review on Chinese digital terrestrial television broadcasting standard and measurements on some working modes," *IEEE Trans. Broadcasting*, vol. 53, no. 1, pp. 1-7, Feb. 2007.
- [76] H. Kobayashi, K. Mori, "Proposal of Channel Estimation Method for OFDM Systems under Time-Varying Fading Environments", *IEICE Technical Report*, vol.190-B, no.12, pp1249-1262, Dec. 2007.
- [77] K. M. M. Prabhu, "*Window Functions and Their Applications in Signal Processing*," CRC press, 2013.
- [78] P. Reangsuntea, P. Boonsrimuang, K. Mori, and H. Kobayashi, "Iterative Based Time Domain Equalization Method for OFDM Signal under High Mobile Environments," in *Proc. of 8th International Conf. on Signal Processing and Commun. Systems (ICSPCS)*, pp. 1-6, Dec. 2014.
- [79] M. Engle, "*Wireless OFDM System: How to make them work?*," Kluwer Academic Publishers, 2002.
- [80] J. Hao, Y. R. Zheng, J. Wang, J. Song, "Dual PN Padding TDS-OFDM for Underwater Acoustic Communication," in *Proc. of Oceans*, pp. 1-4, Oct. 2012.
- [81] J. Hao, J. Wang, and Y. Wu, "A New Equalizer in Doubly-Selective Channels for TDS-OFDM," *IEEE Trans. Broadcasting*, vol. 61, no.1, pp. 91-97, Mar. 2015.
- [82] P. Reangsuntea, P. Boonsrimuang, M. Hourai, K. Mori, and H. Kobayashi, "Iterative Based ML Demodulation Method for OFDM Signal under Higher Mobile Environments," in *Proc. of IEEE 81st Veh. Tech. Conf. (VTC)*, pp. 1-6, May 2015.
- [83] H. Minn, V. K. Bhargava and K. B. Letaief, "A Robust Timing and Frequency Synchronization for OFDM Systems," *IEEE Trans. Wireless Commun.*, vol. 2, no.4, pp. 822-839, Jul. 2003.
- [84] R. M. Gray, "Toeplitz and Circulant Matrices: A Review," *Journal on Foundations and Trends*, vol. 2, no. 3, pp. 155-239, Jan. 2006.
- [85] L. Rugini, P. Banelli, and G. Leus, "Simple Equalization of Time-Varying Channels for OFDM," *IEEE Commun. Lett.*, vol. 9, no. 7, pp.619-621, Jul. 2005.
- [86] A. A. Quadeer, "Enhanced Equalization in OFDM Systems Using Cyclic Prefix," in *Proc. of Wireless Communications, Networking, and Information Security*, pp. 40-44, Jun. 2010.
- [87] L. Lin, J. Lu, L. Ying, R. Car, and W. E, "Fast Algorithm for Extracting the Diagonal of the Inverse Matrix with Application to the Electronic Structure Analysis of Metallic Systems," *Commun. Math. Sci.*, vol. 7, no. 3, pp. 755-777, Jul. 2009.
- [88] Y. Geoffrey Li and Gordon L. Stuber, "*Orthogonal Frequency Division Multiplexing for Wireless Communications*," Springer; 2005.
- [89] M. Liu, M. Crussiere, and J. Helard, "A novel data-aided channel estimation with reduced complexity for TDS-OFDM systems," *IEEE Trans. Broadcasting*, vol. 58, no. 2, pp. 247-260, Jun. 2012.
- [90] Y. Zhao and S. G. Haggman, "Intercarrier interference self-cancellation scheme for OFDM mobile communication systems," *IEEE Trans. Commun.*, vol. 49, pp. 1185-1191, July 2001.
- [91] M. X. Chang, "A novel algorithm of inter-subchannel interference selfcancellation for OFDM systems," *IEEE Trans. Wireless Commun.*, vol. 6, pp. 2881-2893, Aug. 2007.

- [92] D. Shimbo, N. Maeda, H. Mishima, and J. Ido, "Inter-carrier interference compensation for zero padding OFDM," in *Proc. of IEEE 78th Veh. Technol. Conf.*, Las Vegas, NV, USA, pp. 1–5, Sep. 2013.
- [93] N. Benvenuto and S. Tomasin, "On the comparison between OFDM and single carrier modulation with a DFE using a frequency-domain feed forward filter," *IEEE Trans. Commun. Mag.*, vol. 50, pp. 947–955, Jun. 2002.
- [94] G. M. Hyung, L. Junsung, and J. G. David, "Single carrier FDMA for uplink wireless transmission," *IEEE Veh. Tech. Mag.*, vol. 1, no. 3, pp. 30–38, Sep. 2006.
- [95] D. Y. Seol, U. K. Kwon, and G. H. Im, "Performance of single carrier transmission with cooperative diversity over fast fading channels," *IEEE Trans. Commun.*, vol. 57, no. 9, pp. 2799–2807, Sep. 2009.
- [96] A. Ghosh, R. Ratasuk, B. Mondal, N. Mangalvedhe, and T. Thomas, "LTE-advanced: next-generation wireless broadband technology," *IEEE Wireless Commun.*, vol. 17, no. 3, pp. 10–22, Jun. 2010.
- [97] 3GPP TS 36.211, Evolved Universal Terrestrial Radio Access (EUTRA); Physical Channels and Modulation, *3GPP Standard*, Rev. 10.0.0, 2011.
- [98] L. Yang, G. Ren, B. Yang, and Z. Qiu, "Fast Time-Varying Channel Estimation Technique for LTE Uplink in HST Environment," *IEEE Trans. Veh. Tech.*, vol. 61, no. 9, Nov. 2012.
- [99] G. Li, H. Yang, L. Cai and L. Gui, "A Low-complexity Equalization Technique for OFDM System in Time-Variant Multipath Channels," In *Proc. of IEEE on veh. Tech. Conf. (VTC 2003-Fall)*, vol. 4, pp. 2466–2470, Oct. 2003.
- [100] C. Ma, S. Liu and C. Huang, "Low-Complexity ICI Suppression Methods Utilizing Cyclic Prefix for OFDM Systems in High-Mobility Fading Channels," *IEEE Trans. Veh. Tech.*, vol. 63, no. 2, pp. 718–730, Feb. 2014.
- [101] Y. Qi, P. Huang, and M. Rong, "Performance Comparison of TDE and FDE in Single-carrier System," in *Proc. of 69th IEEE on Veh. Tech. Conf. (VTC-Spring)*, pp. 1–5, Apr. 2009.
- [102] P. Reangsuntea, P. Boonsrimuang, K. Mori, and H. Kobayashi, "Time domain equalization method for DFTS-OFDM signal without GI under high mobile environments," In *Proc. of 12nd Inter. Conf. on Electrical Engineering/Electronics, Computer, Telecom. and Info. Tech. (ECTI-CON)*, pp. 1–6, June 2015.
- [103] C. Vulk, "Iterative Solution methods," Delft Institute of Applied Mathematics, Netherlands, 2012.
- [104] Andrew J. Viterbi, "Error Bounds for Convolutional Codes and an Asymptotically Optimum Decoding Algorithm," *IEEE Trans. Information Theory*, Volume IT-13, pp. 260–269, Apr. 1967.